The Impact of Collateral Evolution on Optimal Dosing Strategies and Evolution on Paired Fitness Landscapes

by

Jeffrey Maltas

A dissertation submitted in partial fulfillment
of the requirements for the degree of
Doctor of Philosophy
(Biophysics)
in The University of Michigan
2020

Doctoral Committee:

Assistant Professor Kevin Wood, Chair
Professor Matthew Chapman
Professor Charles Doering
Assistant Professor Jordan Horowitz
Assistant Professor Qiong Yang

Jeffrey Maltas

jamaltas@umich.edu

ORCID iD: 0000-0001-6567-6800

For my mom and dad.

ACKNOWLEDGEMENTS

My unique path to completing this dissertation at the University of Michigan is owed to many outstanding mentors. I would like to first thank Jeff Baker, my high school physics teacher. As a teenager, struggling to cope with the realities of my mom's progressing cancer, I failed out of AP physics. By some cosmic fortune, I landed in Jeff Baker's physics class. He instilled in me a lasting curiosity and passion for physics that has driven me to this day. A sincere thank you Dr. Andrew Kunz, my advisor at Marquette, who gave me the first taste of research and drove an education major toward academia. An important thank you to Dr. John Karkheck, who is the best educator I have ever met, and who advanced my physical intuition more than any other person or book. Thank you to my Miami-Ohio advisor, Dr. Paul Urayama, who first taught me the ins and outs of the academic process and continues to serve as an advisor to this day. Thank you to my advisor here at Michigan, Dr. Kevin Wood. Not only is Kevin an absolutely brilliant scientist, but he deeply cares for the well-being and success of his students. I am also grateful to Dr. Qiong Yang, Dr. Matthew Chapmap, Dr. Jordan Horowitz and Dr. Charles Doering, for serving on my committee. Finally, I am thankful to the members of the Wood lab past and present. Whether it was silly conversations about sports, or important conversations about different cultures and nations, I deeply appreciate the time I have spent with you all.

TABLE OF CONTENTS

LIST OF FIGURES

Figure

LIST OF TABLES

ABSTRACT

Drug resistance is an ever-growing threat to successful treatment of bacterial, cancer and viral infections. As pathogens and cancers continue to find evolutionary solutions to the drugs we treat them with, scientists have begun to focus on more evolutionary-based therapies such as drug cycling. These therapies aim to constrain or control evolution in a particular way such that intractable resistance never evolves. In the same vein, recent work has revealed collateral sensitivity as a promising avenue to guide evolution away from untreatable resistance states. Collateral evolution occurs when a population evolves resistance to the selecting drug and this mechanism of resistance confers "collateral" effects to different drugs it is not exposed to. In this work we show how collateral profiles might be used to slow the acquisition to resistance in a simplified laboratory-based evolution experiment. We demonstrate that intuitive cycling protocols often fail over long time periods, whereas mathematically optimized protocols maintain long-term sensitivity at the cost of transient periods of high resistance. We then extend this work to include nonantibiotic stressors such as pH, salt and food preservatives. This extension highlights that more work is necessary to understand the role these common environments have on the development of multidrug resistance. Finally, using the well-known fitness landscape paradigm, we explore how collateral effects influence the evolutionary dynamics of a pair of landscapes with tunable correlations. We show that alternating evolution in highly correlated environments can lead to higher mean fitness than evolution in either landscape alone, while alternating between two anti-correlated landscapes results in a lower mean fitness. We demonstrate this is due to the location and number

of shared maxima between the two correlated landscapes, which change as a function of ruggedness (epistasis) and paired landscape correlation. Taken together, these results begin to answer many of the important questions required to translate collateral sensitivity into clinical treatments.

CHAPTER I

Introduction

For decades we have generously deployed the use of antibiotics to cure all bacterial ailments. Antibiotics have been seen as a "miracle" drug giving us the ability to cure the incurable almost overnight. Over the last near-century, antibiotics have become intertwined with more than just human health. Antibiotics are regularly and prophylactically used to maintain the agriculture and trade industries worldwide. However, the steady rise of antibiotic-resistant bacteria threatens to usher our world into a post-antibiotic era. A growing number of infections such as gonorrhea and tuberculosis are becoming harder or impossible to treat [1, 2].

With this growing threat challenging effective treatments for viral infections, bacterial infections and cancer [3, 4, 5, 6, 7, 8], the scientific community has turned to evolutionary-based strategies for constraining or reversing resistance. These strategies include optimal dose scheduling [9, 10, 11], antimicrobial stewardship [12, 13], drug cycling [14, 15, 16], exploitation of spatial dynamics [17, 18, 19], cooperative population dynamics [20, 21, 22, 23], phenotypic resistance [24, 25, 26], and drug combinations [27, 28, 29, 30, 31, 32, 33, 34]. One of the most promising recent strategies is the exploitation of collateral sensitivity [35, 36, 37, 38, 39, 40]. Collateral evolution is a term for the unintended increases and decreases in resistance as a direct result of acquiring resistance to the drug applying selection pressure. For example, if a population treated by the fluorquinolone antibiotic ofloxacin were to evolve a general-purpose efflux pump that pumps out both ofloxacin in addition to doxycycline, we would call that additional resistance to doxycyline "collateral resistance". If instead, the conferred mutation altered the way the DNA super-coiled in order to protect itself from ofloxacin, and as a side effect altered its gene expression such that the population became more susceptible to ampicillin, we would call that additional sensitivity to ampicillin "collateral sensitivity".

As a result, it has been proposed that collateral sensitivity can be used to reverse acquired resistance, or to constrain the population from evolving resistance in

the first place via judicious drug scheduling. However, many challenges remain before the exploitation of collateral effects can be used clinically. Collateral profiles to the same selecting drug have been shown to be highly heterogeneous, time-sensitive, and too few studies exist to confirm if these effects differ between species [41, 42, 43]. With these questions in mind, this research seeks to answer several of these questions. We begin with a large systematic study of the collateral profiles in the opportunistic pathogen *E. faecalis* (Chapter 2). A combination of parallel experimental evolution with high-throughput dose-response measurements allow us to measure the collateral profile of 61 different strains evolved to 15 different antibiotics, over 900 strain-drug combinations. We find that collateral effects are pervasive and heterogeneous, even within mutants evolved to the same selecting drug. However, we observe a statistical structure in the collateral profiles, as these profiles cluster into groups characterized by their drug class. In an attempt to exploit this structure, we develop a mathematical framework based based on a Markov Decision Process (MDP) in order to identify the optimal antibiotic schedule that minimizes resistance. Excitingly, we show experimentally that these optimal policies constrain resistance better than more intuitive single, two and four drug cycles. Subsequently, we extend this work on collateral sensitivity by demonstrating that collateral effects between antibiotic and nonantibiotic conditions (pH, acidic, basic, high salt, etc.) are surprisingly common (Chapter 3). While some research has been done looking at the collateral effects from one individual stressor [44, 45, 46, 47, 48, 49, 50, 51, 52, 53], there has yet to be a broader study of the collateral network between antibiotics and nonantibiotics. The prevalence of cross-conditional collateral effects highlight the need for further research on the unintended consequences of food additives, preservatives, biocides, or common natural environments in spreading multidrug resistance. We conclude our experimental collateral sensitivity work by demonstrating that populations evolved to two conditions sequentially can induce increased sensitivity to a larger selection of conditions than

adaptation to either individual stressor alone.

As a model system, all our experiments focus on *Enterococcus faecalis*, a gram-positive opportunistic nosocomial pathogen. *E. faecalis* are found in the gastrointestinal tracts of humans and are known to cause urinary tract infections and between 5 and 15 percent of endocarditis infections [54, 55, 56, 57, 58]. For our own work, *E. faecalis* is a convenient choice of pathogen because it readily evolves resistance to a wide range of antibiotics [59, 60], and much of the current collateral sensitivity literature focuses on gram-negative bacteria. Finally, fully sequenced genomes are available for the common strains such as our preferred strain, V583 [61].

Finally, inspired by the ideas of collateral evolution, we turn to a more abstract evolutionary question: how does evolution proceed when the population is alternating between two environments with a specific correlation (Chapter 4)? Much work has been done investigating evolution on a single fitness landscape, or between many landscapes of no specific correlation [62, 63, 64, 65, 66, 67, 68, 69, 70, 71]. However, we seek to understand the evolutionary dynamics of asexual populations in alternating environments described by a pair of fitness landscapes with some tunable inter-landscape correlation. Interestingly, we find that rapid switching can either increase or decrease the final fitness when compared to evolution in either landscape alone. The resulting fitness is largely governed by shared fitness maximums, or genotypes where both landscapes share a fitness maximum. We show that the location and number of shared fitness maximums are governed by the correlation and ruggedness (epistasis) of the landscapes.

1.1 References

1 S. B. Zaman, M. A. Hussain, R. Nye, *et al.*, "A review on antibiotic resistance: alarm bells are ringing," *Cureus* **9**(6) (2017).

2 B. Aslam, W. Wang, M. I. Arshad, *et al.*, "Antibiotic resistance: a rundown of a global crisis," *Infection and drug resistance* **11**, 1645 (2018).

3 H. W. Boucher, G. H. Talbot, J. Bradley, *et al.*, "Bad bugs, no drugs; no esape! an update from the infections diseases society of america.," *Clin. Infect. Dis.* **48**, 1–12 (2009).

4 D. E. Goldberg, R. Siliciana, and W. R. J. Jr, "Outwitting evolution: Fighting drug-resistant tb, malaria, and hiv.," *Cell* **148**, 1271–1283 (2012).

5 A. Pfaller, "Antifungal drug resistance: Mechanisms, epidemiology, and consequences for treatment.," *Am. J. Med.* **125**, S3–S13 (2012).

6 M. Raviglione, B. Marais, K. Floyd, *et al.*, "Scaling up interentions to achieve global tuberculosis control: Progress and new developments.," *Lancet* **379**, 1902–1913 (2012).

7 P. Borst, "Cancer drug pan-resistance: Pumps, cancer stem cells, quiescence, epithelial to mesenchymal transition, blocked cell death pathways, persister or what?.," *Open Biol.* **2** (2012).

8 K. M. Pluchino, M. D. Hall, A. S. Goldsborough, *et al.*, "Collateral sensitivity as a strategy against cancer multidrug resistance.," *Drug Resis. Updat.* **15**, 98–105 (2012).

9 R. Martin, "Optimal control drug scheduling of cancer chemotherapy.," *Journal of Antimicrobial Chemotherapy* **28**, 1113–1123 (1992).

10 E. Hansen, R. J. Woods, and A. F. Read, "How to use a chemotherapeutic agent when resistance to it threatens the patient," *PLoS biology* **15**(2), e2001110 (2017).

11 A. Fischer, I. Vázquez-García, and V. Mustonen, "The value of monitoring to control evolving populations," *Proceedings of the National Academy of Sciences* **112**(4), 1007–1012 (2015).

12 L. M. Feazel, A. Malhotra, E. N. Perencevich, *et al.*, "Effect of antibiotic stewardship programmes on *clostridium difficile* incidence: a systematic review and meta-analysis.," *Journal of Antimicrobial Chemotherapy* **69**, 1748–1754 (2014).

13 D. L. Smith, S. A. Levin, and R. Laxminarayan, "Strategic interactions in multi-institutional epidemics of antibiotic resistance.," *Proc. Natl. Acad. Sci. USA* **102**, 3153–3158 (2004).

14 C. T. Bergstrom, M. Lo, and M. Lipsitch, "Ecological theory suggests that antimicrobial cycling will not reduce antimicrobial resistance in hospitals.," *Proc. Natl. Acad. Sci. USA* **101**, 13285–13290 (2004).

15 E. M. Brown and D. Nathwani, "Antibiotic cycling or rotation: a systemic review of the evidence of efficacy.," *Journal of Antimicrobial Chemotherapy* **55**, 6–9 (2005).

16 D. Nichol, P. Jeavons, A. G. Fletcher, *et al.*, "Steering evolution with sequential therapy to prevent the emergence of bacterial antibiotic resistance," *PLoS computational biology* **11**(9), e1004493 (2015).

17 M. Baym, T. D. Lieberman, E. D. Kelsic, *et al.*, "Spatiotemporal microbial evolution on antibiotic landscapes," *Science* **353**(6304), 1147–1151 (2016).

18 Q. Zhang, G. Lambert, D. Liao, *et al.*, "Acceleration of emergence of bacterial antibiotic resistance in connected microenvironments," *Science* **333**(6050), 1764–1767 (2011).

19 M. G. De Jong and K. B. Wood, "Tuning spatial profiles of selection pressure to modulate the evolution of drug resistance," *Phys. Rev. Lett.* **120**, 238102 (2018).

20 E. A. Yurtsev, H. X. Chao, M. S. Datta, *et al.*, "Bacterial cheating drives the population dynamics of cooperative antibiotic resistance plasmids," *Molecular systems biology* **9**(1), 683 (2013).

21 H. R. Meredith, A. J. Lopatkin, D. J. Anderson, *et al.*, "Bacterial temporal dynamics enable optimal design of antibiotic treatment," *PLoS computational biology* **11**(4), e1004201 (2015).

22 H. R. Meredith, J. K. Srimani, A. J. Lee, *et al.*, "Collective antibiotic tolerance: mechanisms, dynamics and intervention," *Nature chemical biology* **11**(3), 182–188 (2015).

23 N. M. Vega and J. Gore, "Collective antibiotic resistance: mechanisms and implications," *Current opinion in microbiology* **21**, 28–34 (2014).

24 N. Q. Balaban, J. Merrin, R. Chait, *et al.*, "Bacterial persistence as a phenotypic switch," *Science* **305**(5690), 1622–1625 (2004).

25 C. Tan, R. P. Smith, J. K. Srimani, *et al.*, "The inoculum effect and band-pass bacterial response to periodic antibiotic treatment," *Molecular systems biology* **8**(1), 617 (2012).

26 J. Karslake, J. Maltas, P. Brumm, *et al.*, "Population density modulates drug inhibition and gives rise to potential bistability of treatment outcomes for bacterial infections," *PLoS computational biology* **12**(10), e1005098 (2016).

27 J. P. Torella, R. Chait, and R. Kishony, "Optimal drug synergy in antimicrobial treatments.," *PlOS Comput. Biol.*. **6** (2010).

28 J. Michel, P. J. Yeh, R. Chait, *et al.*, "Drug interactions modulate the potential for evolution of resistance.," *Proc. Natl. Acad. Sci. USA* **105**, 14918–14923 (2008).

29 M. Hegreness, N. Shoresh, D. Damian, *et al.*, "Accelerated evolution of resistance in multi-drug environments.," *Proc. Natl. Acad. Sci. USA* **105**, 13977–13981 (2008).

30 R. Chait, A. Craney, and R. Kishony, "Antibiotic interactions that select against resistance," *Nature* **446**(7136), 668 (2007).

31 M. Baym, L. K. Stone, and R. Kishony, "Multidrug evolutionary strategies to reverse antibiotic resistance," *Science* **351**(6268), aad3292 (2016).

32 K. Wood, S. Nishida, E. D. Sontag, *et al.*, "Mechanism-independent method for predicting response to multidrug combinations in bacteria," *Proceedings of the National Academy of Sciences* **109**(30), 12254–12259 (2012).

33 A. Zimmer, I. Katzir, E. Dekel, *et al.*, "Prediction of multidimensional drug dose responses based on measurements of drug pairs," *Proceedings of the National Academy of Sciences* **113**(37), 10442–10447 (2016).

34 A. Zimmer, A. Tendler, I. Katzir, *et al.*, "Prediction of drug cocktail effects when the number of measurements is limited," *PLoS biology* **15**(10), e2002518 (2017).

35 M. R. de Evgrafov, H. Gumpert, C. Munck, *et al.*, "Collateral resistance and sensitivity modulate evolution in high-level resistance to drug combination treatment in *staphylococcus aureus.*," *Mol. Biol. Evol.* **32**, 1175–1185 (2015).

36 T. Oz, A. Guvenek, S. Yildiz, *et al.*, "Strength of selection pressure is an important parameter contributing to the complexity of antibiotic resistance evolution.," *Mol. Biol. Evol.* **31**, 2387–2401 (2014).

37 V. Lazar, I. Nagy, R. Spohn, *et al.*, "Genome-wide analysis captures the determinants of the antibiotic cross-resistance interaction network.," *Nat. Commun.* **5** (2014).

38 V. Lazar, G. P. Singh, R. Spohn, *et al.*, "Bacterial evolution and antibiotic hypersensitivity.," *Mol. Syst. Biol.* **9** (2013).

39 V. Lazar, A. Martins, R. Spohn, *et al.*, "Antibiotic-resistant bacteria show widespread collateral sensitivity to antimicrobial peptides.," *Nature Microbiology* **3**, 718–731 (2018).

40 L. Imamovic, M. Ellabaan, A. Machado, *et al.*, "Drug-driven phenotypic convergence supports rational treatment strategies of chronic infections.," *Cell* **172**, P121–134 (2018).

41 C. Barbosa, V. Trebosc, C. Kemmer, *et al.*, "Alternative evolutionary paths to bacterial antibiotic resistance cause distinct collateral effects.," *Mol. Biol. Evol.* **34**, 2229–2244 (2017).

42 A. Dhawan, D. Nichol, F. Kinose, *et al.*, "Collateral sensitivity networks reveal evolutionary instability and novel treatment strategies in alk mutated non-small cell lung cancer," *Scientific Reports* **7** (2017).

43 D. Nichol, J. Rutter, C. Bryant, *et al.*, "Antibiotic collateral sensitivity is contingent on the repeatability of evolution," *Nature communications* **10**(1), 334 (2019).

44 C. Seiler and T. U. Berendonk, "Heavy metal driven co-selection of antibiotic resistance in soil and water bodies impacted by agriculture and aquaculture.," *Front Microbiol.* **3** (2012).

45 A. Hassen, N. Saidi, M. Cherif, *et al.*, "Resistance of environmental bacteria to heavy metals.," *Bioresource Technology* **64**, 7–15 (1998).

46 C. Baker-Austin, M. S. Wright, R. Stepanauskas, *et al.*, "Co-selection of antibiotic and metal resistance.," *Trends in Microbiology* **14**, 176–182 (2006).

47 X. Ji, Q. Shen, F. Liu, *et al.*, "Antibiotic resistance gene abundances associated with antibiotics and heavy metals in animal manures and agricultural soils adjacent to feedlots in shanghai; china.," *Journal of Hazardous Materials* **235-236**, 178–185 (2012).

48 P. Bhardwaj, A. Hans, K. Ruikar, *et al.*, "Reduced chlorhexidine and daptomycin susceptibility in vancomycin-resistant enterococcus faecium after serial chlorhexidine exposure," *Antimicrobial agents and chemotherapy* **62**(1), e01235–17 (2018).

49 D. E. Carey and P. J. McNamara, "The impact of triclosan on the spread of antibiotic resistance in the environment.," *Frontiers in Microbiology* **5** (2015).

50 S. P. Yazdankhah, A. A. Scheie, E. A. Høiby, *et al.*, "Triclosan and antimicrobial resistance in bacteria: an overview," *Microbial drug resistance* **12**(2), 83–90 (2006).

51 M. E. Wand, L. J. Bock, L. C. Bonney, *et al.*, "Mechanisms of increased resistance to chlorhexidine and cross-resistance to colistin following exposure of klebsiella pneumoniae clinical isolates to chlorhexidine.," *Antimicrobial agents and chemotherapy* **61** (2017).

52 C. Horner, D. Mawer, and M. Wilcox, "Reduced susceptibility to chlorhexidine in staphylococci: is it increasing and does it matter?," *Journal of antimicrobial chemotherapy* **67**, 2547–2559 (2012).

53 A. Knöppel, J. Näsvall, and D. I. Andersson, "Evolution of antibiotic resistance without antibiotic exposure," *Antimicrobial agents and chemotherapy* **61**(11), e01495–17 (2017).

54 D. B. Clewell, M. S. Gilmore, Y. Ike, *et al.*, *Enterococci: from commensals to leading causes of drug resistant infection*, Massachusetts Eye and Ear Infirmary (2014).

55 R. M. Donlan, "Biofilms and device-associated infections.," *Emerging infectious diseases* **7**(2), 277 (2001).

56 T. O'Driscoll and C. W. Crank, "Vancomycin-resistant enterococcal infections: epidemiology, clinical manifestations and optimal management.," *Drug Resis. Updat.* **8**, 217–230 (2015).

57 Y. Cetinkaya, P. Falk, and C. G. Mayhall, "Vancomycin resistant enterococci.," *Clin. Microbiol. Rev.* **13**, 686–707 (2000).

58 M. M. Huycke, D. F. Sahm, and M. S. Gilmore, "Multiple-drug resistant enterococci: the nature of the problem and an agenda for the future.," *Emerging infectious diseases* **4**(2), 239 (1998).

59 K. L. Palmer, A. Daniel, C. Hardy, *et al.*, "Genetic basis for daptomycin resistance in enterococci," *Antimicrobial Agents and Chemotherapy* **55**(7), 3345–3356 (2011).

60 C. Miller, J. Kong, T. T. Tran, *et al.*, "Adaptation of enterococcus faecalis to daptomycin reveals an ordered progression to resistance," *Antimicrobial agents and chemotherapy* , AAC–01473 (2013).

61 I. T. Paulsen, L. Banerjei, G. Myers, *et al.*, "Role of mobile dna in the evolution of vancomycin-resistant enterococcus faecalis," *Science* **299**(5615), 2071–2074 (2003).

62 I. Cvijović, B. H. Good, E. R. Jerison, *et al.*, "Fate of a mutation in a fluctuating environment," *Proceedings of the National Academy of Sciences* **112**(36), E5021–E5028 (2015).

63 V. Mustonen and M. Lässig, "Molecular evolution under fitness fluctuations," *Phys. Rev. Lett.* **100**, 108101 (2008).

64 R. C. Lewontin and D. Cohen, "On population growth in a randomly varying environment," *Proceedings of the National Academy of Sciences* **62**(4), 1056–1060 (1969).

65 R. Hermsen and T. Hwa, "Sources and sinks: a stochastic model of evolution in heterogeneous environments," *Physical review letters* **105**(24), 248104 (2010).

66 M. C. Whitlock and R. Gomulkiewicz, "Probability of fixation in a heterogeneous environment," *Genetics* **171**(3), 1407–1417 (2005).

67 S. Farhang-Sardroodi, A. Darooneh, M. Nikbakht, *et al.*, "The effect of spatial randomness on the average fixation time of mutants.," *PLoS computational biology* **13**(11), e1005864 (2017).

68 N. Kashtan, E. Noor, and U. Alon, "Varying environments can speed up evolution," *Proceedings of the National Academy of Sciences* **104**(34), 13711–13716 (2007).

69 J. H. Gillespie, "Some properties of finite populations experiencing strong selection and weak mutation," *The American Naturalist* **121**(5), 691–708 (1983).

70 J. H. Gillespie, "A simple stochastic gene substitution model," *Theoretical Population Biology* **23**(2), 202 – 215 (1983).

71 J. H. Gillespie, "Molecular evolution over the mutational landscape," *Evolution* **38**(5), 1116–1129 (1984).

CHAPTER II

Pervasive and Diverse Collateral Sensitivity Profiles Inform Optimal Strategies to Limit Antibiotic Resistance

This chapter was amended from: Jeff Maltas and Kevin B. Wood. 'Pervasive and diverse collateral sensitivity profiles inform optimal strategies to limit antibiotic resistance' PLOS Biology 17(10), e300515, 2019.

2.1 Introduction

As mentioned briefly in the introduction, the rapid emergence of drug resistance is an urgent threat to effective treatments for bacterial infections, cancers and many viral infections [1, 2, 3, 4, 5, 6]. Unfortunately, the development of novel drugs is a long and arduous process, underscoring the need for alternative approaches to forestall resistance evolution. Recent work has highlighted the promise of evolution-based strategies for optimizing and prolonging the efficacy of established drugs, including optimal dose scheduling [7, 8, 9], antimicrobial stewardship [10, 11], drug cycling [12, 13, 14], consideration of spatial dynamics [15, 16, 17], cooperative dynamics [18, 19, 20, 21], or phenotypic resistance [22, 23, 24], and judicious use of drug combinations [25, 26, 27, 28, 29, 30, 31, 32]. In a similar spirit, a number of recent studies have suggested exploiting collateral sensitivity as a means for slowing or even reversing antibiotic resistance [33, 34, 35, 36, 37, 38]. Collateral evolution occurs when a population evolves resistance to a target drug while simultaneously exhibiting increased sensitivity or resistance to a different drug. From an evolutionary perspective, collateral effects are reminiscent of the trade-offs inherent when organisms are required to simultaneously adapt to different tasks, an optimization that is often surprisingly simple because it takes place on a low-dimensional phenotypic space [39, 40]. If similarly tractable dynamics occur in the evolution of multi-drug resistance, systematic optimization of drug deployment has the promise to mitigate the effects of resistance.

Indeed, recent studies in bacteria have shown that the sequential [41, 42, 43, 44, 45, 38, 46] or simultaneous [47, 48] deployment of antibiotics with mutual collateral

sensitivity can sometimes slow the emergence of resistance. Unfortunately, collateral profiles have also been shown to be highly heterogeneous [49, 50] and often not repeatable [51], potentially complicating the design of successful collateral sensitivity cycles. The picture that emerges is enticing, but complex; while collateral effects offer a promising new dimension for improving therapies, the design of drug cycling protocols is an extremely difficult problem that requires optimization at multiple scales, from dynamics within individual hosts to those that occur at the hospital or community scale. Despite many promising recent advances, it is not yet clear how to optimally harness collateral evolutionary effects to design drug policies, even in simplified laboratory scenarios. The problem is challenging for many reasons, including the stochastic nature of evolutionary trajectories and–at an empirical level– the relative paucity of data regarding the prevalence and repeatability of collateral sensitivity profiles in different species.

In this chapter, we take a step towards answering these questions by investigating how drug sequences might be used to slow resistance in a simplified, single-species bacterial population. We show that even in this idealized scenario, intuitive cycling protocols–for example, sequential application of two drugs exhibiting reciprocal collateral sensitivity–are expected to fail over long time periods, though mathematically optimized policies can maintain long-term drug sensitivity at the price of transient periods of high resistance. As a model system, we focus on *Enterococcus faecalis*, a gram-positive opportunistic bacterial pathogen. *E. faecalis* are found in the gastrointestinal tracts of humans and are implicated in numerous clinical infections, ranging from urinary tract infections to infective endocarditis, where they are responsible for between 5 and 15 percent of cases [52, 53, 54, 55, 56]. For our purposes, *E. faecalis* is a convenient model species because it rapidly evolves resistance to antibiotics in the laboratory [57, 58], and fully sequenced reference genomes are available [59].

By combining parallel experimental evolution of *E. faecalis* with high-throughput

dose-response measurements, we provide collateral sensitivity and resistance profiles for 60 strains evolved to 15 different antibiotics, yielding a total of 900 mutant-drug combinations. We find that cross resistance and collateral sensitivity are pervasive in drug-resistant mutants, though patterns of collateral effects can vary significantly, even for mutants evolved to the same drug. Notably, however, the sensitivity profiles cluster into groups characterized by selecting drugs from similar drug classes, indicating the existence of large scale statistical structure in the collateral sensitivity profiles. To exploit that structure, we develop a simple mathematical framework based on a Markov Decision Process (MDP) to identify optimal antibiotic policies that minimize resistance. These policies yield drug sequences that can be tuned to optimize either short-term or long-term evolutionary outcomes, and they codify the trade-offs between instantaneous drug efficacy and delayed evolutionary consequences. While clearly too simple to capture evolution in realistic clinical scenarios, the model points to new conceptual strategies for mitigating resistance by balancing short-term growth inhibition with infrequent use of drugs intended to steer pathogen populations to a more vulnerable future state.

2.2 Results

2.2.1 Collateral effects are pervasive and heterogeneous

To investigate collateral drug effects in *E. faecalis*, we exposed four independent populations of strain V583 to increasing concentrations of a single drug over 8 days (a maximum of roughly 60 generations) using serial passage laboratory evolution (Figure 2.1). We repeated this laboratory evolution for a total of 15 antibiotics spanning a wide range of classes and mechanisms of action (Table 2.2). Many, but not all, of these drugs are clinically relevant for the treatment of enterococcal infections. As a control, we also evolved 4 independent populations of the ancestral V583 strain to

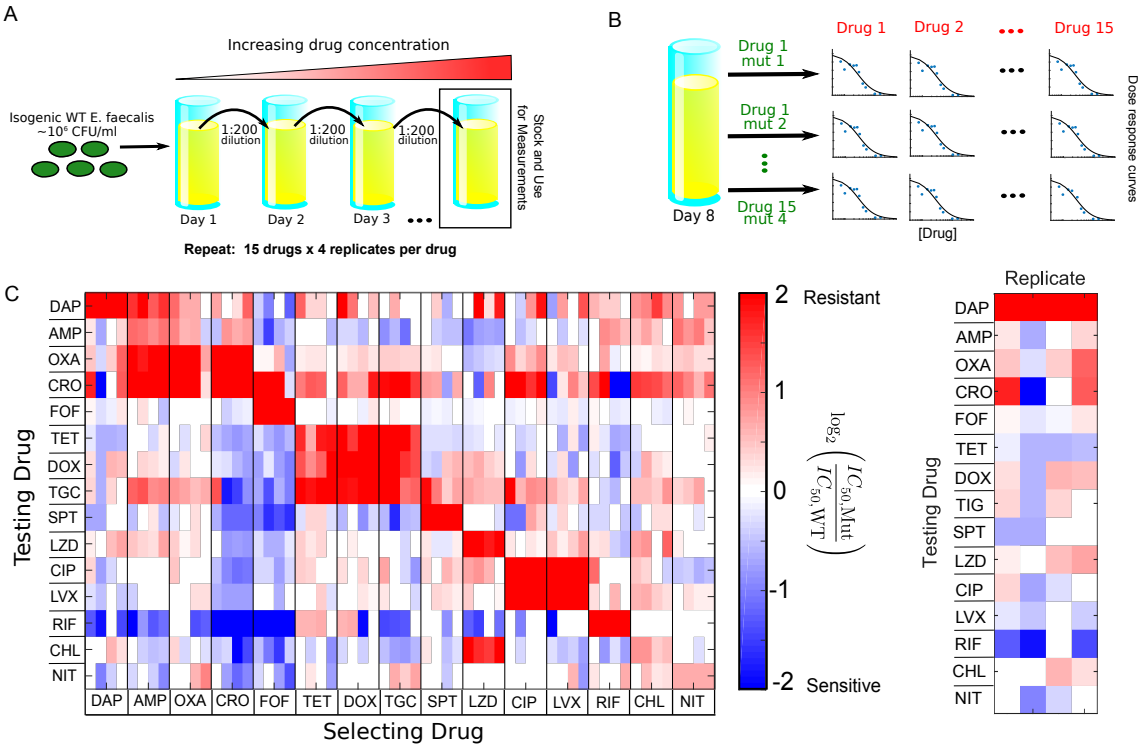

Figure 2.1: **Collateral effects are pervasive and vary across parallel evolution experiments in *E. faecalis*.** A. *E. faecalis* strain V583 was exposed to increasing concentrations of a single antibiotic over an 8-day serial passage experiment with daily 200-fold dilutions (maximally 60 generations total; see Methods). The evolution was performed in quadruplicate for each drug and repeated for a total of 15 drugs (Table 2.2). After 8 days, a single mutant was isolated from each population. B. The half maximal inhibitory concentration (IC_{50}) for each of 15 drugs was estimated for all 60 mutants by nonlinear fitting of a dose response curve (relative OD) to a Hill-like function (Methods). C. Main panel: resistance (red) or sensitivity (blue) of each evolved mutant (horizontal axis; 15 drugs x 4 mutants per drug) to each drug (vertical axis) is quantified by the $\log_2$-transformed relative increase in the IC_{50} of the testing drug relative to that of wild-type (V583) cells. While the color scale ranges from a 4x decrease to a 4x increase in IC_{50}, it should be noted that both resistance to the selecting drug (diagonal blocks) and collateral effects can be significantly higher. Each column of the heat map represents a collateral sensitivity profile for one mutant. Right panel: enlarged first column from main panel. Mutants isolated from replicate populations evolved to daptomcyin exhibit diverse sensitivity profiles. While all mutants are resistant to the selecting drug (daptomycin), mutants may exhibit either sensitivity or resistance to other drugs. For example, the first and last replicates exhibit cross resistance to ceftriaxone (CRO), while replicate 2 exhibits collateral sensitivity and replicate 3 shows little effect.

media (BHI) alone. After a maximum of 60 generations, we isolated a single colony (hereafter termed a "mutant") from each population and measured its response to all 15 drugs using replicate dose-response experiments (Figure 2.1B). To quantify resistance, we estimated the half maximal inhibitory concentration (IC_{50}) for each mutant-drug combination using nonlinear least squares fitting to a Hill-like dose response function (Methods; see Figure 2.7 for examples). A mutant strain was defined to be collaterally sensitive if its IC_{50} had decreased by more than $3\sigma_{WT}$ relative to the ancestral strain (σ_{WT} is defined as the uncertainty–standard error across replicates–of the IC_{50} measured in the ancestral strain). Similarly, an increase in IC_{50} by more than $3\sigma_{WT}$ relative to the ancestral strain corresponds to cross-resistance. As a measure of cross resistance / sensitivity, we then calculate $C \equiv \log_2(IC_{50,Mut}/IC_{50,WT})$, the (log-scaled) fold change in IC_{50} of each mutant relative to wild-type (WT); values of $C > 0$ indicate cross resistance, while values of $C < 0$ indicate collateral sensitivity (Figure 2.1C). For each mutant, we refer to the set of C values (one for each testing drug) as its collateral sensitivity profile $\bar{C}$.

Our results indicate that collateral effects–including sensitivity–are pervasive, with approximately 73 percent (612/840) of all (collateral) drug-mutant combinations exhibiting a statistically significant change in IC_{50}. By contrast, none of the four V583 strains propagated in BHI alone showed any collateral effects. The isolates exhibit collateral sensitivity to a median of 4 drugs, with only 3 of the 60 mutants (5 percent) exhibiting no collateral sensitivity at all; on the other hand, mutants selected by ceftriaxone (CRO) and fosfomycin (FOF) exhibit particularly widespread collateral sensitivity. Cross resistance is similarly prevalent, with only 2 strains failing to exhibit cross resistance to at least one drug. Somewhat surprisingly, 56 of 60 mutants exhibit cross resistance to at least one drug from a different class (e.g. all mutants evolved to ciprofloxacin (CIP), a DNA synthesis inhibitor, show increased resistance CRO, an inhibitor of cell wall synthesis). The collateral effects can also

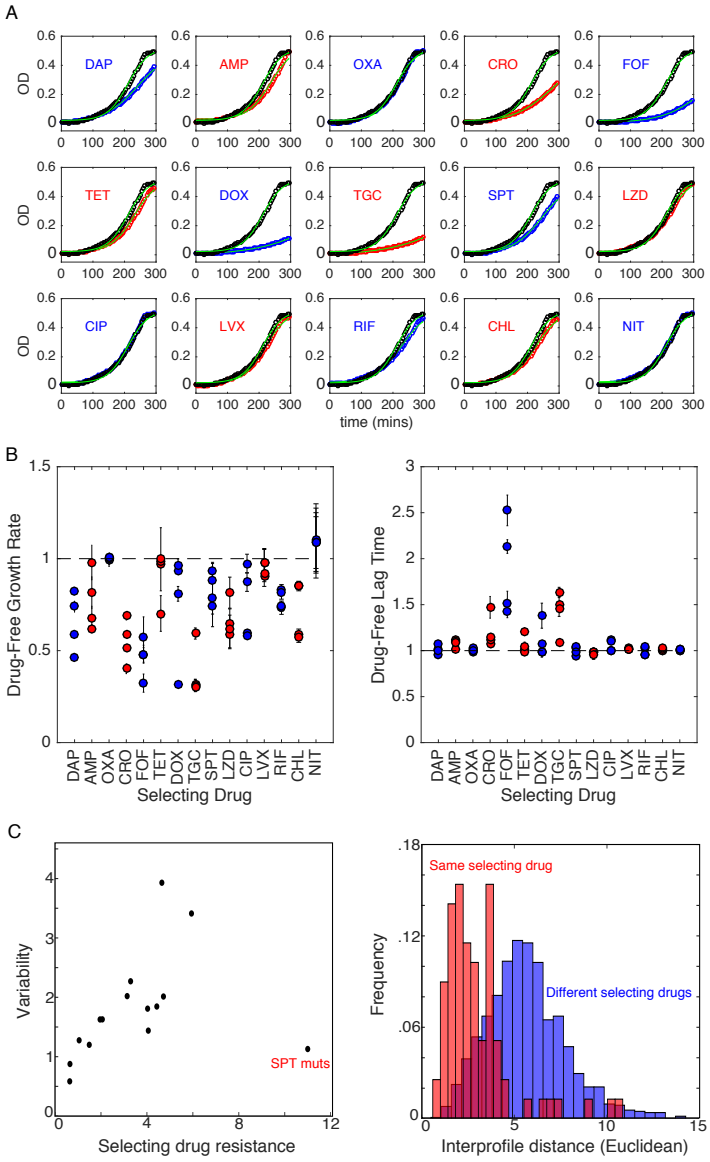

Figure 2.2: **Growth costs and lag times for isolates selected by different antibiotics** A. Example optical density (OD) time series for single isolates selected by each of the 15 drugs. Blue or red circles correspond to the isolate, black circles to ancestral strains. Light green lines show fits to logistic growth function [60] given by $g(t) = g_0 + K\left(1 + \exp(4\mu(\lambda - t)/K + 2)\right)^{-1}$, where μ is the maximum specific growth rate, λ is the lag time, and K is the carrying capacity. To reduce the number of free parameters, we fix $K = 0.5$ to match that of the ancestral strain. B. Maximum specific growth rate (μ, left) and lag time (λ, right) in drug-free media for isolates from each of the four populations selected by each drug. All values are normalized by the values measured in the ancestral strain. Errorbars are standard errors of the mean estimated from 3 technical replicates for each isolate (cont'd on next page).

Figure 2.2: C. Left panel: variability in replicates for all 15 drugs vs the (log2-scaled) fold increase in IC_{50} to the selecting drug (Spearman correlation of 0.58, $p = 0.03$ including the SPT mutants; 0.82 $p < 10^{-3}$, without the SPT mutants.). Variability is defined as $V \equiv \sum_{i=1}^{m} d_i/m$, where $m = 4$ is the number of replicates and d_i is the Euclidean distance between mutant i and the centroid formed by all vectors corresponding to a given selecting drug (Figure 2.8). Right panel: histogram of Euclidean distances between collateral profiles in pairs of isolates selected by the same (red) or different (blue) drugs. To emphasize collateral, rather than direct, effects, the component(s) of each collateral profile corresponding to the selecting drug(s) were removed prior to calculating variability (panel C) and pairwise Euclidean distances (D).

be quite large; we measured 8 instances of collateral sensitivity where the IC_{50} decreases by 16 fold or more. We observe a strong, repeatable collateral sensitivity to rifampicin (RIF) when mutants were selected by inhibitors of cell wall synthesis, an effect that–to our knowledge–has not been reported elsewhere. More typically, however, collateral effects are smaller than the direct effects to the selecting drug, with 46 percent (384/840) exhibiting more than a factor 2 change in IC_{50} and only 7 percent (61/840) exhibiting more than a factor 4 change.

2.2.2 Isolates exhibit variability in fitness costs and collateral profiles

To investigate the potential impact of resistance selection on fitness, we estimated the specific growth rate and the lag time in drug-free media for isolates selected from each of the 60 populations (4 populations per selecting drug). Our measured growth costs, or the difference between drug-free growth of the wild-type and mutant, exhibit significant variability, even across different populations selected by the same drug (Figure 2.2, similar to results in other species [49]. In some isolates–such as those selected by oxacillin (OXA) or nitrofurantoin (NIT)–growth rate and lag times are indistinguishable from those of the ancestral strains. On the other hand, isolates selected by CRO and FOF–selecting conditions that frequently result in collateral sensitivity–show dramatically reduced growth and an increased lag time, suggesting

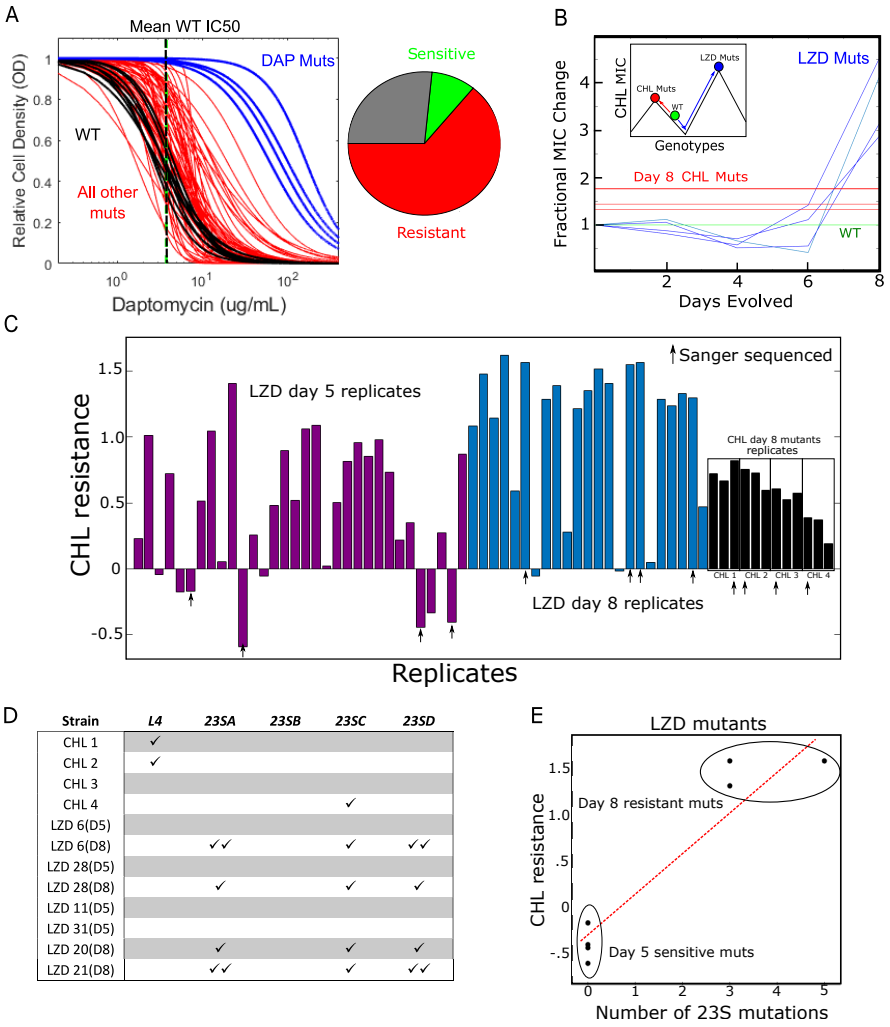

Figure 2.3: **Collateral effects can lead to frequent or high-level resistance to non-selecting drugs.** A. Estimated dose response curves (fit to Hill-like function) for all mutants tested against daptomycin. Strains evolved to daptomycin (blue) and all other drugs (red) frequently exhibit increased resistance to daptomycin relative to wild-type (black, individual replicates; dotted black line, mean IC_{50}). Right inset: Approximately 64 percent of all drug-evolved mutants exhibit increased daptomycin resistance, while only 11 percent exhibit collateral sensitivity. B. Fractional change in chloramphenicol (CHL) IC_{50} for mutants evolved to linezolid (blue). The width of the green line represents the confidence interval ($\pm$ 3 standard errors of the mean measured over 8 replicate measurements) for the (normalized) choramphenicol IC_{50} in wild-type cells. For comparison, the red lines represent the final (day 8) CHL resistance achieved in populations evolved directly to CHL. Inset: Schematic depicting two hypothetical paths to different CHL resistance maximums.

Figure 2.3: The green circle represents the sensitive wild-type. Evolution can occur to CHL directly (red line) or to CHL collaterally through LZD resistance (blue line). The LZD evolution depicts early collateral sensitivity before ultimately achieving a higher total resistance. C. CHL resistance ($\log_2$-scaled change in IC_{50} relative to ancestor) for LZD-selected isolates at day 5 (purple) and day 8 (blue), and for individual colony isolates (4) for each of the four CHL-selected populations (black). Arrows indicate 12 isolates chosen for Sanger sequencing. D. Mutations observed in four different genes associated with LZD-resistance in each of the 12 selected isolates from panel C. E. CHL resistance and number of 23S mutations in LZD isolates on days 5 and 8.

that the selected resistance determinants are associated with strong pleiotropic effects even in drug-free media.

Our results indicate that collateral profiles can vary significantly even when mutants are evolved in parallel to the same drug (Figure 2.1C). For example, all 4 mutants selected by daptomycin (DAP) exhibit high-level resistance to the selecting drug, but replicates 1 and 4 exhibit collateral resistance to CRO, while replicate 2 exhibits collateral sensitivity and replicate 3 shows little effect (Figure 2.1C, right panel). To quantify the variation between replicates selected by the same drug, we considered the collateral profile of each mutant (i.e. a column of the collateral sensitivity matrix) as a vector in 15-dimensional drug resistance space. Then, for each set of replicates, we defined the variability $V \equiv \sum_{i=1}^{m} d_i/m$, where $m = 4$ is the number of replicates and d_i is the Euclidean distance between mutant i and the centroid formed by all vectors corresponding to a given selecting drug (Figure 2.8). Variability differs for different selecting drugs, with DAP and RIF showing the largest variability and NIT the smallest (Figure 2.8). We find that the variability is significantly correlated with average resistance to the selecting drug, even when one removes contributions to variability from the selecting drug itself (Figure 2.2C, left), indicating that collateral (rather than direct) effects underlie the correlation. Such a correlation might be expected if, for example, resistance arises from an accumulation of stochastic events

following a Poisson-like distribution, where the mean is proportional to the variance. We do note, however, that selection by spectinomcyin (SPT) represents a notable exception to this trend. These results suggest that the repeatability of collateral effects is sensitive to the drug used for selection. As a result, certain drugs may be more appropriate for establishing robust antibiotic cycling profiles.

To further quantify the variability within and between isolates selected by different drug, we calculated the pairwise Euclidian distance between collateral profiles of isolates selected in the same drug and pairs of isolates selected in different drugs (Figure 2.2C, right). We see the distributions do have some overlap; that is, pairs of isolates selected by the same drug are sometimes more distinct from one another, by this metric, than pairs selected by different drugs. However, the distribution for different selecting drugs (blue) is shifted significantly to the right, indicating that isolates selected by the same drug are more similar to one another (on average) than to isolates selected by different drugs.

2.2.3 Cross resistance to daptomycin appears frequently under selection by different drugs

Daptomycin is a lipopeptide antibiotic sometimes used as a last line of defense against gram-positive bacterial infections, including vancomycin resistant enterococci (VRE). While DAP resistance was initially believed to be rare [61], it has become increasingly documented in clinical settings [62]. Recent work in a related enterococcal species has shown that cross resistance to DAP can arise from serial exposure to chlorhexidine, a common antiseptic [63], but less is known about DAP cross resistance following exposure to other antimicrobial agents. Surprisingly, our results indicate that DAP resistance is common when populations are selected by other antibiotics, with 64 percent of all evolved lineages displaying DAP cross resistance and only 11 percent displaying collateral sensitivity (Figure 2.3A).

2.2.4 Selection by LZD leads to higher CHL resistance than direct selection by CHL

Surprisingly, we found that isolates selected by linezolid (LZD) developed higher resistance to chloramphenicol (CHL) than isolates selected directly by CHL (Figure 2.3B). The isolates from LZD and from CHL exhibit similar growth and lag-time distributions in drug-free media (Figure 2.2), suggesting that this effect is not driven by fitness costs alone. To investigate further, we isolated LZD-selected mutants at days 2, 4, 6 and 8 of the laboratory evolution and measured the resistance of each to CHL. We find that early-stage (days 4-6) mutants exhibit low level CHL sensitivity just prior to a dramatic increase in cross resistance around day 8. These findings suggest LZD selection drives the population across a CHL fitness valley, ultimately leading to levels of resistance that exceed those observed by direct CHL selection (Figure 2.3B, inset).

To further investigate the repeatability of this phenomenon, we exposed 32 additional populations to increasing LZD concentrations in parallel over 8 days. Using the four initial LZD mutants as a guide, we measured the CHL susceptibility of isolates from each population at day 5 (Figure 2.3C, purple) and day 8 (Figure 2.3C, blue). In addition, to account for potential heterogeneity in the original populations, we measured CHL susceptibility in three different (single colony) isolates from each of the original four populations selected in CHL (Figure 2.3C, black). Nine of the populations became contaminated between days 5 and 8, and were thus excluded from the day 8 analysis. On day 5, almost a third (10 of 32) of the LZD-selected strains exhibited CHL resistance greater than that of any day 8 CHL-selected strains, while 25 percent (8 of 32) were more CHL-sensitive than even the ancestral strains. By contrast, on day 8 the vast majority of isolates (17 of 23) were highly CHL-resistant, with only a few strains (2 of 23) exhibiting small levels collateral sensitivity.

To identify genes that may be responsible for collateral CHL resistance, we PCR-

amplified and (Sanger) sequenced seven genes (*rpsJ, L3, L4*, which are genes for ribosomal proteins, and four genes for 23S rRNA, *23SA, 23SB, 23SC, 23SD*) previously associated with LZD resistance [64] in a subset of 12 isolates. We selected the most CHL-resistant isolate from each CHL population, two pairs of day 5/day 8 LZD-selected isolates that exhibited collateral sensitivity on day 5 and cross resistance on day 8, two LZD-selected isolates with high-level collateral sensitivity to CHL on day 5, and two LZD isolates with large cross resistance on day 8 (Figure 2.3C; specific isolates marked by black arrows). We did not observe mutations in *rpsJ, L3* or *23SB* in any strain. In addition, the four LZD-selected isolates showed no mutations in any of the sequenced genes on day 5 (Figure 2.3D). By contrast, all 4 of the LZD-selected strains contained at least 3 mutations in the 23S rRNA genes on day 8. Two of the CHL-selected isolates had mutations in *L4* and one had a single mutation in the 23SC gene.

We observe a strong correlation between the level of CHL resistance and the total number of 23S rRNA mutations, similar to the dosing behavior previously observed for LZD [64]. This correlation suggests that the 23S mutations found in LZD-selected (and CHL-resistant) isolates from day 8–but missing in the CHL-sensitive isolates from day 5– may be responsible for the later-stage, high-level cross resistance to CHL. Elucidating the precise evolutionary dynamics underlying differential selection for these mutations in LZD and CHL remains an open question, though the early (day 5) CHL-sensitivity observed in LZD-selected isolates suggests it may be necessary to cross a fitness valley in CHL resistance in order to eventually achieve higher CHL resistance.

Table 2.1: **Mutations identified in selected populations.** Check marks indicate the same mutation was also identified in clonal isolates from the same population.

Strain	Gene	Pop (%)	Clonal	Description
Dap1	*rpsJ*	100.0	✓	30S ribosomal protein S10
	Intergenic *EF_0871 / EF_0872*	41.1		
	comG1	100.0		
	EF_3010	100.0		
Amp4	*pyrR*	43.0		
	hexA	31.7		
	Intergenic *EF_3191 / EF_3192*	100.0	✓	
	EF_3290	93.0	✓	Sensor histidine kinase
Ox1	*EF_1820*	40.0		
	EF_3290	40.0		Sensor histidine kinase
Dox4	*rpsJ*	87.0	✓	30S ribosomal protein S10
	rpsJ	100.0	✓	30S ribosomal protein S10
	prgB	100.0	✓	
Spt4	*rpsE*	100.0	✓	40S ribosomal protein S5
Lzd2	*EF_0149*	100	✓	
	23S ribosomal RNA	66.2	✓	23S ribosomal RNA
Cip1	Intergenic *EF_0115 / EF_0116*	30.5		
	Intergenic *EF_1077 / EF_1078*	100.0	✓	
	parC	100.0	✓	topoisomerase IV
	EF_2485	40.9		
	nusG	45.6		
	EF_2981	44.3		
Lvx3	*gyrA*	100	✓	DNA gyrase
	gyrA	100	✓	DNA gyrase
	parC	100	✓	topoisomerase IV
	EF_1692	100	✓	

2.2.5 Whole-genome sequencing reveals known resistance determinants and mutations in genes previously linked with collateral sensitivity

To investigate the genetic changes in drug-selected populations, we sequenced population samples from one evolved population per drug. In addition, we isolated and sequenced a single clone from each population. As controls, we sequenced two different isolates from the ancestral V583 stock as well as both single isolates and a population sample propagated in drug-free media. We then used breseq [65], an established computational pipeline capable of mutant identification in both clonal and population samples (Methods). To minimize potential artifacts from sample preparation or analysis, we excluded from further analysis four populations where variants identified by clonal and population samples did not overlap. In addition, we limit our focus to those mutations estimated to occur with frequency greater than 30 percent in the population samples.

This analysis revealed a total of 29 mutations in the 11 populations (Table 2.1; note that the population selected in NIT contained no identifiable mutations). The control strain propagated in BHI contained no mutations relative to the ancestral strains. For 9 of the 11 selecting drugs, we identified mutations that likely confer resistance to the selecting drug. For example, we observed mutations in drug targets associated with protein synthesis inhibitors (*rpsJ [66], rpsE [67]*), fluoroquinolones (*parC, gyrA* [68]), and RNA synthesis inhibitors (*rpoB* [68]). We also identified mutations in a sensor histidine kinases [69, 70] (EF_3290) in populations selected by cell-wall inhibitors and mutations in 23S rRNA genes in the LZD-selected population [64, 71]. Surprisingly, the DAP-selected population did not contain mutations in genes previously identified with DAP resistance [57, 58], though we observe a mutation in *rpsJ* in both the clonal and population sequences. While previous experiments have shown rpsJ not to confer DAP resistance in one genetic background of *E. faecalis* strain S613 [66], it may underlie the observed cross resistance to other antibiotics. Finally, we observe

no mutations in either the clonal or population sequencing for the Nit1 population, despite repeated experiments confirming increased resistance to NIT. Because the resistance is relatively low-level (IC_{50} increases by approximately 50 percent relative to ancestor), it is possible the observed resistance corresponds to transient phenotypic resistance, similar to the post-antibiotic effect or the cellular hysteresis observed when drugs are rapidly cycled [46]. Finally, the TGC-selected population contains a mutation in EF_0926, the response regulator in a two-component signaling system (TCS) with the sensor kinase EF_0927. While this specific system has not been implicated in tigecycline (TGC) resistance, similar TCS have been linked to TGC resistance in *A. baumannii* [72].

Several of the mutations we identified occur in genes previously linked with collateral effects in other species. For example, mutations in the topisomerase gene *gyrA* have been posited to induce collateral sensitivities via global transcriptional changes induced by modulated DNA supercoiling [35, 73, 74]. Similarly, mutations in ribosomal genes, such as *rpsE*, have been linked with multi-drug resistance modulated by large-scale changes in the transcriptome [75].

2.2.6 Sensitivity profiles cluster into groups based on known classes of selecting drug

Our results indicate that there is significant heterogeneity in collateral sensitivity profiles, even when parallel populations are selected with the same antibiotic. While the genetic networks underlying these phenotypic responses are complex and, in many cases, poorly understood, one might expect that selection by chemically or mechanistically similar drugs would lead to profiles with shared statistical properties. For example, previous work showed (in a different context) that pairwise interactions between simultaneously applied antibiotics can be used to cluster drugs into groups that interact monochromatically with one another; these groups correspond to known

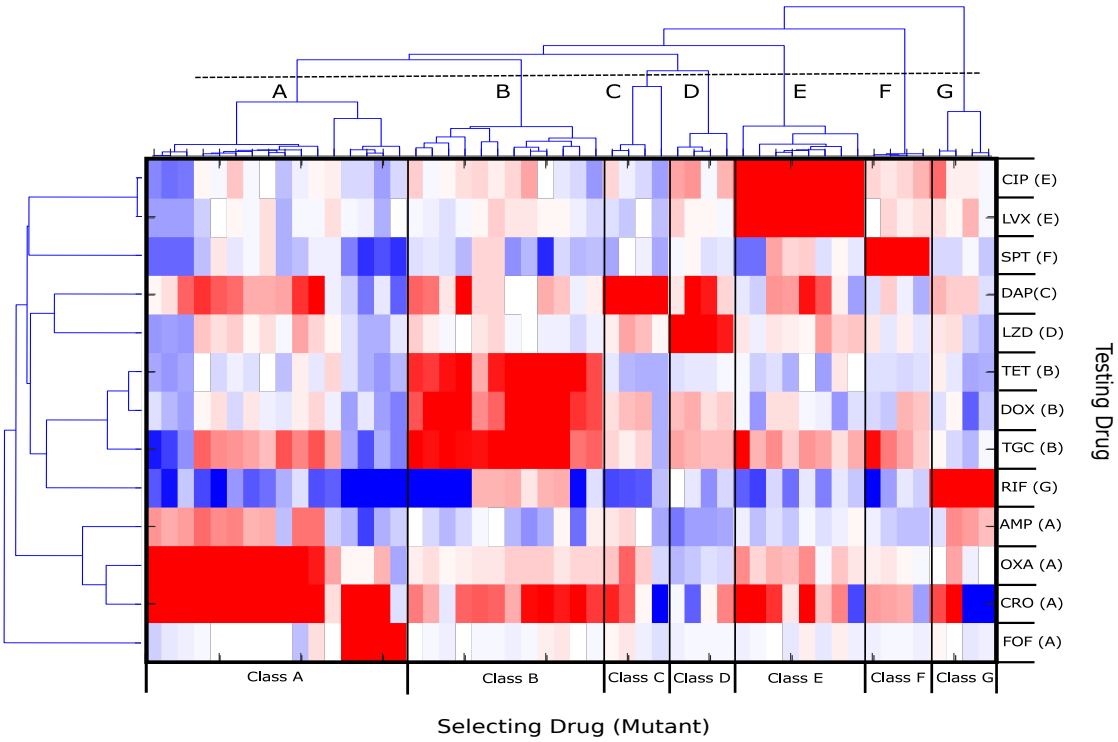

Figure 2.4: **Hierarchical clustering of collateral sensitivity profiles partitions mutants into groups selected by known drug classes.** Heatmap with ordering of rows (testing drug) and columns (4 replicate experiments with the same selecting drug) determined via hierarchical clustering. Colormap and scale are identical to those used in Figure 1. Collateral profiles (columns) for mutants selected by drugs from known drug classes (here labeled A-G) cluster together; if clusters are defined using the dashed line (top), there are 7 distinct clusters, each corresponding to a particular drug class: A. Cell-wall synthesis inhibitors (AMP, OXA, CRO, FOF), B. Tetracyclines (TET, DOX, TGC), C. Lipopeptides (DAP), D. Oxazolidinones (LZD), E. Fluoroquinolones (CIP, LVX), F. Aminocyclitols (SPT), and G. Antimycobacterials (RIF). When clustering the testing drugs (rows), drugs from the same class are frequently but not always clustered together. For example, cell-wall drugs such as AMP, OXA, and CRO form a distinct cluster that does not include FOF (bottom 4 rows).

drug classes [76], highlighting statistical structure in drug interaction networks that appear, on the surface, to be extremely heterogeneous. Recent work in bacteria has also shown that phenotypic profiles of mutants selected by drugs from the same class tend to cluster together in *P. aeruginosa* [38] and *E. coli* [77].

Similarly, we asked whether collateral sensitivity profiles in *E. faeaclis* can be used to cluster resistant mutants into statistically similar classes. We first performed hierarchical clustering (Methods) on collateral profiles of 52 different mutants (Figure 2.4, x-axis; note that we excluded mutants selected by CHL and NIT, which did not achieve resistance of at least 2x to the selecting drug). Despite the heterogeneity in collateral profiles, they cluster into groups characterized–exclusively–by selecting drugs from the same drug classes before grouping mutants from any two different drug classes. For example, inhibitors of cell wall synthesis (AMP, CRO, FOF, OXA) cluster into one group (noted by A in Figure 3), while tetracycline-like drugs (TET, DOX, TGC) cluster into another (noted by B). This approach also separates spectinomycin (SPT, aminoglycoside antibiotic class) from the tetracycline class of antibiotics (TET, DOX, TGC) despite the fact that they both target the 30S subunit of the ribosome, suggesting that it may help identify drugs with similar mechanisms but statistically distinct collateral profiles.

We then performed a similar clustering analysis of the collateral responses across the 14 different testing drugs (Figure 2.4, y-axis), which again leads to groupings the correspond to known drug classes. One drug, FOF, provides an interesting exception. Mutants selected for FOF resistance cluster with those of other cell-wall synthesis inhibitors (Class A, columns). However, the behavior of FOF as a testing drug (last row) is noticeably distinct from that of other cell-wall synthesis inhibitors (the 3 rows directly above FOF). Taken together, the clustering analysis reveals clear statistical patterns that connect known mechanisms of antibiotics to their behavior as both selecting and testing agents.

2.2.7 A Markov decision process (MDP) model predicts optimal drug policies to constrain resistance

Our results indicate that collateral sensitivity is pervasive, and while collateral sensitivity profiles are highly heterogeneous, clustering suggests the existence of statistical structure in the data. Nevertheless, because of the stochastic nature of the sensitivity profiles, it is not clear whether this information can be leveraged to design drug sequences that constrain evolution. It is important to note that our goal, at this stage, is not to design specific drug sequences that might be transferred directly to the clinic, but instead to evaluate–in a simple setting–the feasibility of slowing resistance in even the most optimized cases. Given that resistance to the selecting drugs is often larger in magnitude than collateral (off-diagonal) effects, it is not clear a priori that a feasible strategy exists that prevents the inevitable march to high-level resistance, even in a highly idealized setting.

To address this problem, we develop a simple mathematical model based on a Markov decision process (MDP) to predict optimal drug policies. MDP's are widely used in applied mathematics and finance and have a well-developed theoretical basis [78, 79, 80]. In a MDP, a system transitions stochastically between discrete states. At each time step, we must make a decision (called an "action"), and for each state-action combination there is an associated instantaneous "reward" (or cost). The action influences not only the instantaneous reward, but also which state will occur next. The goal of the MDP is to develop a policy–a set of actions corresponding to each state–that will optimize some objective function (e.g. maximize some cumulative reward) over a given time period.

For our system, the state s_t at time step $t = 0, 1, 2, ...$ is defined by the resistance profile of the population, a vector that describes the resistance level to each available drug. At each time step, an action a_t is chosen that determines the drug to be applied. The system–which is assumed to be Markovian–then transitions with probability

$P_a(s_{t+1}|s_t, a_t)$ to a new state s_{t_i+1}, and the transition probabilities are estimated from evolutionary experiments (or any available data). The instantaneous reward function $R_a(s)$ is chosen to be the (negative of the) resistance to the currently applied drug; intuitively, it provides a measure of how well the current drug inhibits the current population. The optimal policy $\pi^*(s)$ is formally a mapping from each state to the optimal action; intuitively, it tells which drug should be applied for a given resistance profile. The policy is chosen to maximize a cumulative reward function $R_c \equiv \langle \sum_{t=0}^{\infty} \gamma^t R_\pi(s_t) \rangle$, where brackets indicate an expectation value conditioned on the initial state s_0 and the choice of policy π. The parameter γ ($0 \leq \gamma < 1$) is a discount factor that determines the timescale for the optimization; $\gamma \approx 1$ leads to a solution that performs optimally on long timescales, while $\gamma \approx 0$ leads to solutions that maximize near-term success.

To apply the MDP framework to collateral sensitivity profiles, we must infer from our data a set of (stochastic) rules for transitioning between states (i.e. we must estimate $P_a(s_{t+1}|s_t, a_t)$). While many choices are possible–and different rules may be useful to describing different evolutionary scenarios–here we consider a simple model where the resistance to each drug is increased/decreased additively according to the collateral effects measured for the selecting drug in question. Specifically, the state s_{t+1} following application of a drug at time t is given by $s_t + \bar{C}$, where $\bar{C}$ is one of the four collateral profiles (see Figure 2.1) measured following selection by that drug. Because resistance/sensitivity is measured using log-scaled ratios of IC_{50}'s, these additive changes in the resistance profile correspond to multiplicative changes in the relative IC_{50} for each drug. For instance, if one selection step increases the IC_{50} by a factor of 3, then two consecutive selection steps would increase IC_{50} by a factor of 9. This model assumes that selection by a given drug always produces changes in the resistance profile with the same statistical properties. For example, selection by DAP increases the resistance to DAP (with probability 1) while simultaneously

either increasing resistance to AMP (with probability 1/4), decreasing resistance to AMP (with probability 1/4), or leaving resistance to AMP unchanged (probability 1/2). Repeated application of the same drug will steadily increase the population's resistance to that drug, but the process could potentially sensitize the population to other drugs. This model implicitly assumes sufficiently strong selection that, at each step, the state of the system is fully described by a single "effective" resistance profile (rather than, for example, an ensemble of profiles that would be required to model clonal interference). While we focus here on this particular model, we stress that this MDP framework can be easily adopted to other scenarios by modifying $P_a(s_{t+1}|s_t, a_t)$.

For numerical efficiency, we discretized both the state space (i.e. the resistance to each drug is restricted to a finite number of levels) as well as the measured collateral profiles (exposure to a drug leads to an increase/decrease of 0, 1, or 2 resistance levels; Figure 2.5A, Figure 2.9). In practice, this means that resistance will eventually saturate at a finite value if a single drug is applied repeatedly. In addition, we restrict our calculations to a representative subset of six drugs (DAP, AMP, FOF, TGC, LZD, RIF). The set includes inhibitors of cell wall, protein, or RNA synthesis, and five of the six drugs (excluding RIF) are clinically relevant for enterococcus infections. We note, however, that the results are qualitatively similar for different discretization schemes (Figure 2.10) and for different drug choices (Figures 2.11-2.13).

2.2.8 Drug policies can be tuned to minimize resistance on different timescales

The optimal policy $\pi^*(s)$ is a high-dimensional mapping that is difficult to directly visualize. For intuition on the policy, we calculated the frequency with which each drug is prescribed as a function of resistance to each of the six individual drugs (Figures 2.14, 2.15; top panels). Not surprisingly, we found that when resistance to a particular drug is very low, that drug is often chosen as optimal. In addition,

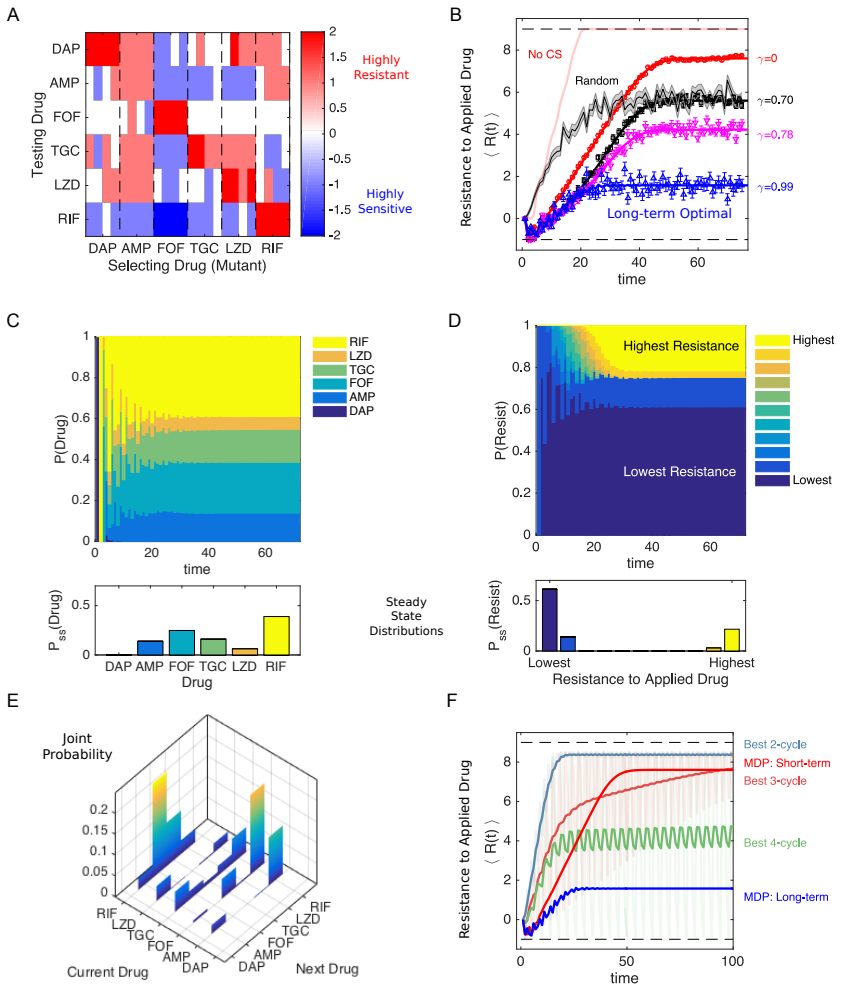

Figure 2.5: **Simulated optimal drug sequences constrain resistance on long timescales and outperform simple collateral sensitivity cycles** A. Discretized collateral sensitivity or resistance $C_d \in \{-2, -1, 0, 1, 2\}$ for a selection of six drugs. For each selecting drug, the heat map shows the level of cross resistance or sensitivity (C_d) to each testing drug (the subscript d indicates the profiles are discretized) for $n_r = 4$ independently evolved populations. See Figure 2.1 for original (non-discretized) data. B. Average level of resistance ($\langle R(t) \rangle$) to the applied drug for policies with $\gamma = 0$ (red),$\gamma = 0.7$ (black),$\gamma = 0.78$ (magenta), and $\gamma = 0.99$ (blue). Resistance to each drug is characterized by 11 discrete levels arbitrary labeled with integer values from -1 (least resistant) to 9 (most resistant). At time 0, the population starts in the second lowest resistance level (0) for all drugs. Symbols (circles, triangles, squares) are the mean of 10^3 independent simulations of the MDP, with error bars ± SEM. Solid lines are numerical calculations using exact Markov chain calculations (see Methods).

Figure 2.5: Light red line, long-term optimal policy ($\gamma = 0.99$) calculated using the data in A but with collateral sensitivity values set to 0. Black shaded line, randomly cycled drugs ($\pm$ SEM). C. The time-dependent probability P(Drug) of choosing each of the six drugs when the optimal policy ($\gamma = 0.99$) is used. Inset, steady state distribution P$_s s$(Drug). D. The probability P(Resist) of the population exhibiting a particular level of resistance to the applied drug when the optimal policy ($\gamma = 0.99$) is used. Inset, steady state distribution P$_s s$(Drug). E. Steady state joint probability distribution P(current drug, next drug) for consecutive time steps when the optimal policy ($\gamma = 0.99$) is used. F. Average level of resistance ($\langle R(t) \rangle$) to the applied drug for collateral sensitivity cycles of 2 (dark green, LZD-RIF), 3 (pink, AMP-RIF-LZD), or 4 (dark green, AMP-RIF-TGC-LZD) drugs are compared with MDP policies with $\gamma = 0$ (short-term, red) and $\gamma = 0.99$ (long-term, blue). For visualizing the results of the collateral sensitivity cycles, which give rise to periodic behavior with large amplitude, the curves show a moving time average (window size 10 steps), but the original curves are shown transparently in the background.

the specific frequency distributions vary significantly depending on γ, which sets the timescale of the optimization. For example, the long-term optimal policy ($\gamma = 0.99$) yields a frequency distribution that is approximately independent of the level of resistance to FOF (Figure 2.14, upper right panel). By contrast, the frequency distribution for a short-term policy ($\gamma = 0.1$) changes with FOF resistance; at low levels of resistance, FOF is frequently applied as the optimal drug, but it is essentially never applied once FOF resistance reaches a certain threshold (Figure 2.15, upper right panel). Both the short- and long-term optimal policies lead to aperiodic drug sequences, but the resulting resistance levels vary significantly (Figures 2.14, 2.15, bottom panels). These differences reflect a key distinction in the policies: short-term policies depend sensitively on the current resistance level and maximize efficacy (minimize resistance) at early times, while long-term policies may tolerate short-term performance failure in exchange for success on longer timescales.

2.2.9 Optimal policies outperform random cycling and rely on collateral sensitivity

To compare the outcomes of different policies, we simulated the MDP and calculated the expected resistance level to the applied drug over time, $\langle R(t) \rangle$, from 1000 independent realizations (Figure 2.5B). All MDP policies perform significantly better than random drug cycling for the first 10-20 time steps and even lead to an initial decrease in resistance. The long-term policy ($\gamma = 0.99$, blue) is able to maintain low-level resistance indefinitely, while the short-term policy ($\gamma = 0$) eventually gives rise to high-level (almost saturating) resistance. Notably, if we repeat this calculation on an identical data set but with all collateral sensitivities set to 0, the level of resistance rapidly increases to its saturating value (Figure 2.5B, light red line), indicating that collateral sensitivity is critical to the success of these policies. We note that the timescales used here are not necessarily reflective of a clinical situation, and instead our goal is to understand the performance of the optimization over a wide range of timescales.

2.2.10 Optimal policies highlight new strategy for minimizing resistance

To understand the optimal policy dynamics, we calculated the time-dependent probability distributions P(Drug)–the probability of applying a particular drug–and P(Resist)–the probability of observing a given level of resistance to the applied drug–for the MDP following the long-term policy ($\gamma = 0.99$, Figure 2.5C-D). We also calculated the (steady state) joint probability distribution characterizing the prescribed drugs at consecutive time steps (Figure 2.5E). The distributions reveal highly non-uniform behavior; after an initial transient period, RIF is applied most often, followed by FOF, while DAP is essentially never prescribed. Certain patterns also emerge between consecutively applied drugs; for example, FOF is frequently followed by RIF. Somewhat surprisingly, the distribution of resistance levels is highly bimodal,

with the lowest possible resistance level occurring most often, followed by the highest possible level, then the second lowest level, and then the second highest level (Figure 2.5D). The policy achieves a low average level of resistance not by consistently maintaining some intermediate level of resistance to the applied drug, but instead by switching between highly-effective drugs and highly-ineffective drugs, with the latter occurring much less frequently. In words, rare periods of high resistance are the price of frequent periods of very low resistance. These qualitative trends occur for other drug choices (Figures 2.11-2.13) and are relatively insensitive to the number of discretization levels chosen (Figure 2.10). The results suggest a new conceptual strategy for minimizing resistance: interspersing frequent steps of instantly effective drugs (low resistance)–which provide short-term inhibition of pathogen growth–with rare steps of relatively ineffective drugs (high resistance), which provide little short-term inhibition but shepherd the population to a more vulnerable future state.

2.2.11 Optimal policies maintain lower long-term resistance than collateral sensitivity cycles

The resurgent interest in collateral sensitivity was sparked, in part, by innovative recent work that demonstrated the successful application of collateral sensitivity cycles, where each drug in a sequence promotes evolved sensitivity to the next drug [41]. To compare the performance of the MDP to that expected from collateral sensitivity cycles, we identified all collateral sensitivity cycles for the six drug network and calculated $\langle R(t) \rangle$ for 100 time steps of each cycle. We then determined the "best" cycle of a given length–defined as the cycle with the lowest mean value of $\langle R(t) \rangle$ over the last ten time steps–and compared the performance of those cycles to the short- and long-term MDP policies (Figure 2.5F). The MDP long-term optimal solution ($\gamma = 0.99$) maintains resistance at a lower average value than for all of the collateral sensitivity cycles. For MDP policies with shorter time horizons (e.g. the instant gratification

cycle, $\gamma = 0$), however, the collateral sensitivity cycles of 3 and 4 drugs (as well as the long-term MDP solution) lead to lower resistance at intermediate or longer time scales, reflecting the inherent trade-offs between instantaneous drug efficacy and long-term sustainability. One advantage of the MDP optimization is that it allows for explicit tuning of the policy (via γ) to achieve maximal efficacy over the desired time horizon.

2.2.12 Optimized drug sequences improve growth inhibition and reduce adaptation rates in lab evolution experiments

The MDP-based optimal policies perform well in stochastic simulations and highlight new strategies for potentially slowing resistance. However, the model contains a number of assumptions that lead to an oversimplified picture of the true evolutionary dynamics. As a result, it is not clear whether optimized drug sequences from this model will be effective in real, evolving pathogen populations.

To test the performance of MDP-based drug cycles, we designed a lab evolution experiment comparing inhibitory effects of different drug cycling protocols over 20 days. For experimental feasibility, we restrict our focus to a subset of four drugs (FOF, RIF, AMP, TGC) and reduced the length of each evolutionary time step from 8 days–as in the original collateral sensitivity experiment (Figure 2.1)– to 2 days. First, we experimentally measured the collateral sensitivity matrix for the four drug set following 2 days of lab evolution in eight replicate populations per drug (Figure 2.6A). We then calculated the optimal policy for two different values of γ ($\gamma = 0.9$, $\gamma = 0.78$), both corresponding to timescales commensurate with the planned experiment. In both cases, the steady state distribution of drug application P(Drug) calls for frequent use of TGC and relatively rare use of FOF, though the specific distribution depends on the particular choice of γ (Figure 2.6B, top panel; see also Figure 2.16).

An exact application of the optimal policy requires measuring the full sensitiv-

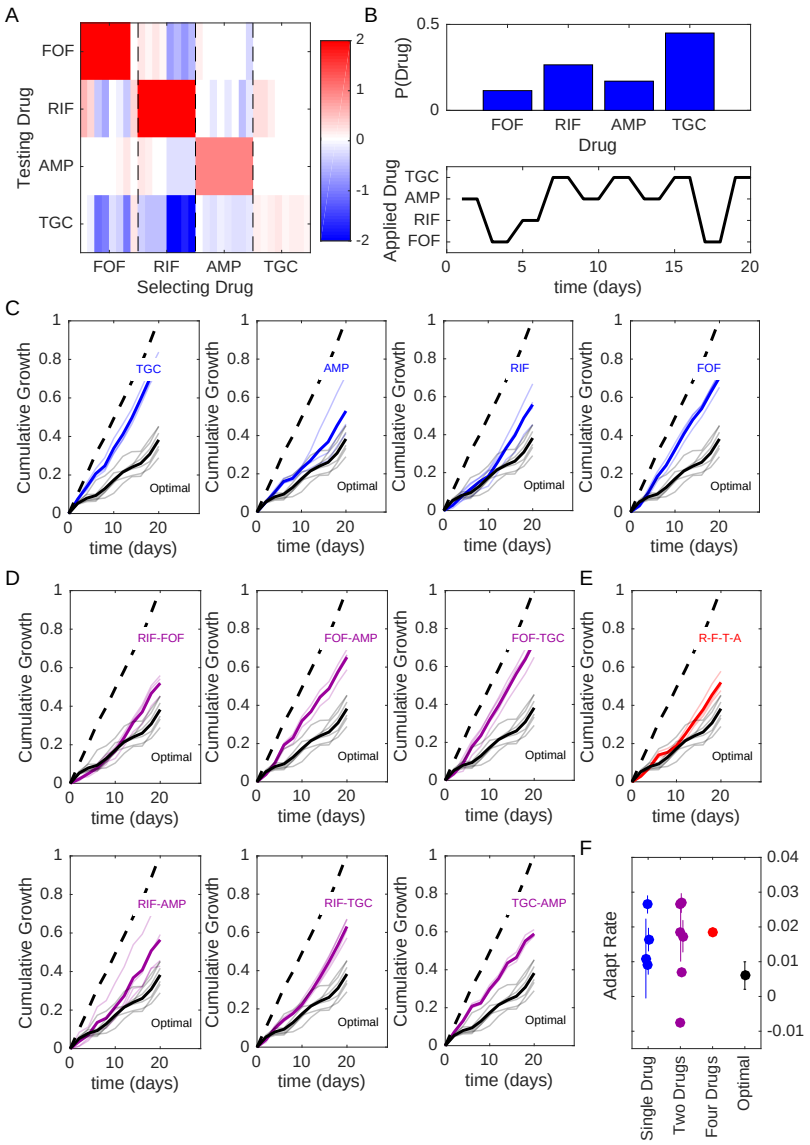

Figure 2.6: **Optimized drug sequences reduce cumulative growth and adaptation rates in lab evolution experiments.** A. Resistance (red) or sensitivity (blue) of each evolved mutant (horizontal axis; 4 drugs x 8 mutant per drug) to each drug (vertical axis) following 2 days of selection is quantified by the $\log_2$-transformed relative increase in the IC_{50} of the testing drug relative to that of wild-type (V583) cells. B. Top: distribution of applied drug at time step 20 (approximate steady state) calculated using an optimal policy with $\gamma = 0.9$. Bottom: sequence of applied drug from one particular realization of the stochastic process with the optimal policy ($\gamma = 0.9$). C-E. Cumulative population growth over time for populations exposed to single drug sequences (C, blue), two-drug sequences (D,magenta), a four drug sequence (E, red), or the optimal sequence from panel B (black curves, all panels).

Figure 2.6: Transparent lines represent individual replicate experiments and each thicker dark line corresponds to a mean over replicates. Dashed line, drug-free control (normalized to a growth of 1 at the end of the experiment). F. Adaptation rate for single drug (blue), two-drug (magenta), four drug (red), and optimal sequences (black). Error bars are standard errors across replicates. Adaptation rate is defined as the slope of the best fit linear regression describing time series of daily growth (see Figure 2.20).

ity profile at each step and using that profile, in accordance with the policy, to choose the next drug in the sequence. However, simulations suggest that choosing a pre-determined drug cycle–that is, a cycle drawn from a particular realization of the stochastic process–is expected to perform near-optimally on the timescale of the experiment (Figures 2.17, 2.18). For experimental convenience, we choose a single MDP-derived cycle for each value of γ. For example, for $\gamma = 0.9$ the sequence involves ten 2-day time steps, with drugs applied in the following order: AMP-FOF-RIF-TGC-AMP-TGC-AMP-TGC-FOF-TGC (Figure 2.6B, bottom; see Figure 2.16 for $\gamma = 0.78$ example). To evaluate the efficacy of the MDP-derived cycle, we exposed a total of 60 replicate populations to one of 13 different drug cycle protocols (including the two MDP-derived cycles) over a 20-day serial passage lab evolution experiment. Every 40 hours, we measured the optical density of each population and then diluted each into fresh media containing the prescribed drug (added after a brief drug-free outgrowth phase, see Methods). Drug concentrations were chosen to be just above the MIC for ancestral populations–with MIC determined by complete absence of growth in ancestral strains after 24 hours under identical conditions–and the same concentration was applied at every time step calling for the associated drug. As a measure of drug efficacy, we defined the cumulative growth of a population at time t as the sum of the optical density measurements up to and including time t. Note that because drug-resistant populations often reach a steady-state carrying capacity–in our case, about OD=0.6–considerably faster than the 40-hour time window, cumulative

growth is a conservative measure that underestimates differences in population size that would occur in exponentially-growing populations (for example, in a chemostat).

In addition to the two MDP-derived drug protocols, we also tested protocols calling for repeated application of each drug alone (Figure 2.6C), each of the six possible 2-drug cycles (Figure 2.6D), a four drug cycle consisting of repeated application of RIF-FOF-TGC-AMP ((Figure 2.6E), and a drug-free control (dashed lines, Figure 2.6C-E). In all cases, cumulative growth was normalized to the value of the drug-free control at the end of the 20-day experiment. To compare results from the model with experiment, we mapped each of the discrete resistance levels to an OD value, with the highest level of resistance corresponding to drug-free growth (OD$\approx$ 0.6 each day) and the lowest resistance level corresponding to no growth (OD=0); see Figures 2.17, 2.18. We found experimentally that cycles involving sequential application of drugs with (on average) mutual collateral sensitivity–for example, cycles of RIF-FOF or RIF-AMP (see (Figure 2.6A)–are among the best-performing two-drug cycles, as predicted by previous studies [41]. However, the MDP-derived protocols led to a significant reduction in cumulative growth, outperforming every other protocol, often by significant margins (Figure 2.6; Figure 2.16). In addition to cumulative growth, we characterized each trajectory by calculating the adaptation rate, which is defined as the average rate of increase of instantaneous growth over time (i.e. the slope of the best-fit regression line for instantaneous growth vs time over days 2-20, Figures 2.19-2.20). Adaptation rate, which is essentially an estimate of the average convexity of the cumulative growth curves, provides no information on the magnitude of the growth at each step, but instead measures how rapidly that growth is increasing over time (starting with the first measurement after day 2). In addition to reducing cumulative growth, the MDP-derived sequences led to lower rates of adaptation than nearly every other protocol (Figure 2.6F; Figure 2.16F). A notable exception is the TGC-AMP cycle, which exhibits a (small) negative adaptation rate, reflecting that

fact that growth at day 2 has already achieved relatively high levels–roughly 60 percent of drug-free growth–suggesting that adaptation largely occurs in that first period but is nearly absent after that.

2.3 Discussion

Our work provides an extensive quantitative study of phenotypic and genetic collateral drug effects in *E. faecalis*. We have shown that cross resistance and collateral sensitivity are widespread but heterogeneous, with patterns of collateral effects often varying even between mutants evolved to the same drug. Our results contain a number of surprising, drug-specific observations; for example, we observed a strong, repeatable collateral sensitivity to RIF when mutants were selected by inhibitors of cell wall synthesis. Additionally, cross-resistance to DAP is particularly common when cells are selected by other frequently used antibiotics. Because the FDA/CLSI breakpoint for DAP resistance is not dramatically different than the MIC distributions found in clinical isolates prior to DAP use [81], one may speculate that even small collateral effects could have potentially harmful consequences for clinical treatments involving DAP. In addition, we found that selection by one drug, LZD, led to higher overall resistance to CHL than direct selection by CHL. While choramphenicol is rarely used clinically, the result illustrates that 1) collateral effects can be highly dynamic, and 2) indirect selection may drive a population across a fitness valley to an otherwise inaccessible fitness peak.

Our findings also point to global trends in collateral sensitivity profiles. For example, we found that the repeatability of collateral effects is sensitive to the drug used for selection, meaning that some drugs may be better than others for establishing robust antibiotic cycling profiles. On the other hand, despite the apparent unpredictability of collateral effects at the level of individual mutants, the sensitivity profiles for mutants selected by drugs from known classes tend to cluster into statistically similar groups.

As proof-of-principle, we show how these profiles can be incorporated into a simple mathematical framework that optimizes drug protocols while accounting for effects of both stochasticity and different time horizons. Within this framework, drug policies can be tuned to optimize either short-term or long-term evolutionary outcomes. The ability to systematically tune these timescales may eventually be useful in designing drug protocols that interpolate between short-term, patient-centric outcomes and long-term, hospital-level optimization.

Our results complement recent studies on collateral sensitivity and also raise a number of new questions for future work. Much of the previous work on collateral networks in bacteria has focused on gram-negative bacteria and highlighted the role of aminoglycosides in collateral sensitivity [41, 36]. Many gram-positive bacteria, including enterococci, are intrinsically resistant to aminoglycosides [82], and we therefore included only one (SPT) in our study. In that case, however, we did observe collateral sensitivity to cell wall inhibitors (AMP and FOF) in SPT-selected populations, consistent with findings in other species [41, 36], though it is not clear from our results whether aminoglycoside resistance would be associated with more widespread collateral sensitivity in *E. faecalis*. Recent work demonstrates that collateral profiles may be largely conserved across a wide range of *E. coli* isolates [77], offering hope that large scale analysis of clinical isolates may soon identify similar patterns in enterococci.

Multiple studies have shown that collateral profiles are heterogeneous [49, 50], and optimization will therefore require incorporation of stochastic effects such as likelihood scores [51]. These likelihood scores could potentially inform transition probabilities in our MDP approach, leading to specific predictions for optimal drug sequences based on known fitness landscapes. While we have quantified the variability in evolved populations in several ways (e.g. variability scores, interprofile distance, population sequencing), we cannot definitely comment on the source of that variability; it

could arise, for example, from different fixation events in independent populations or, alternatively, from clonal interference and random sampling in isolating individual clones. Indeed, population sequencing does suggest some measure of heterogeneity, even when we limit our analysis to mutations occurring at greater than 30 percent. In any event, our results point to a rich collection of possible collateral profiles, meaning that successful approaches for limiting resistance will likely require incorporation of variability and heterogeneity.

Several previous studies have indicated that cycles involving mutually collaterally sensitive drugs may be chosen to minimize the evolution of resistance [41, 42]. In the context of our MDP model, these cycles fall somewhere between the short-time-horizon optimization and the long-term optimal strategy, and in some cases, the collateral sensitivity cycling can lead to considerable slowing of resistance. However, our results indicate that the MDP optimizations on longer time-horizons lead to systematically lower resistance, a consequence of intermixing (locally) sub-optimal steps where the drug is instantaneously less effective but shepherds the population to a more vulnerable evolutionary state. We also find experimentally that mutual collateral sensitivity cycles with two drugs do generally outperform most other two-drug and single-drug protocols–as predicted by previous studies–but they generally underperform the MDP-based sequences.

It is important to keep in mind several limitations of our work. Designing effective drug protocols for clinical use is an extremely challenging and multi-scale problem. Our approach was not to develop a detailed, clinically accurate model, but instead to focus on a simpler question: optimizing drug cycles in single-species host-free populations. Even in this idealized scenario, which corresponds most closely to in vitro lab experiments, slowing resistance is a difficult and poorly understood problem (despite much recent progress). Our results are promising because they show systematic optimization is indeed possible given the measured collateral sensitivity profiles.

We have chosen to focus on a simple evolutionary scenario where collateral effects accumulate over time based on the history of drug exposure. By using a simple model that can be analyzed in detail, our goal was to identify new conceptual strategies–and with them, experimentally testable predictions–for exploiting correlations in phenotypic resistance profiles. While we have focused on an extremely simple model, the MDP framework can be readily extended to account for different evolutionary scenarios and to incorporate more complex clinically-inspired considerations. For example, it would be straightforward to include fitness costs associated with different resistance profiles; in turn, the model might be extended to allow for drug-free periods ("drug holidays"), which potentially exploit these fitness costs to minimize resistance [50]. In addition, the current model inherently assumes that the dominant collateral effects are independent of the genetic background. In fact, collateral sensitivity profiles in cancer have been previously shown to be time-dependent [83, 50], epistasis certainly occurs [49, 84], and population heterogeneity could limit efficacy of this strategy under some conditions [85]. Unfortunately, the frequency and relative impact of these confounding effects are difficult to gauge. However, the relative success of the MDP-inspired sequences in lab evolution experiments underscores the potential of the approach. In particular, our findings offer hope that strategies combining frequent use of highly effective drugs with rare periods of "evolutionary steering" by less effective drugs may be promising even when the detailed assumptions of the model do not strictly hold.

Our future work will focus on experimentally characterizing dynamic properties of collateral effects and expanding the MDP approach to account for time-varying sensitivity profiles and epistasis. It may also be interesting to investigate collateral effects in microbial biofilms, where antibiotics can have counterintuitive effects even on evolutionarily short timescales [86]. On longer timescales, elegant experimental approaches to biofilm evolution have revealed that spatial structure can give rise to

rich evolutionary dynamics [87, 88] and potentially, but not necessarily, divergent results for biofilm and planktonic populations [89]

Finally, our results raise questions about the potential molecular and genetic mechanisms underlying the observed collateral effects. The phenotypic clustering analysis presented here may point to shared mechanistic explanations for sensitivity profiles selected by similar drugs, and the full genome sequencing identifies candidate genes associated with increased resistance. However, fully elucidating the detailed genetic underpinnings of collateral sensitivity remains an ongoing challenge for future work. At the same time, because the MDP framework depends only on phenotypic measurements, it may allow for systematic optimization of drug cycling policies even when molecular mechanisms are not fully known.

2.4 Materials and Methods

2.4.1 Strains, antibiotics and media

All resistant lineages were derived from *E. faecalis* V583, a fully sequenced vancomycin-resistant clinical isolate [90]. The 15 antibiotics used are listed in Table 2.2. Each antibiotic was prepared from powder stock and stored at -20°C with the exception of ampicillin, which was stored at -80°C. Evolution and IC_{50} measurements were conducted in BHI medium alone with the exception of DAP, which requires an addition of 50 mM calcium for antimicrobial activity.

2.4.2 Laboratory evolution experiments

Evolution experiments to each antibiotic were performed in quadruplicate. Evolutions were performed using 1 mL BHI medium in 96-well plates with maximum volume 2 mL. Each day, populations were grown in at least three different antibiotic concentrations spanning both sub- and super-MIC doses. After 16-20 hours of incubation at 37°C, the well with the highest drug concentration that contained visual growth was propagated into 2 higher concentrations (typically a factor 2x and 4x increase in drug concentration) and 1 lower concentration to maintain a living mutant lineage (always half the concentration that most recently produced growth). A 1/200 dilution was used to inoculate the next day's evolution plate, and the process was repeated for a total of 8 days of selection. On the final day of evolution all strains were stocked in 30 percent glycerol. Strains were then plated on a pure BHI plate and a single colony was selected for IC_{50} determination. In the case of LZD mutants, days 2, 4, and 6 were also stocked for further testing.

Table 2.2: **Table of antibiotics used in this study and their targets.**

Drug Name (abbreviation)	**Drug Class**	**Mechanism of Action**
Daptomycin (DAP)	Lipopeptide	Cell membrane insertion
Ampicillin (AMP)	β-lactam	Inhibits cell wall synthesis
Oxacillin (OXA)	β-lactam	Inhibits cell wall synthesis
Ceftriaxone (CRO)	β-lactam	Inhibits cell wall synthesis
Fosfomycin (FOF)	Fosfomycin	Inhibits cell wall synthesis
Tetracycline (TET)	Tetracycline	30S protein synthesis inhibitor
Doxycycline (DOX)	Tetracycline	30S protein synthesis inhibitor
Tigecycline (TGC)	Tetracycline	30S protein synthesis inhibitor
Spectinomycin (SPT)	Aminoglycosides	30S protein synthesis inhibitor
Linezolid (LZD)	Oxazolidinone	50S protein synthesis inhibitor
Chloramphenicol (CHL)	Amphenicol	50S protein synthesis inhibitor
Ciprofloxacin (CIP)	Quinolone	DNA gyrase inhibitor
Levofloxacin (LVX)	Quinolone	DNA gyrase inhibitor
Nitrofurantoin (NIT)	Nitrofuran	Multiple mechanisms
Rifampicin (RIF)	Rifamycin	RNA polymerase inhibitor

2.4.3 Measuring drug resistance and sensitivity

Experiments to estimate IC_{50} were performed in replicate in 96-well plates by exposing mutants to a drug gradient consisting of 6-14 points–one per well–typically in a linear dilution series prepared in BHI medium with a total volume of 205 uL (200 uL of BHI, 5 uL of 1.5OD cells) per well. After 20 hours of growth the optical density at 600 nm (OD600) was measured using an Enspire Multimodal Plate Reader (Perkin Elmer) with an automated 20-plate stacker assembly. This process was repeated for all 60 mutants as well as the wild-type, which was measured in replicates of 8.

The optical density (OD600) measurements for each drug concentration were normalized by the OD600 in the absence of drug. To quantify drug resistance, the resulting dose response curve was fit to a Hill-like function $f(x) = (1 + (x/K)^h)^{-1}$ using nonlinear least squares fitting, where K is the half-maximal inhibitory concentration (IC_{50}) and h is a Hill coefficient describing the steepness of the dose-response relationship. A mutant strain was defined to be collaterally sensitive if its IC_{50} had decreased by more than $3\sigma_{WT}$ relative to the ancestral strain (σ_{WT} is defined as the uncertainty–standard error across replicates–of the IC_{50} measured in the ancestral strain). Similarly, an increase in IC_{50} by more than $3\sigma_{WT}$ relative to the ancestral strain corresponds to cross-resistance.

2.4.4 Hierarchical clustering

Hierarchical clustering was performed in Matlab using, as input, the collateral profiles $\bar{C}$ for each mutant. The distance between each pair of mutants was calculated using a correlation metric (Matlab function pdist with parameter 'correlation'), and the linkage criteria was chosen to be the mean average linkage clustering.

2.4.5 Markov decision process (MDP) model

The MDP model consists of a finite set of states (S), a finite set of actions (A), a conditional probability ($P_a(s'|s,a)$) describing (action-dependent) Markovian transitions between these states, and an instantaneous reward function ($R_a(s)$) associated with each state and action combination. The state of the system $s \in S$ is an n_d-dimensional vector, with n_d the number of drugs and each component $s^i \in \{r_{min}, r_{min}+1, ..., r_{max}\}$ indicating the level of resistance to drug i. The action $a \in A \equiv \{1, 2, ..., n_d\}$ is the choice of drug at the current step, and we take the reward function $R_a(s)$ to be the (negative of the) resistance level to the currently applied drug (i.e. the a-th component of s). The goal of the MDP is to identify a policy $\pi(s)$, which is a mapping from S to A that specifies an optimal action for each state. The policy is chosen to maximize a cumulative reward function $R_c = \sum_{t=0}^{\infty} \gamma^t \langle R_\pi(s_t) \rangle$, where t is the time step, s_t is the state of the system at time t, $R_\pi(s_t)$ is a random variable describing the instantaneous reward assuming that the actions are chosen according to policy π, and brackets indicate an expectation value. The parameter γ ($0 \leq \gamma < 1$) is a discount factor that determines the relative importance of instantaneous vs long-term optimization. In words, we seek an optimal policy–which associates the resistance profile of a given population to an optimal drug choice–that minimizes the cumulative expected resistance to the applied drug.

The MDP problem was solved using value iteration, a standard dynamic programming algorithm for MDP models. Briefly, the optimization was performed by first computing the optimal value function $V(s)$, which associates to each state s the expected reward obtained by following a particular policy and starting in that state. Following the well-established value iteration algorithm [80, 78, 79], we iterate according to $V_{i+1}(s) = \max_{\{a\}} \left(R_a(s) + \gamma \sum_{s'} P(s'|s,a) V_i(s') \right)$. Given the optimal value function, the optimal policy is then given by the action that minimizes the optimal value function at the next time step.

Once the optimal policy $\pi = \pi^*$ is found, the system is reduced to a simple Markov chain with transition matrix $T_{\pi^*} = P_{\pi^*(s)}(s'|s, \pi^*(s))$, where the subscript π^* means that the decision in each state is determined by the policy π^* (i.e. that $a = \pi^*(s)$ for a system in state s). Explicitly, the Markov chain dynamics are given by $P_{t+1}(s) = T_{\pi^*} P_t(s)$, with $P_t(s)$ the probability to be in state s at time step t. All quantities of interest–including P(Drug), P(Resist) (see Figure 2.5), and $\langle R(t) \rangle$–can be calculated directly from $P_t(s)$. For example, $\langle R(t) \rangle = \sum_{s \in S} P_t(s) R_{\pi^*}(s)$, with $R_{\pi^*}(s)$ the instantaneous reward for a system in state s under optimal policy π^*.

2.4.6 Experiments to evaluate different drug sequence protocols

Experiments to evaluate different drug sequence protocols were performed in replicate in 96-well plates by exposing populations to antibiotic concentrations just above the wild-type MIC value, determined by an absence of measurable growth after 24 hours. Seed populations were grown overnight from single colonies and then diluted 1:200 into fresh BHI plates with appropriate antibiotic concentration according to each prescribed policy. Populations were left to grow inside a plate reader for 40 hours, while OD readings were taken every 20 minutes for at least the first 6 hours. To estimate daily growth, we took a final OD reading for each population after 40 hours. The populations were then diluted 1:200 into fresh BHI media, following a brief 2-hour outgrowth phase, populations were then diluted immediately into pre-prepared plates containing the appropriate drug concentrations. The purpose of the outgrowth phase is to minimize drug-drug interactions and post-antibiotic effects that may occur if the population were to be diluted into the next drug-plate immediately. To avoid contamination, each plate was covered during growth phase. In addition, each experimental plate contained 36 control wells with BHI alone – no cells. If any of these wells displayed visible growth, the plate was considered to be contaminated and discarded; the experiment was then started again from the previous night's stock.

During the 20 day experiment, only one such restart was required. Strains were stocked at -80C in 15 percent glycerol at the end of each 40 hour growth.

2.4.7 Whole-genome sequencing

To identify any genomic changes that contributed to the measured collateral phenotypes identified, we sequenced 15 independently evolved drug mutants along with two V583 ancestors as well as a control V583 strain propagated in BHI for the 8 days. Each of the 15 drug-selected mutants and BHI-control were subjected to both clonal and population sequencing. Populations were streaked from a frozen stock, grown up in BHI, triple washed in PBS and DNA was isolated using a Quick-DNA Fungal/Bacterial Kit (Zymo Reserach). The clonal samples were sequenced in two batches via the University of Michigan sequencing core while the population samples were sequenced via the Microbial Genome Sequencing Center (MiGS) at University of Pittsburgh.

The resulting genomic data was analyzed using the high-throughput computational pipeline breseq, with default settings. Average read coverage depth was about 50 on batch 1, 300 on batch 2 and 200 on the population sequencing batch. Briefly, genomes were trimmed and subsequently aligned to E. faecalis strain V583 (Accession numbers: AE016830 - AE016833) via Bowtie 2. A sequence read was discarded if less than 90 percent of the length of the read did not match the reference genome or a predicted candidate junction. At each position a Bayesian posterior probability is calculated and the log10 ratio of that probability versus the probability of another base (A, T, C, G, gap) is calculated. Sufficiently high consensus scores are marked as read alignment evidence (in our case a consensus score of 10). Any mutation that occurred in either of the 2 control V583 strains was filtered from the results.

2.5 Appendix

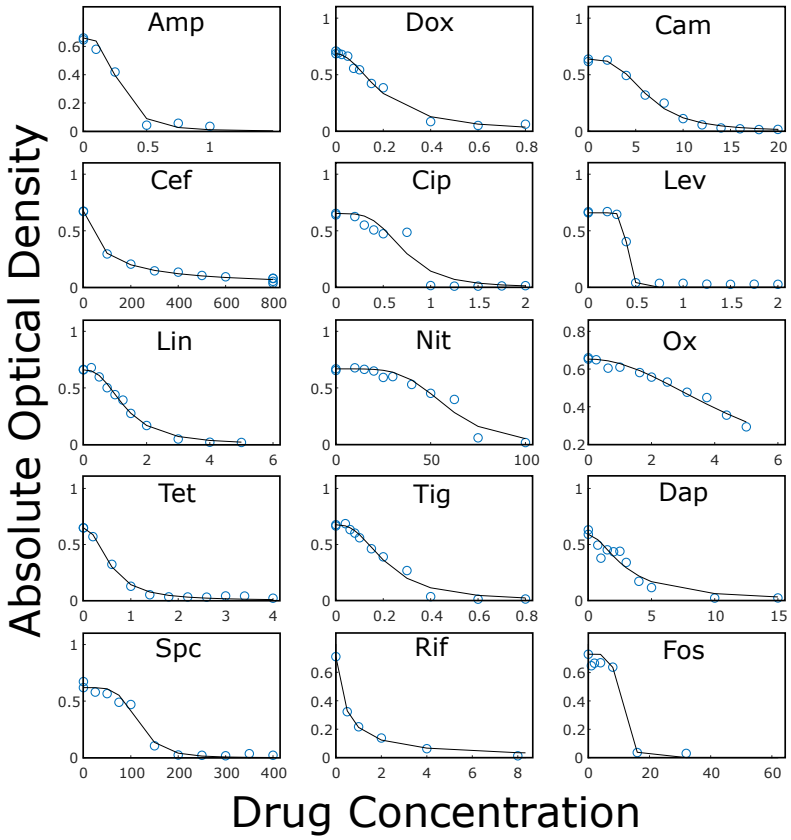

Figure 2.7: **Example dose response curves for each drug** Optical density (OD) of V583 cultures after 12 hours of incubation at various drug concentrations (blue circles). All drug concentrations are measured in μg/mL. Lines: fit of normalized dose response curve to Hill-like function $f(x) = (1 + (x/K)^h)^{-1}$, with K the IC_{50} and h a Hill coefficient.

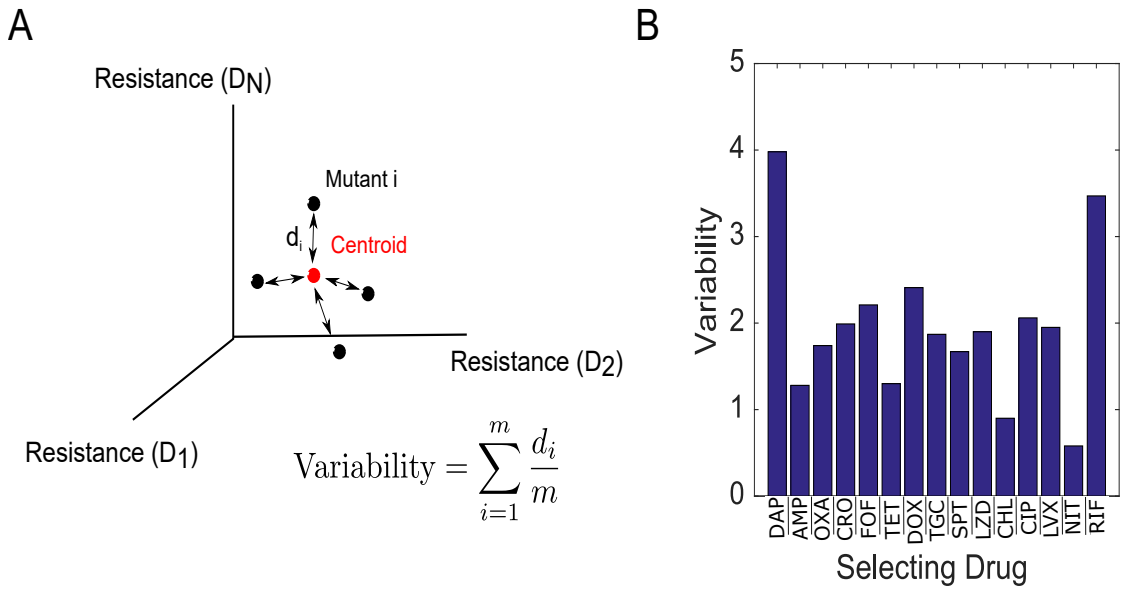

Figure 2.8: **Variation within replicate populations.** A. Variability in collateral profiles between mutants selected by the same drug is defined by first representing each mutant's collateral profile as a vector $\bar{C}$ in 15-dimensional drug space. Dimension i represents the log2-scaled fold increase in IC_{50} (relative to wild-type) for drug i. The variability for a set of mutants evolved to the same drug is then given by the average Euclidean distance d_i for a mutant from the centroid. B. Variability in replicates (defined in panel A) for all 15 drugs used for selection.

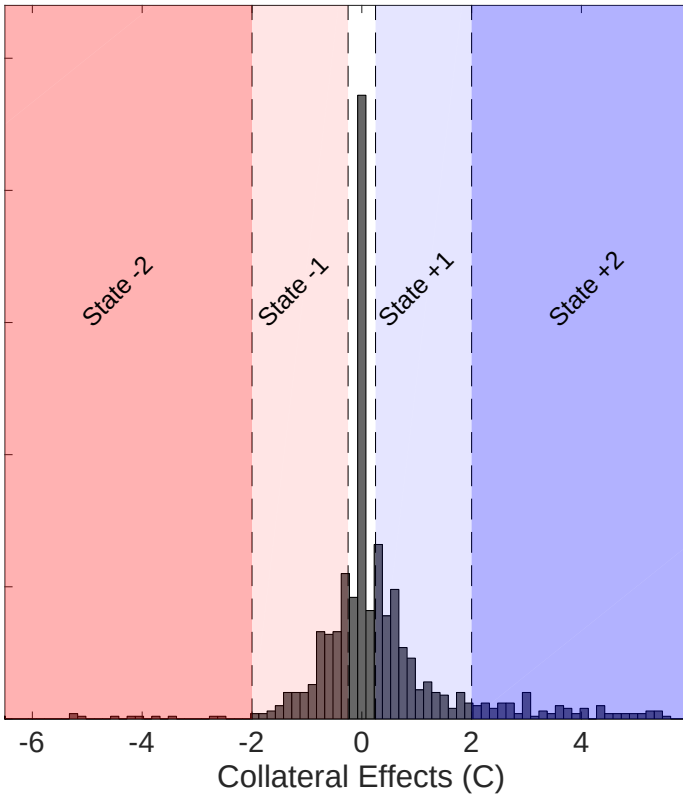

Figure 2.9: **Discretization of collateral effects** Histogram of collateral effects ($C > 0$ resistance, $C < 0$ sensitivity). Shaded regions indicate the five levels of discretization chosen for the MDP model ($C < -2$, red; $-2 \leq C < -0.25$, light red; $-0.25 \leq C \leq 0.25$, white; $0.25 < C \leq 2$, light blue; $C > 2$, dark blue). The discretized values range from -2 (reducing resistance by two levels) to +2 (increasing resistance by two levels).

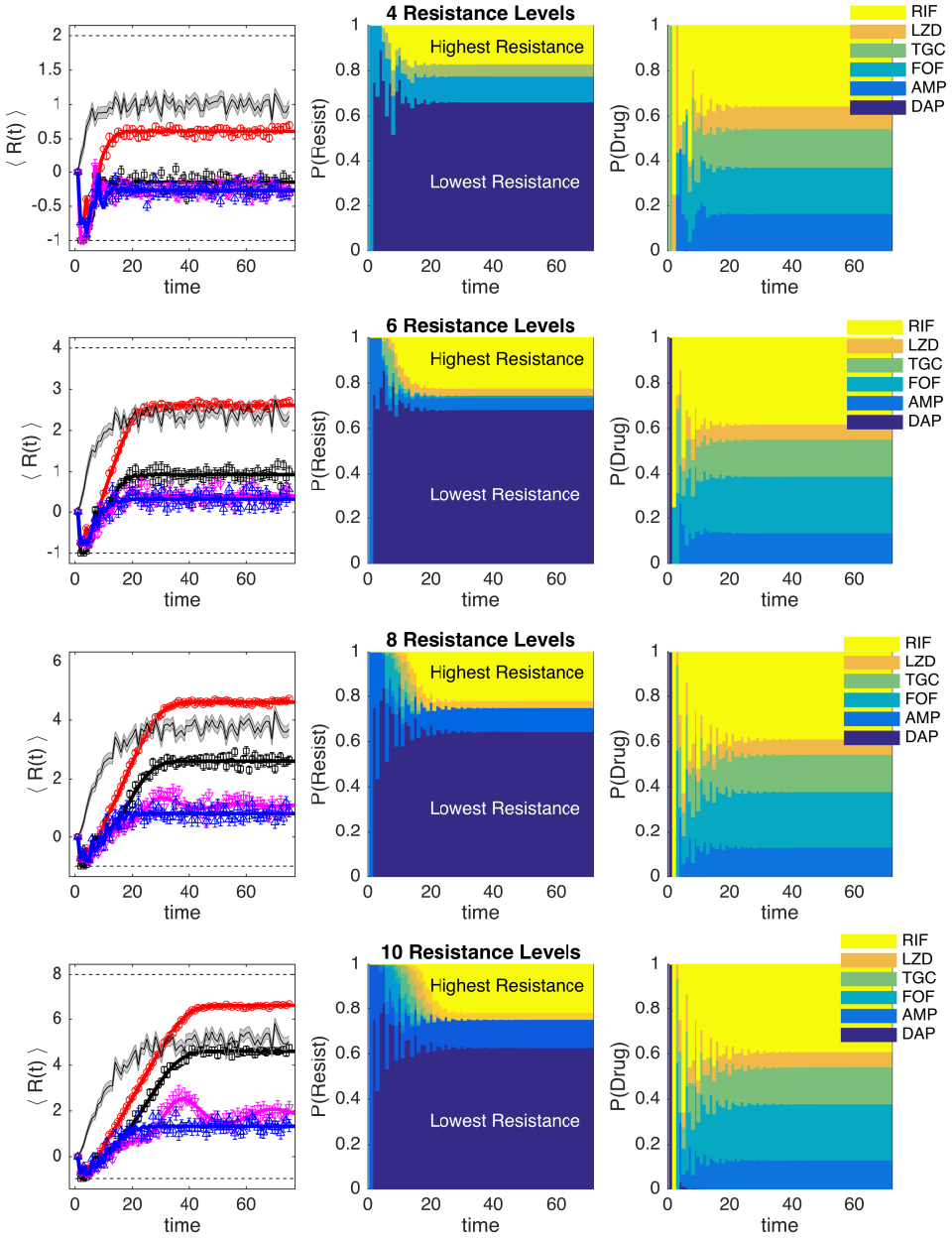

Figure 2.10: **MDP models with different numbers of states show similar qualitative behavior** In all panels, the MDP is solved for a selection of six drugs: daptomycin (DAP), ampicillin (AMP), fosfomycin (FOF), tigecycline (TGC), linezolid (LZD), and rifampicin (RIF). Left column: Average level of resistance ($\langle R(t) \rangle$) to the applied drug for policies with $\gamma = 0$ (red),$\gamma = 0.7$ (black),$\gamma = 0.9$ (magenta), and $\gamma = 0.99$ (blue). Resistance to each drug is characterized by 4 (top row), 6, 8, or 10 (bottom row) discrete levels. At time 0, the population starts in the second lowest resistance level (0) for all drugs. Symbols (circles, triangles, squares) are the mean of 10^3 independent simulations of the MDP, with error bars $\pm$ SEM.

Table 2.3: **Mutant Number Table For Dendrograms.**

Mutant Number	**Drug Name**
1-4	Daptomycin
5-8	Ampicillin
9-12	Oxacillin
13-16	Ceftriaxone
17-20	Fosfomycin
21-24	Tetracycline
25-28	Doxycycline
29-32	Tigecycline
33-36	Spectinomycin
37-40	Linezolid
41-44	Ciprofloxacin
45-48	Levofloxacin
49-52	Rifampicin
53-56	Chloramphenicol
57-60	Nitrofurantoin

Figure 2.10: Solid lines are numerical calculations using exact Markov chain calculations (see Methods). Black shaded line, randomly cycled drugs. Middle column: The probability P(Resist) of the population exhibiting a particular level of resistance to the applied drug when the optimal policy ($\gamma = 0.99$) is used. Right column: The time-dependent probability P(Drug) of choosing each of the six drugs when the optimal policy ($\gamma = 0.99$) is used.

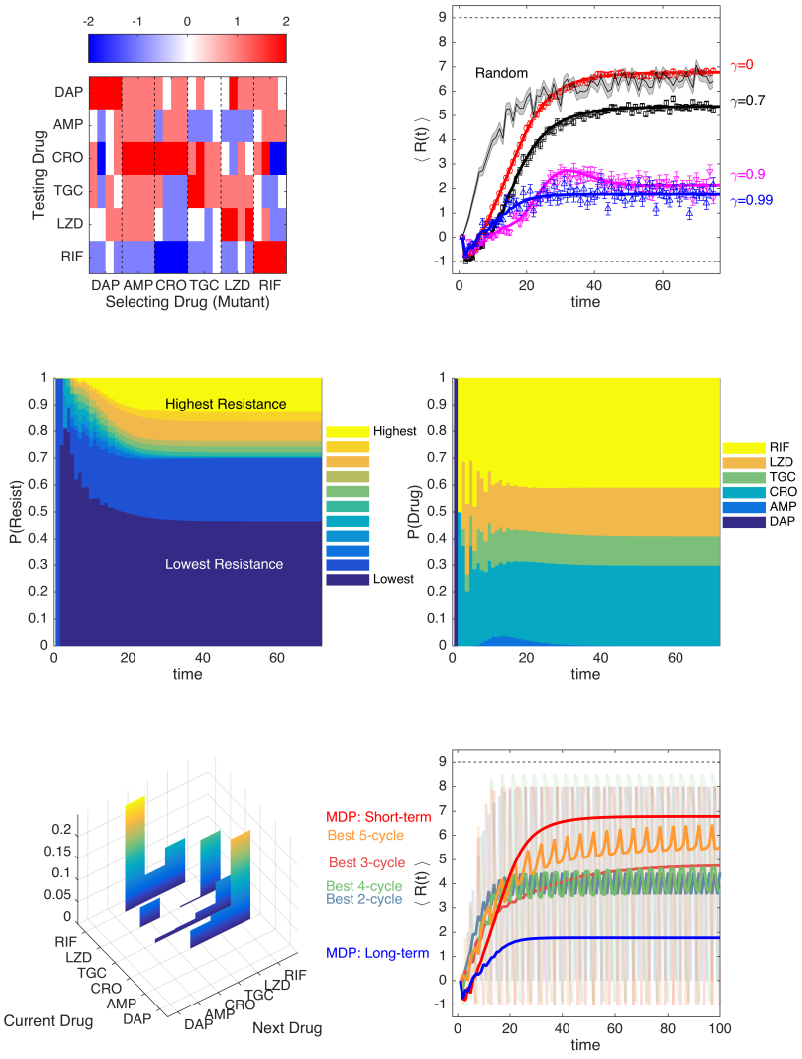

Figure 2.11: **Optimal drug sequences constrain resistance on long timescales and outperform simple collateral sensitivity cycles** A. Average of discretized collateral sensitivity or resistance $C_d \in \{-2, -1, 0, 1, 2\}$ for a selection of six drugs: daptomycin (DAP), ampicillin (AMP), ceftriaxone (CRO), tigecycline (TGC), linezolid (LZD), and rifampicin (RIF). For each selecting drug, the heat map shows the average value of C_d from $n_r = 4$ independently evolved populations. See Fig 1 for original (non-discretized) data. B. Average level of resistance ($\langle R(t) \rangle$) to the applied drug for policies with $\gamma = 0$ (red),$\gamma = 0.7$ (black), $\gamma = 0.9$ (magenta), and $\gamma = 0.99$ (blue). Resistance to each drug is characterized by 11 discrete levels ranging from -1 (least resistant) to 9 (most resistant). At time 0, the population starts in the second lowest resistance level (0) for all drugs. Symbols (circles, triangles, squares) are the mean of 10^3 independent simulations of the MDP, with error bars ± SEM. Solid lines are numerical calculations using exact Markov chain calculations (see Methods).

Figure 2.11: Black shaded line, randomly cycled drugs. C. The probability P(Resist) of the population exhibiting a particular level of resistance to the applied drug when the optimal policy ($\gamma = 0.99$) is used. D. The time-dependent probability P(Drug) of choosing each of the six drugs when the optimal policy ($\gamma = 0.99$) is used. E. Steady state joint probability distribution P(current drug, next drug) for consecutive time steps when the optimal policy ($\gamma = 0.99$) is used. F. Average level of resistance ($\langle R(t) \rangle$) to the applied drug for collateral sensitivity cycles of 2 (dark green, CRO-RIF), 3 (pink, RIF-CRO-TGC), 4 (light green, TGC-LZD-AMP-RIF), and 5 (orange, AMP-RIF-CRO-TGC-LZD) drugs are compared with MDP policies with $\gamma = 0$ (short-term, red) and $\gamma = 0.99$ (long-term, blue). For visualizing the results of the collateral sensitivity cycles, which give rise to periodic behavior with large amplitude, the curves show a moving time average (window size 10 steps), but the smoothed curves are shown transparently in the background.

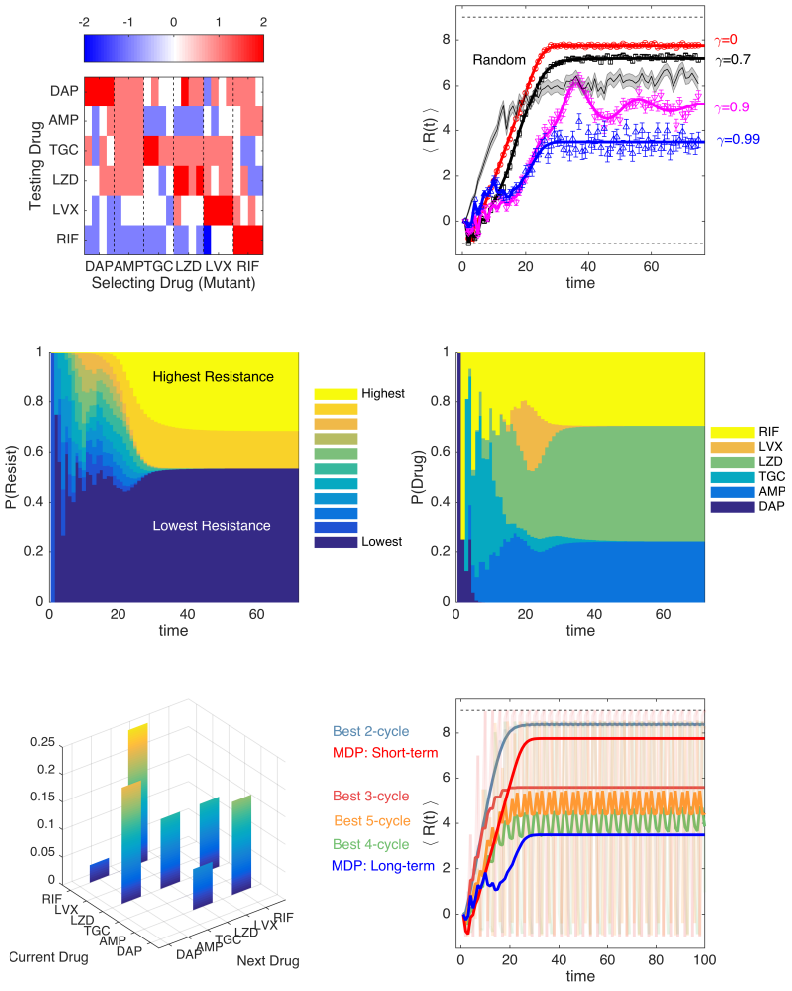

Figure 2.12: **Optimal drug sequences constrain resistance on long timescales and outperform simple collateral sensitivity cycles** A. Average of discretized collateral sensitivity or resistance $C_d \in \{-2, -1, 0, 1, 2\}$ for a selection of six drugs: daptomycin (DAP), ampicillin (AMP), tigecycline (TGC), linezolid (LZD), levofloxacin (LVX), and rifampicin (RIF). For each selecting drug, the heat map shows the average value of C_d from $n_r = 4$ independently evolved populations. See Fig 1 for original (non-discretized) data. B. Average level of resistance ($\langle R(t) \rangle$) to the applied drug for policies with $\gamma = 0$ (red),$\gamma = 0.7$ (black), $\gamma = 0.9$ (magenta), and $\gamma = 0.99$ (blue). Resistance to each drug is characterized by 11 discrete levels ranging from -1 (least resistant) to 9 (most resistant). At time 0, the population starts in the second lowest resistance level (0) for all drugs. Symbols (circles, triangles, squares) are the mean of 10^3 independent simulations of the MDP, with error bars ± SEM. Solid lines are numerical calculations using exact Markov chain calculations (see Methods).

Figure 2.12: Black shaded line, randomly cycled drugs. C. The probability P(Resist) of the population exhibiting a particular level of resistance to the applied drug when the optimal policy ($\gamma = 0.99$) is used. D. The time-dependent probability P(Drug) of choosing each of the six drugs when the optimal policy ($\gamma = 0.99$) is used. E. Steady state joint probability distribution P(current drug, next drug) for consecutive time steps when the optimal policy ($\gamma = 0.99$) is used. F. Average level of resistance ($\langle R(t) \rangle$) to the applied drug for collateral sensitivity cycles of 2 (dark green, TGC-RIF), 3 (pink, LZD-AMP-LVX), 4 (light green, RIF-TGC-LZD-AMP), and 5 (orange, AMP-LVX-RIF-TGC-LZD) drugs are compared with MDP policies with $\gamma = 0$ (short-term, red) and $\gamma = 0.99$ (long-term, blue). For visualizing the results of the collateral sensitivity cycles, which give rise to periodic behavior with large amplitude, the curves show a moving time average (window size 10 steps), but the smoothed curves are shown transparently in the background.

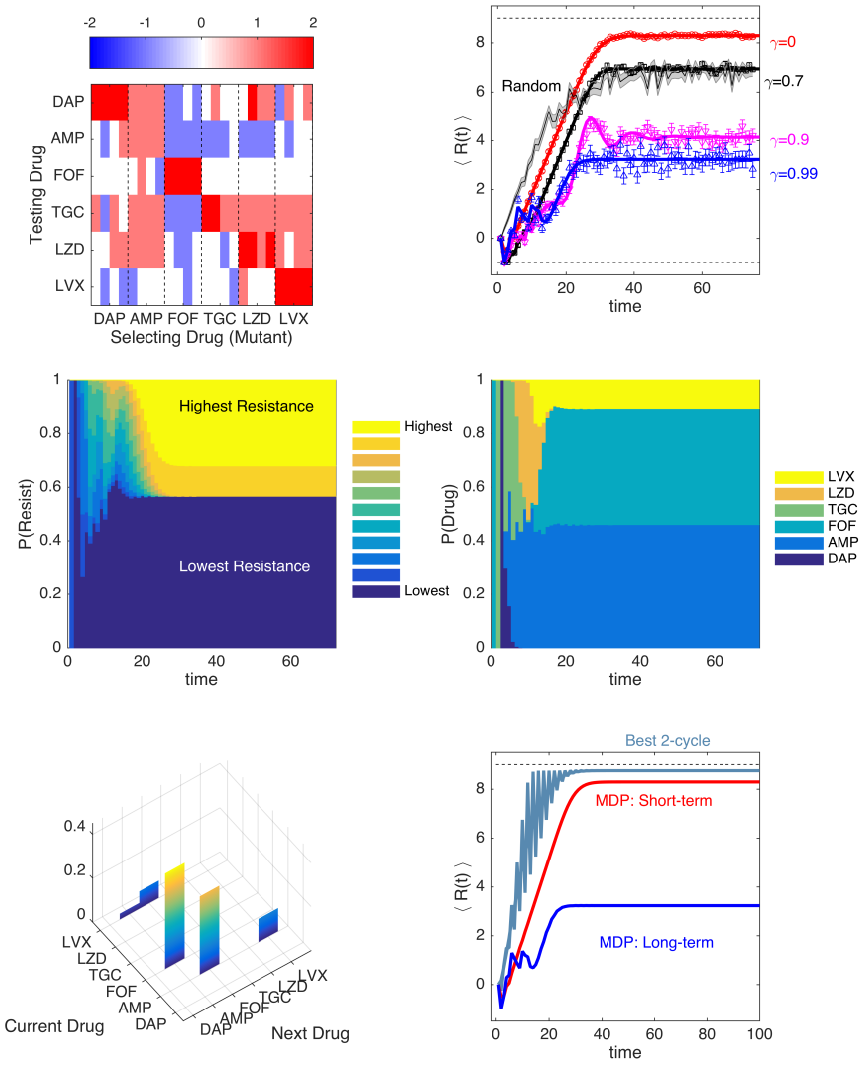

Figure 2.13: **Optimal drug sequences constrain resistance on long timescales and outperform simple collateral sensitivity cycles** A. Average of discretized collateral sensitivity or resistance $C_d \in \{-2, -1, 0, 1, 2\}$ for a selection of six drugs: daptomycin (DAP), ampicillin (AMP), tigecycline (TGC), linezolid (LZD), levofloxacin (LVX), and rifampicin (RIF). For each selecting drug, the heat map shows the average value of C_d from $n_r = 4$ independently evolved populations. See Fig 1 for original (non-discretized) data. B. Average level of resistance ($\langle R(t) \rangle$) to the applied drug for policies with $\gamma = 0$ (red),$\gamma = 0.7$ (black), $\gamma = 0.9$ (magenta), and $\gamma = 0.99$ (blue). Resistance to each drug is characterized by 11 discrete levels ranging from -1 (least resistant) to 9 (most resistant). At time 0, the population starts in the second lowest resistance level (0) for all drugs.

Figure 2.13: Symbols (circles, triangles, squares) are the mean of 10^3 independent simulations of the MDP, with error bars ± SEM. Solid lines are numerical calculations using exact Markov chain calculations (see Methods). Black shaded line, randomly cycled drugs. C. The probability P(Resist) of the population exhibiting a particular level of resistance to the applied drug when the optimal policy ($\gamma = 0.99$) is used. D. The time-dependent probability P(Drug) of choosing each of the six drugs when the optimal policy ($\gamma = 0.99$) is used. E. Steady state joint probability distribution P(current drug, next drug) for consecutive time steps when the optimal policy ($\gamma = 0.99$) is used. F. Average level of resistance ($\langle R(t) \rangle$) to the applied drug for collateral sensitivity cycles of 2 (dark green, AMP-LVX) drugs are compared with MDP policies with $\gamma = 0$ (short-term, red) and $\gamma = 0.99$ (long-term, blue). For visualizing the results of the collateral sensitivity cycles, which give rise to periodic behavior with large amplitude, the curves show a moving time average (window size 10 steps), but the smoothed curves are shown transparently in the background.

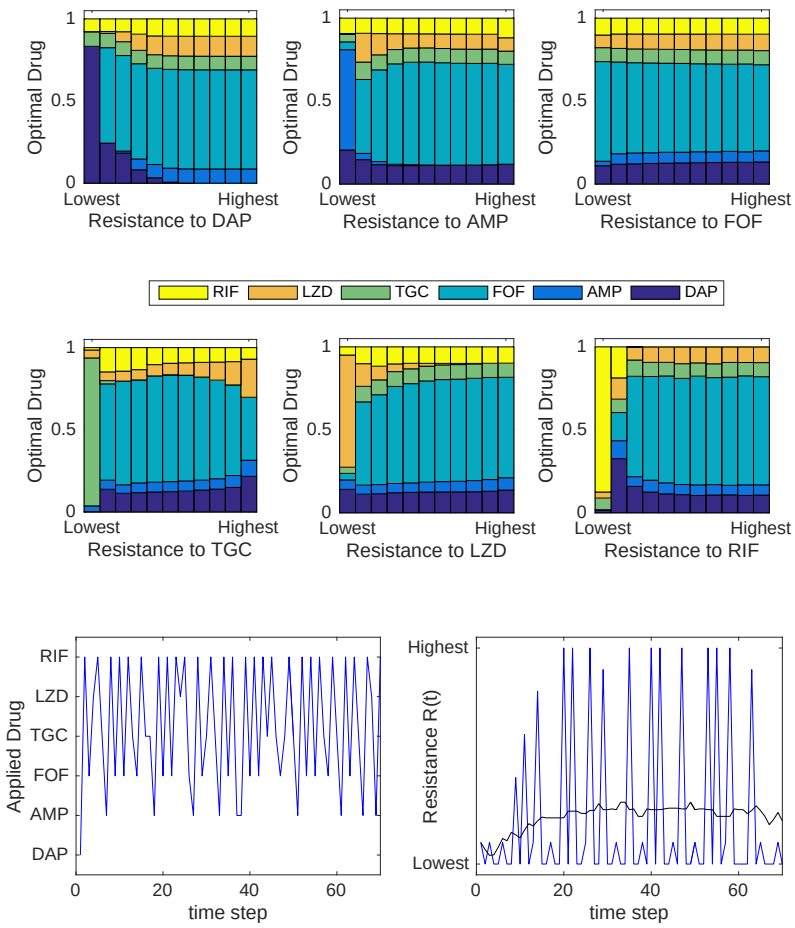

Figure 2.14: **Optimal policy statistics and sample trajectories for $\gamma = 0.99$** The optimal policy $\pi^*(s)$ is a mapping from the set of all possible resistance profiles (S) to the set of drugs (A). The policy associates each resistance profile with a unique (optimal) drug. Top panels: Frequency with which each drug is prescribed (according to the optimal policy) as a function of the level of resistance to an individual drug (horizontal axis). More specifically, for each of the six panels, the state space is partitioned into eleven distinct subsets, with each subset containing all states characterized by a given level of resistance to the particular drug in question (horizontal axis). The colored bars then show how frequently each of the six drugs is prescribed (according to the optimal policy) across all states within that subset. Bottom left panel: single simulated trajectory showing drug choice over time. Bottom right panel: single simulated trajectory of the instantaneous reward R, which corresponds to the resistance level to the applied drug. Blue curve is the specific trajectory; black curve is a moving average of the trajectory with a window size of 20.

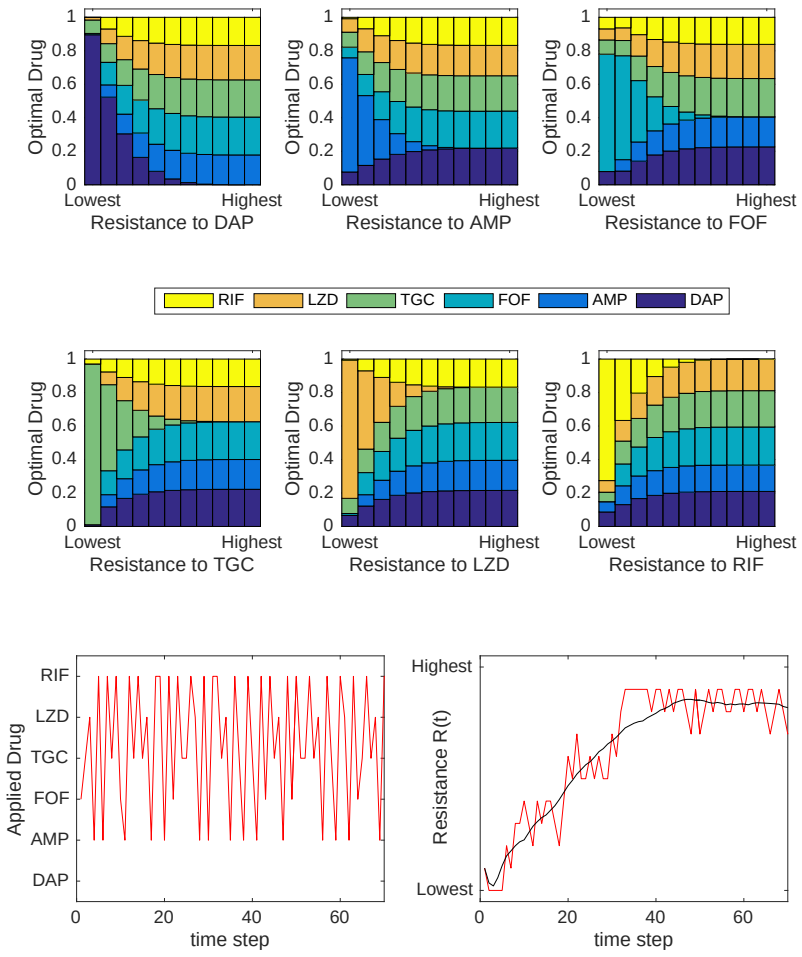

Figure 2.15: **Optimal policy statistics and sample trajectories for** $\gamma = 0.1$ Top panels: Frequency with which each drug is prescribed (according to the optimal policy) as a function of the level of resistance to an individual drug (horizontal axis). In each of the six panels, the state space is partitioned into eleven distinct subsets, with each subset containing all states with a given level of resistance to the particular drug in question. The colored bars then show how frequently each of the six drugs is prescribed across all states within that subset. Bottom left panel: single simulated trajectory showing drug choice over time. Bottom right panel: single simulated trajectory of the instantaneous reward R, which corresponds to the resistance level to the applied drug. Red curve is the specific trajectory; black curve is a moving average of the trajectory with a window size of 20.

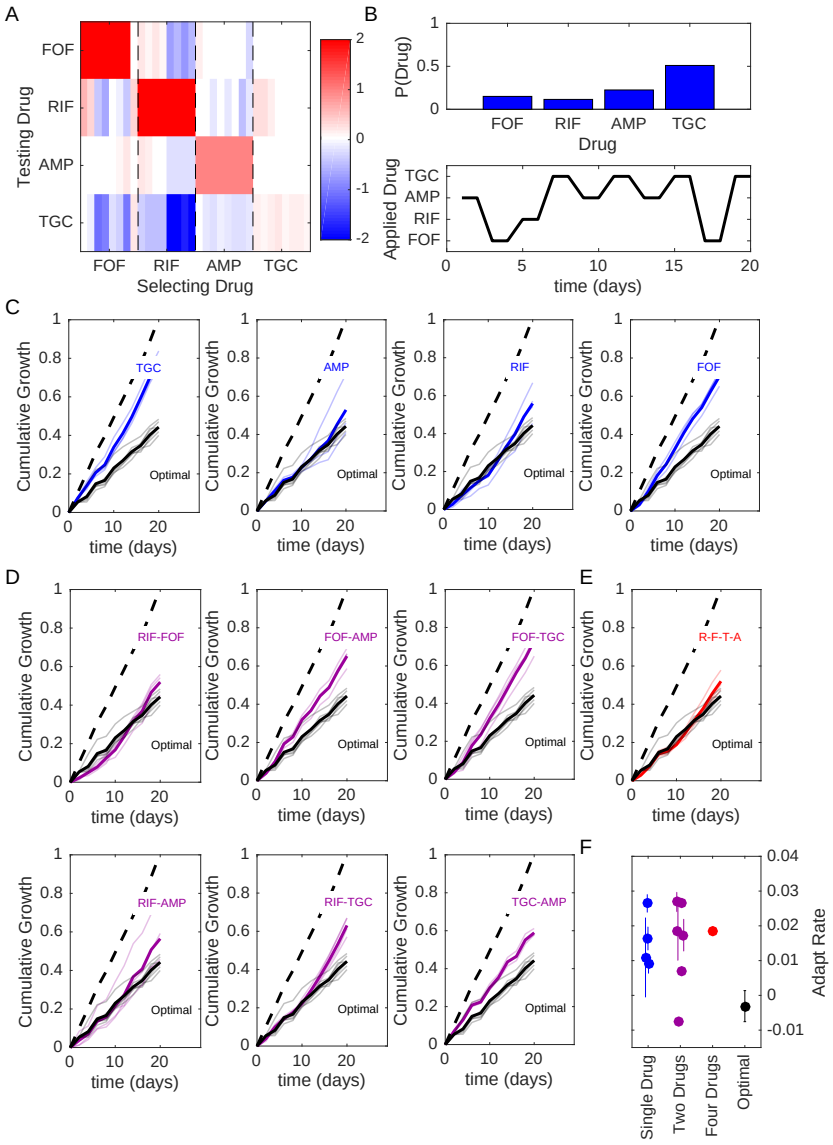

Figure 2.16: **Optimized drug sequences reduce cumulative growth and adaptation rates in lab evolution experiments.** A. Resistance (red) or sensitivity (blue) of each evolved mutant (horizontal axis; 4 drugs x 8 mutant per drug) to each drug (vertical axis) following 2 days of selection is quantified by the $\log_2$-transformed relative increase in the IC_{50} of the testing drug relative to that of wild-type (V583) cells. B. Top: distribution of applied drug at time step 20 (approximate steady state) calculated using an optimal policy with $\gamma = 0.78$. Bottom: sequence of applied drug from one particular realization of the stochastic process with the optimal policy ($\gamma = 0.78$). C-E.

Figure 2.16: Cumulative population growth over time for populations exposed to single drug sequences (C, blue), two-drug sequences (D,magenta), a four drug sequence (E, red), or the optimal sequence from panel B (black curves, all panels). Transparent lines represent individual replicate experiments and each thicker dark line corresponds to a mean over replicates. Dashed line, drug-free control (normalized to a growth of 1 at the end of the experiment). F. Adaptation rate for single drug (blue), two-drug (magenta), four drug (red), and optimal sequences (black). Error bars are standard errors across replicates. Adaptation rate is defined as the slope of the best fit linear regression describing time series of daily growth (see Figure 2.20).

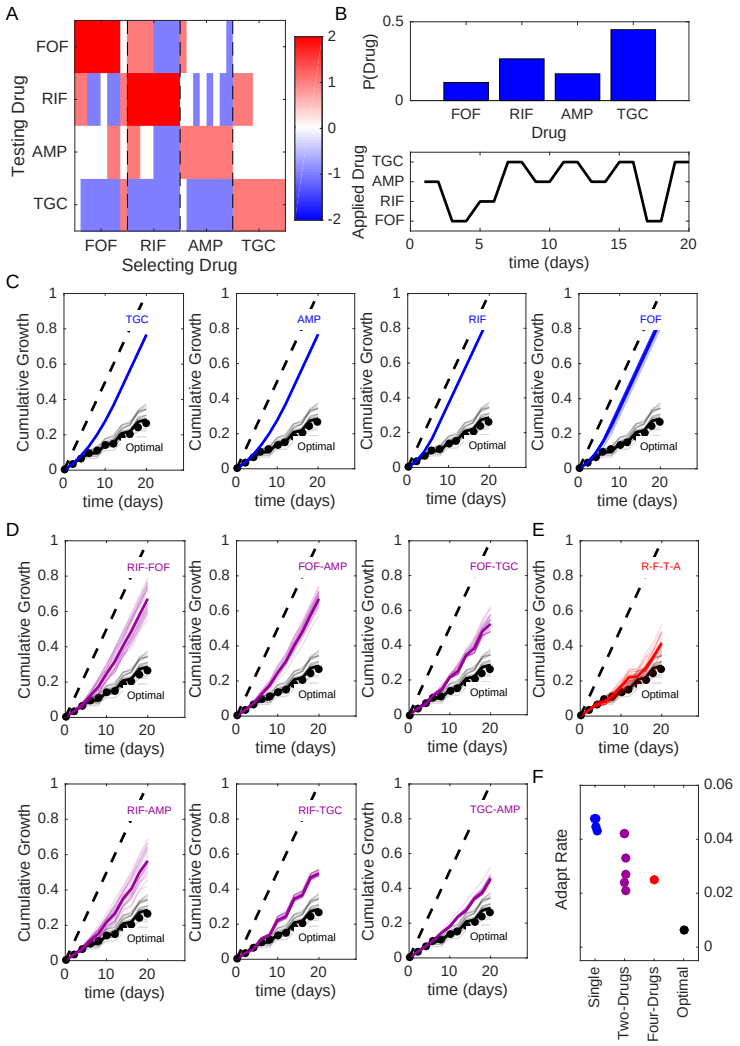

Figure 2.17: **Optimized drug sequences reduce cumulative growth and adaptation rates in numerical simulations of the laboratory evolution experiments.** Compare to Figure 2.6 (main text). A. Resistance (red) or sensitivity (blue) of each evolved mutant (horizontal axis; 4 drugs x 8 mutant per drug) to each drug (vertical axis) following 2 days of selection is quantified by the $\log_2$-transformed relative increase in the IC_{50} of the testing drug relative to that of wild-type (V583) cells. The profile is then discretized into 4 levels of resistance. B. Top: distribution of applied drug at time step 20 (approximate steady state) calculated using an optimal policy with $\gamma = 0.9$. Bottom: sequence of applied drug from one particular realization of the stochastic process with the optimal policy ($\gamma = 0.9$). C-E.

Figure 2.17: Cumulative population growth (simulations) over time for populations exposed to single drug sequences (C, blue), two-drug sequences (D,magenta), a four drug sequence (E, red), or the optimal sequence from panel B (black curves, all panels). Black circles correspond to the true optimal (i.e. applying the MDP policy directly) and performs only slightly better, on average, than the fixed sequence in panel B. At each time step, resistance level to each drug is converted to an OD value using a linear conversion with the highest resistance level corresponding to growth of drug-free cells (OD$\approx$ 0.6) and the lowest resistance level corresponding to OD=0. Transparent lines represent individual replicate experiments and each thicker dark line corresponds to a mean over replicates. Dashed line, drug-free control (normalized to a growth of 1 at the end of the experiment). F. Adaptation rate for single drug (blue), two-drug (magenta), four drug (red), and optimal sequences (black). Error bars are standard errors across replicates. Adaptation rate is defined as the slope of the best fit linear regression describing time series of daily growth.

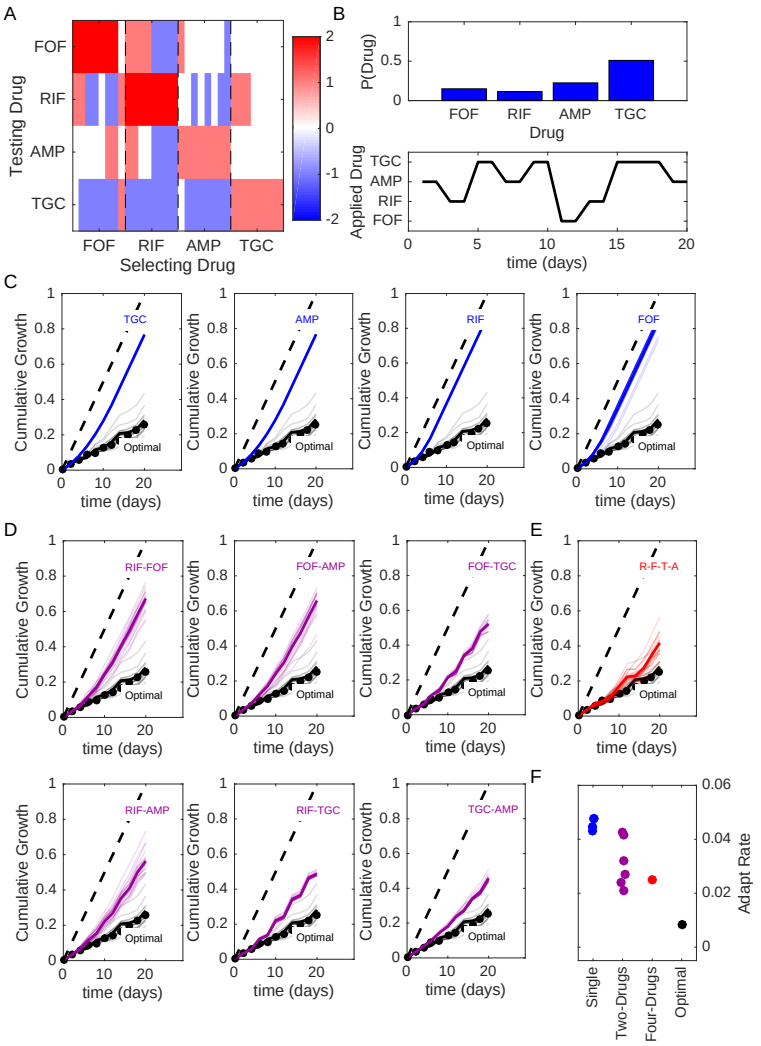

Figure 2.18: **Optimized drug sequences reduce cumulative growth and adaptation rates in numerical simulations of the laboratory evolution experiments.** Compare to Figure 2.16. A. Resistance (red) or sensitivity (blue) of each evolved mutant (horizontal axis; 4 drugs x 8 mutant per drug) to each drug (vertical axis) following 2 days of selection is quantified by the $\log_2$-transformed relative increase in the IC_{50} of the testing drug relative to that of wild-type (V583) cells. The profile is then discretized into 4 levels of resistance. B. Top: distribution of applied drug at time step 20 (approximate steady state) calculated using an optimal policy with $\gamma = 0.78$. Bottom: sequence of applied drug from one particular realization of the stochastic process with the optimal policy ($\gamma = 0.78$). C-E.

Figure 2.18: Cumulative population growth (simulations) over time for populations exposed to single drug sequences (C, blue), two-drug sequences (D,magenta), a four drug sequence (E, red), or the optimal sequence from panel B (black curves, all panels). Black circles correspond to the true optimal (i.e. applying the MDP policy directly) and performs only slightly better, on average, than the fixed sequence in panel B. At each time step, resistance level to each drug is converted to an OD value using a linear conversion with the highest resistance level corresponding to growth of drug-free cells (OD$\approx$ 0.6) and the lowest resistance level corresponding to OD=0. Transparent lines represent individual replicate experiments and each thicker dark line corresponds to a mean over replicates. Dashed line, drug-free control (normalized to a growth of 1 at the end of the experiment). F. Adaptation rate for single drug (blue), two-drug (magenta), four drug (red), and optimal sequences (black). Error bars are standard errors across replicates. Adaptation rate is defined as the slope of the best fit linear regression describing time series of daily growth.

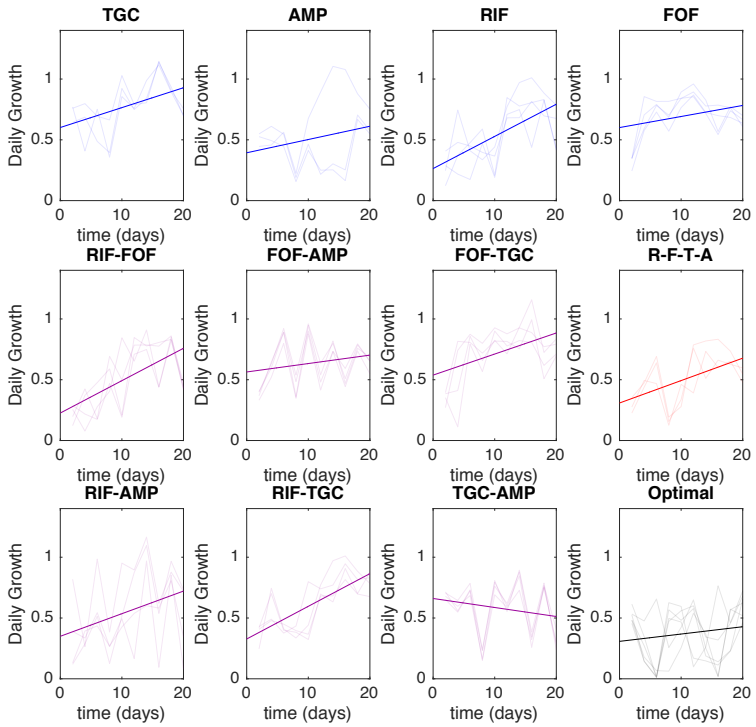

Figure 2.19: **Estimated adaptation rate in lab evolution experiments based on γ=0.9 MDP policy.** Daily growth, which is defined as the OD measured at the end of each 48-hour period (normalized to drug-free control), for populations exposed to single drug (blue), two-drug (magenta), four-drug (red), and optimal (black) drug sequences. All time series start at day 2 (i.e. following 48 hours of adaption). Transaprent curves correspond to individual replicate experiments; solid dark lines show the (average) best fit linear regression. Adaptation rate is defined as the slope of the regression line.

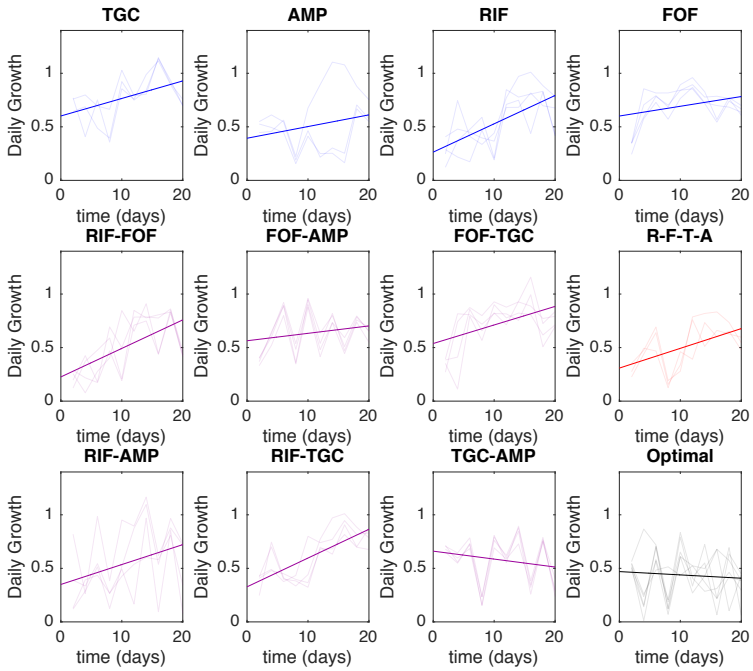

Figure 2.20: **Estimated adaptation rate in lab evolution experiments based on γ=0.78 MDP policy.** Daily growth, which is defined as the OD measured at the end of each 48-hour period (normalized to drug-free control), for populations exposed to single drug (blue), two-drug (magenta), four-drug (red), and optimal (black) drug sequences. All time series start at day 2 (i.e. following 48 hours of adaption). Transparent curves correspond to individual replicate experiments; solid dark lines show the (average) best fit linear regression. Adaptation rate is defined as the slope of the regression line.

2.6 References

1 H. W. Boucher, G. H. Talbot, J. Bradley, *et al.*, "Bad bugs, no drugs; no esape! an update from the infections diseases society of america.," *Clin. Infect. Dis.* **48**, 1–12 (2009).

2 D. E. Goldberg, R. Siliciana, and W. R. J. Jr, "Outwitting evolution: Fighting drug-resistant tb, malaria, and hiv.," *Cell* **148**, 1271–1283 (2012).

3 A. Pfaller, "Antifungal drug resistance: Mechanisms, epidemiology, and consequences for treatment.," *Am. J. Med.* **125**, S3–S13 (2012).

4 M. Raviglione, B. Marais, K. Floyd, *et al.*, "Scaling up interentions to achieve global tuberculosis control: Progress and new developments.," *Lancet* **379**, 1902–1913 (2012).

5 P. Borst, "Cancer drug pan-resistance: Pumps, cancer stem cells, quiescence, epithelial to mesenchymal transition, blocked cell death pathways, persister or what?.," *Open Biol.* **2** (2012).

6 K. M. Pluchino, M. D. Hall, A. S. Goldsborough, *et al.*, "Collateral sensitivity as a strategy against cancer multidrug resistance.," *Drug Resis. Updat.* **15**, 98–105 (2012).

7 R. Martin, "Optimal control drug scheduling of cancer chemotherapy.," *Journal of Antimicrobial Chemotherapy* **28**, 1113–1123 (1992).

8 E. Hansen, R. J. Woods, and A. F. Read, "How to use a chemotherapeutic agent when resistance to it threatens the patient," *PLoS biology* **15**(2), e2001110 (2017).

9 A. Fischer, I. Vázquez-García, and V. Mustonen, "The value of monitoring to control evolving populations," *Proceedings of the National Academy of Sciences* **112**(4), 1007–1012 (2015).

10 L. M. Feazel, A. Malhotra, E. N. Perencevich, *et al.*, "Effect of antibiotic stewardship programmes on *clostridium difficile* incidence: a systematic review and meta-analysis.," *Journal of Antimicrobial Chemotherapy* **69**, 1748–1754 (2014).

11 D. L. Smith, S. A. Levin, and R. Laxminarayan, "Strategic interactions in multi-institutional epidemics of antibiotic resistance.," *Proc. Natl. Acad. Sci. USA* **102**, 3153–3158 (2004).

12 C. T. Bergstrom, M. Lo, and M. Lipsitch, "Ecological theory suggests that antimicrobial cycling will not reduce antimicrobial resistance in hospitals.," *Proc. Natl. Acad. Sci. USA* **101**, 13285–13290 (2004).

13 E. M. Brown and D. Nathwani, "Antibiotic cycling or rotation: a systemic review of the evidence of efficacy.," *Journal of Antimicrobial Chemotherapy* **55**, 6–9 (2005).

14 D. Nichol, P. Jeavons, A. G. Fletcher, *et al.*, "Steering evolution with sequential therapy to prevent the emergence of bacterial antibiotic resistance," *PLoS computational biology* **11**(9), e1004493 (2015).

15 M. Baym, T. D. Lieberman, E. D. Kelsic, *et al.*, "Spatiotemporal microbial evolution on antibiotic landscapes," *Science* **353**(6304), 1147–1151 (2016).

16 Q. Zhang, G. Lambert, D. Liao, *et al.*, "Acceleration of emergence of bacterial antibiotic resistance in connected microenvironments," *Science* **333**(6050), 1764–1767 (2011).

17 M. G. De Jong and K. B. Wood, "Tuning spatial profiles of selection pressure to modulate the evolution of drug resistance," *Phys. Rev. Lett.* **120**, 238102 (2018).

18 E. A. Yurtsev, H. X. Chao, M. S. Datta, *et al.*, "Bacterial cheating drives the population dynamics of cooperative antibiotic resistance plasmids," *Molecular systems biology* **9**(1), 683 (2013).

19 H. R. Meredith, A. J. Lopatkin, D. J. Anderson, *et al.*, "Bacterial temporal dynamics enable optimal design of antibiotic treatment," *PLoS computational biology* **11**(4), e1004201 (2015).

20 H. R. Meredith, J. K. Srimani, A. J. Lee, *et al.*, "Collective antibiotic tolerance: mechanisms, dynamics and intervention," *Nature chemical biology* **11**(3), 182–188 (2015).

21 N. M. Vega and J. Gore, "Collective antibiotic resistance: mechanisms and implications," *Current opinion in microbiology* **21**, 28–34 (2014).

22 N. Q. Balaban, J. Merrin, R. Chait, *et al.*, "Bacterial persistence as a phenotypic switch," *Science* **305**(5690), 1622–1625 (2004).

23 C. Tan, R. P. Smith, J. K. Srimani, *et al.*, "The inoculum effect and band-pass bacterial response to periodic antibiotic treatment," *Molecular systems biology* **8**(1), 617 (2012).

24 J. Karslake, J. Maltas, P. Brumm, *et al.*, "Population density modulates drug inhibition and gives rise to potential bistability of treatment outcomes for bacterial infections," *PLoS computational biology* **12**(10), e1005098 (2016).

25 J. P. Torella, R. Chait, and R. Kishony, "Optimal drug synergy in antimicrobial treatments.," *PlOS Comput. Biol.*. **6** (2010).

26 J. Michel, P. J. Yeh, R. Chait, *et al.*, "Drug interactions modulate the potential for evolution of resistance.," *Proc. Natl. Acad. Sci. USA* **105**, 14918–14923 (2008).

27 M. Hegreness, N. Shoresh, D. Damian, *et al.*, "Accelerated evolution of resistance in multi-drug environments.," *Proc. Natl. Acad. Sci. USA* **105**, 13977–13981 (2008).

28 R. Chait, A. Craney, and R. Kishony, "Antibiotic interactions that select against resistance," *Nature* **446**(7136), 668 (2007).

29 M. Baym, L. K. Stone, and R. Kishony, "Multidrug evolutionary strategies to reverse antibiotic resistance," *Science* **351**(6268), aad3292 (2016).

30 K. Wood, S. Nishida, E. D. Sontag, *et al.*, "Mechanism-independent method for predicting response to multidrug combinations in bacteria," *Proceedings of the National Academy of Sciences* **109**(30), 12254–12259 (2012).

31 A. Zimmer, I. Katzir, E. Dekel, *et al.*, "Prediction of multidimensional drug dose responses based on measurements of drug pairs," *Proceedings of the National Academy of Sciences* **113**(37), 10442–10447 (2016).

32 A. Zimmer, A. Tendler, I. Katzir, *et al.*, "Prediction of drug cocktail effects when the number of measurements is limited," *PLoS biology* **15**(10), e2002518 (2017).

33 M. R. de Evgrafov, H. Gumpert, C. Munck, *et al.*, "Collateral resistance and sensitivity modulate evolution in high-level resistance to drug combination treatment in *staphylococcus aureus.*," *Mol. Biol. Evol.* **32**, 1175–1185 (2015).

34 T. Oz, A. Guvenek, S. Yildiz, *et al.*, "Strength of selection pressure is an important parameter contributing to the complexity of antibiotic resistance evolution.," *Mol. Biol. Evol.* **31**, 2387–2401 (2014).

35 V. Lazar, I. Nagy, R. Spohn, *et al.*, "Genome-wide analysis captures the determinants of the antibiotic cross-resistance interaction network.," *Nat. Commun.* **5** (2014).

36 V. Lazar, G. P. Singh, R. Spohn, *et al.*, "Bacterial evolution and antibiotic hypersensitivity.," *Mol. Syst. Biol.* **9** (2013).

37 V. Lazar, A. Martins, R. Spohn, *et al.*, "Antibiotic-resistant bacteria show widespread collateral sensitivity to antimicrobial peptides.," *Nature Microbiology* **3**, 718–731 (2018).

38 L. Imamovic, M. Ellabaan, A. Machado, *et al.*, "Drug-driven phenotypic convergence supports rational treatment strategies of chronic infections.," *Cell* **172**, P121–134 (2018).

39 O. Shoval, H. Sheftel, G. Shinar, *et al.*, "Evolutionary trade-offs, pareto optimality, and the geometry of phenotype space," *Science* **336**(6085), 1157–1160 (2012).

40 Y. Hart, H. Sheftel, J. Hausser, *et al.*, "Inferring biological tasks using pareto analysis of high-dimensional data," *Nature methods* **12**(3), 233–235 (2015).

41 L. Imamovic and M. O. A. Sommer, "Use of collateral sensitivity networks to design drug cycling protocols that avoid resistance development.," *Sci. Transl. Med* **5**, 204ra132 (2013).

42 S. Kim, T. D. Lieberman, and R. Kishony, "Alternating antibiotic treatments constrain evolutionary paths to multidrug resistance.," *Proc. Natl. Acad. Sci. USA* **111**, 14494–14499 (2014).

43 A. Fuentes-Hernandez, J. Plucain, F. Gori, *et al.*, "Using a sequential regimen to eliminate bacteria at sublethal antibiotic dosages," *PLoS biology* **13**(4), e1002104 (2015).

44 R. Roemhild, C. Barbosa, R. E. Beardmore, *et al.*, "Temporal variation in antibiotic environments slows down resistance evolution in pathogenic pseudomonas aeruginosa," *Evolutionary applications* **8**(10), 945–955 (2015).

45 M. Yoshida, S. G. Reyes, S. Tsudo, *et al.*, "Time-programmable dosing allows the manipulation, suppression and reversal of antibiotic drug resistance *in vitro*.," *Nat. Commun.* **8** (2017).

46 R. Roemhild, C. S. Gokhale, P. Dirksen, *et al.*, "Cellular hysteresis as a principle to maximize the efficacy of antibiotic therapy," *Proceedings of the National Academy of Sciences* **115**(39), 9767–9772 (2018).

47 C. Munck, H. K. Gumpert, A. I. N. Wallin, *et al.*, "Prediction of resistance development against drug components by collateral responses to component drugs.," *Sci. Transl. Med* **6**, 262ra156 (2014).

48 C. Barbosa, R. Beardmore, H. Schulenburg, *et al.*, "Antibiotic combination efficacy (ace) networks for a pseudomonas aeruginosa model," *PLoS biology* **16**(4), e2004356 (2018).

49 C. Barbosa, V. Trebosc, C. Kemmer, *et al.*, "Alternative evolutionary paths to bacterial antibiotic resistance cause distinct collateral effects.," *Mol. Biol. Evol.* **34**, 2229–2244 (2017).

50 A. Dhawan, D. Nichol, F. Kinose, *et al.*, "Collateral sensitivity networks reveal evolutionary instability and novel treatment strategies in alk mutated non-small cell lung cancer," *Scientific Reports* **7** (2017).

51 D. Nichol, J. Rutter, C. Bryant, *et al.*, "Antibiotic collateral sensitivity is contingent on the repeatability of evolution," *Nature communications* **10**(1), 334 (2019).

52 D. B. Clewell, M. S. Gilmore, Y. Ike, *et al.*, *Enterococci: from commensals to leading causes of drug resistant infection*, Massachusetts Eye and Ear Infirmary (2014).

53 R. M. Donlan, "Biofilms and device-associated infections.," *Emerging infectious diseases* **7**(2), 277 (2001).

54 T. O'Driscoll and C. W. Crank, "Vancomycin-resistant enterococcal infections: epidemiology, clinical manifestations and optimal management.," *Drug Resis. Updat.* **8**, 217–230 (2015).

55 Y. Cetinkaya, P. Falk, and C. G. Mayhall, "Vancomycin resistant enterococci.," *Clin. Microbiol. Rev.* **13**, 686–707 (2000).

56 M. M. Huycke, D. F. Sahm, and M. S. Gilmore, "Multiple-drug resistant enterococci: the nature of the problem and an agenda for the future.," *Emerging infectious diseases* **4**(2), 239 (1998).

57 K. L. Palmer, A. Daniel, C. Hardy, *et al.*, "Genetic basis for daptomycin resistance in enterococci," *Antimicrobial Agents and Chemotherapy* **55**(7), 3345–3356 (2011).

58 C. Miller, J. Kong, T. T. Tran, *et al.*, "Adaptation of enterococcus faecalis to daptomycin reveals an ordered progression to resistance," *Antimicrobial agents and chemotherapy* , AAC–01473 (2013).

59 I. T. Paulsen, L. Banerjei, G. Myers, *et al.*, "Role of mobile dna in the evolution of vancomycin-resistant enterococcus faecalis," *Science* **299**(5615), 2071–2074 (2003).

60 M. Zwietering, I. Jongenburger, F. Rombouts, *et al.*, "Modeling of the bacterial growth curve," *Appl. Environ. Microbiol.* **56**(6), 1875–1881 (1990).

61 T. Kelesidis, R. Humphries, D. Z. Uslan, *et al.*, "Daptomycin nonsusceptible enterococci: an emerging challenge for clinicians," *Clinical Infectious Diseases* **52**(2), 228–234 (2011).

62 T. T. Tran, J. M. Munita, and C. A. Arias, "Mechanisms of drug resistance: daptomycin resistance," *Annals of the New York Academy of Sciences* **1354**(1), 32–53 (2015).

63 P. Bhardwaj, A. Hans, K. Ruikar, *et al.*, "Reduced chlorhexidine and daptomycin susceptibility in vancomycin-resistant enterococcus faecium after serial chlorhexidine exposure," *Antimicrobial agents and chemotherapy* **62**(1), e01235–17 (2018).

64 N. Bourgeois-Nicolaos, L. Massias, B. Couson, *et al.*, "Dose Dependence of Emergence of Resistance to Linezolid in Enterococcus faecalis In Vivo," *The Journal of Infectious Diseases* **195**, 1480–1488 (2007).

65 D. E. Deatherage and J. E. Barrick, "Identification of mutations in laboratory-evolved microbes from next-generation sequencing data using breseq.," *Methods Mol. Biol.* **1151**, 165–188 (2014).

66 K. Beabout, T. G. Hammerstrom, A. M. Perez, *et al.*, "The ribosomal s10 protein is a general target for decreased tigecycline susceptibility," *Antimicrobial Agents and Chemotherapy* **59**(9), 5561–5566 (2015).

67 D. Criswell, V. L. Tobiason, J. S. Lodmell, *et al.*, "Mutations conferring aminoglycoside and spectinomycin resistance in borrelia burgdorferi," *Antimicrobial Agents and Chemotherapy* **50**(2), 445–452 (2006).

68 W. R. Miller, J. M. Munita, and C. A. Arias, "Mechanisms of antibiotic resistance in enterococci," *Expert review of anti-infective therapy* **12**(10), 1221–1236 (2014).

69 L. Li, Q. Wang, H. Zhang, *et al.*, "Sensor histidine kinase is a β-lactam receptor and induces resistance to β-lactam antibiotics," *Proceedings of the National Academy of Sciences* **113**(6), 1648–1653 (2016).

70 S. L. Kellogg and C. J. Kristich, "Convergence of pasta kinase and two-component signaling in response to cell wall stress in enterococcus faecalis," *Journal of Bacteriology* **200**(12) (2018).

71 K. S. Long and B. Vester, "Resistance to linezolid caused by modifications at its binding site on the ribosome," *Antimicrobial Agents and Chemotherapy* **56**(2), 603–612 (2012).

72 P. M. De Silva and A. Kumar, "Signal transduction proteins in acinetobacter baumannii: Role in antibiotic resistance, virulence, and potential as drug targets," *Frontiers in Microbiology* **10**, 49 (2019).

73 C. Pál, B. Papp, and V. Lázár, "Collateral sensitivity of antibiotic-resistant microbes," *Trends in microbiology* **23**(7), 401–407 (2015).

74 M. A. Webber, V. Ricci, R. Whitehead, *et al.*, "Clinically relevant mutant dna gyrase alters supercoiling, changes the transcriptome, and confers multidrug resistance," *mBio* **4**(4) (2013).

75 J. E. Gomez, B. B. Kaufmann-Malaga, C. N. Wivagg, *et al.*, "Ribosomal mutations promote the evolution of antibiotic resistance in a multidrug environment.," *eLife* **6** (2017).

76 P. Yeh, A. I. Tschumi, and R. Kishony, "Functional classification of drugs by properties of their pairwise interactions.," *Nature Genetics* **38**, 489–494 (2006).

77 N. L. Podnecky, E. G. Fredheim, J. Kloos, *et al.*, "Conserved collateral antibiotic susceptibility networks in diverse clinical strains of escherichia coli.," *Nature Communications* **9** (2018).

78 R. E. Bellman and S. E. Dreyfus, *Applied dynamic programming*, vol. 2050, Princeton university press (2015).

79 E. A. Feinberg and A. Shwartz, *Handbook of Markov decision processes: methods and applications*, vol. 40, Springer Science & Business Media (2012).

80 R. Bellman, "A markovian decision process," *Journal of Mathematics and Mechanics* **6**(5), 679–684 (1957).

81 R. M. Humphries, S. Pollett, and G. Sakoulas, "A current perspective on daptomycin for the clinical microbiologist.," *Clin. Microbiol. Rev.* **26**, 759–780 (2013).

82 J. W. Chow, "Aminoglycoside Resistance in Enterococci," *Clinical Infectious Diseases* **31**, 586–589 (2000).

83 B. Zhao, J. C. Sedlak, R. Srinivas, *et al.*, "Exploiting temporal collateral sensitivity in tumor clonal evolution.," *Cell.* **165**, 1–13 (2016).

84 C. Barbosa, R. Roemhild, P. Rosenstiel, *et al.*, "Evolutionary stability of collateral sensitivity to antibiotics in the model pathogen pseudomonas aeruginosa," *bioRxiv* , 570663 (2019).

85 Y. J. Jiao, M. Baym, A. Veres, *et al.*, "Population diversity jeopardizes the efficacy of antibiotic cycling," *BioRxiv* , 082107 (2016).

86 W. Yu, K. M. Hallinen, and K. B. Wood, "Interplay between antibiotic efficacy and drug-induced lysis underlies enhanced biofilm formation at subinhibitory

drug concentrations," *Antimicrobial agents and chemotherapy* **62**(1), e01603–17 (2018).

87 M. Martin, T. Hölscher, A. Dragoš, *et al.*, "Laboratory evolution of microbial interactions in bacterial biofilms," *Journal of bacteriology* **198**(19), 2564–2571 (2016).

88 H. P. Steenackers, I. Parijs, K. R. Foster, *et al.*, "Experimental evolution in biofilm populations," *FEMS microbiology reviews* **40**(3), 373–397 (2016).

89 C. B. Turner, C. W. Marshall, and V. S. Cooper, "Parallel genetic adaptation across environments differing in mode of growth or resource availability," *Evolution letters* **2**(4), 355–367 (2018).

90 D. F. Sahm, J. Kissinger, M. S. Gilmore, *et al.*, "In vitro susceptibility studies of vancomycin-resistant enterococcus faecalis," *Antimicrobial Agents and Chemotherapy* **33**, 1588–1591 (1989).

CHAPTER III

Using Selection By Nonantibiotic Stressors to Sensitize Bacteria to Antibiotics

This chapter was amended from: Jeff Maltas, Brian Krasnick, and Kevin B. Wood. 'Using selection by nonantibiotic stressors to sensitize bacteria to antibiotics' Molecular Biology and Evolution 37(5), May 2020.

3.1 Introduction

As noted and demonstrated in the previous chapter, the emergence of drug resistance is continually shrinking an ever-smaller pool of drugs necessary for the successful treatment of infectious disease [1, 2, 3, 4, 5, 6, 7]. Interestingly, in addition to antibiotics, many studies have shown that exposure to non-antibiotic conditions, such as heavy metals, biocides, extreme temperatures, acidic or osmotic stress, and even growth media may also lead to reduced susceptibility to antimicrobials [8, 9, 10, 11, 12, 13, 14, 15, 16, 17]. For example, adaptation to the antiseptic chlorhexidine (CHX) was recently shown to be associated with collateral resistance to daptomycin, a lipopeptide antibiotic used to treat multidrug-resistant Gram-positive infections [12]. On the other hand, antibiotic resistant strains may exhibit increased sensitivity to antimicrobial peptides [18], and bacteria undergoing long-term evolution without drug generally show decreased antibiotic resistance [19]. As a whole, these studies point to overlapping evolutionary constraints that govern adaptation to a large and chemically diverse collection of deleterious environments. In turn, they raise the question of whether non-antibiotic stressors–which are frequently encountered in both clinical and natural environments–might play an important role in the evolution of drug resistance and, at the same time, represent an untapped set of environmental "levers" for steering evolutionary trajectories [20].

While there has been extensive progress identifying the molecular mechanisms governing cross-resistance between specific pairs of antibiotic and non-antibiotic stressors, relatively little is known about the systems-level properties of these evolutionary trade-offs. Phenotypic studies may complement mechanistic approaches by identify-

ing statistical relationships between large collections of stressors, offering new insights into questions that are difficult to answer from molecular information alone. For example, does adaptation to non-antibiotic stressors frequently lead to modulated antibiotic resistance, or are these effects relatively rare, restricted–perhaps–to structurally or mechanistically similar agents? When these collateral effects appear, are they dominated by cross-resistance, pointing to an ever-accelerating march to resistant pathogens with broad multi-agent resistance? Or do these conditions co-select for increased sensitivities, potentially leading to multi-agent environmental sequences that trap cells in evolutionarily vulnerable states? Recent evolution-based approaches have revolutionized our view of multidrug therapies [21]. Non-antibiotic stressors may offer a complementary set of unappreciated selective forces for simultaneously sensitizing pathogens to multiple drugs.

In this work we start to answer some of these questions using laboratory evolution and phenotypic profiling in an opportunistic bacteria pathogen. Specifically, we investigate phenotypic collateral effects arising during bacterial adaptation to 6 antibiotics and 7 non-antibiotic environments, including common biocides, extreme pH, and osmotic stress. As a model system, we focus on *E. faecalis*, a Gram-positive bacterial species frequently found in the gastrointestinal tracts of humans. *E. faecalis* can survive in a range of harsh environments, making it a good candidate for adaptation to many different environmental conditions. At the same time, *E. faecalis* is an important clinical pathogen that contributes to multiple human infections, including urinary tract infections and infective endocarditis [22, 23, 24, 25].

In the work done in Chapter 2, we used laboratory evolution to characterize the phenotypic collateral sensitivity profiles between multiple antibiotics in *E. faecalis* [26]. In this study, we show that collateral resistance and sensitivity are also surprisingly common between more general environmental stressors, both between different non-antibiotic stressors and between antibiotics and non-antibiotic condi-

tions. While the specific resistance profiles vary between independent populations, even when selected by the same condition, the collateral sensitivities remain common. For example, 25 of 32 isolates selected by the antimicrobial triclosan (TCS) exhibited increased sensitivity to at least one of the 6 antibiotics tested. Finally, we show experimentally that populations evolved to a sequence of two conditions (the antibiotic linezolid and the preservative sodium benzoate (NaBz)) can induce increased sensitivity to more conditions than adaptation to either stressor alone. The results demonstrate how sequential adaptation to drug and non-drug environments can be used to sensitize bacterial to antibiotics and highlight new potential approaches for leveraging evolutionary trade-offs inherent in adaptation to diverse environments.

3.2 Results

3.2.1 Collateral effects between antibiotic and non-antibiotic stressors are common.

To investigate collateral effects between antibiotic and non-antibiotic conditions, we exposed populations of *E. faecalis* strain V583, a clinical isolate [27], to increasing concentrations of a single condition for up to 60 days (approximately 450 generations) via serial passage evolution (Figure 3.1A, Methods). We repeated this laboratory evolution for 13 different selecting conditions, including extreme pH, osmotic stress, biocides, preservatives and traditionally known antibiotics (Table 2). Following laboratory evolution, we isolated a single colony ("mutant") from each population and measured its susceptibility to all 7 conditions as well as to 6 antibiotics spanning multiple classes via high-throughput dose-response experiments. In addition, we measured susceptibility of 6 previously isolated strains (one for each antibiotic; strains were originally isolated in [26]) to all 7 non-antibiotic stressors. To quantify resistance to each condition, we estimated the half maximal inhibitory concentration

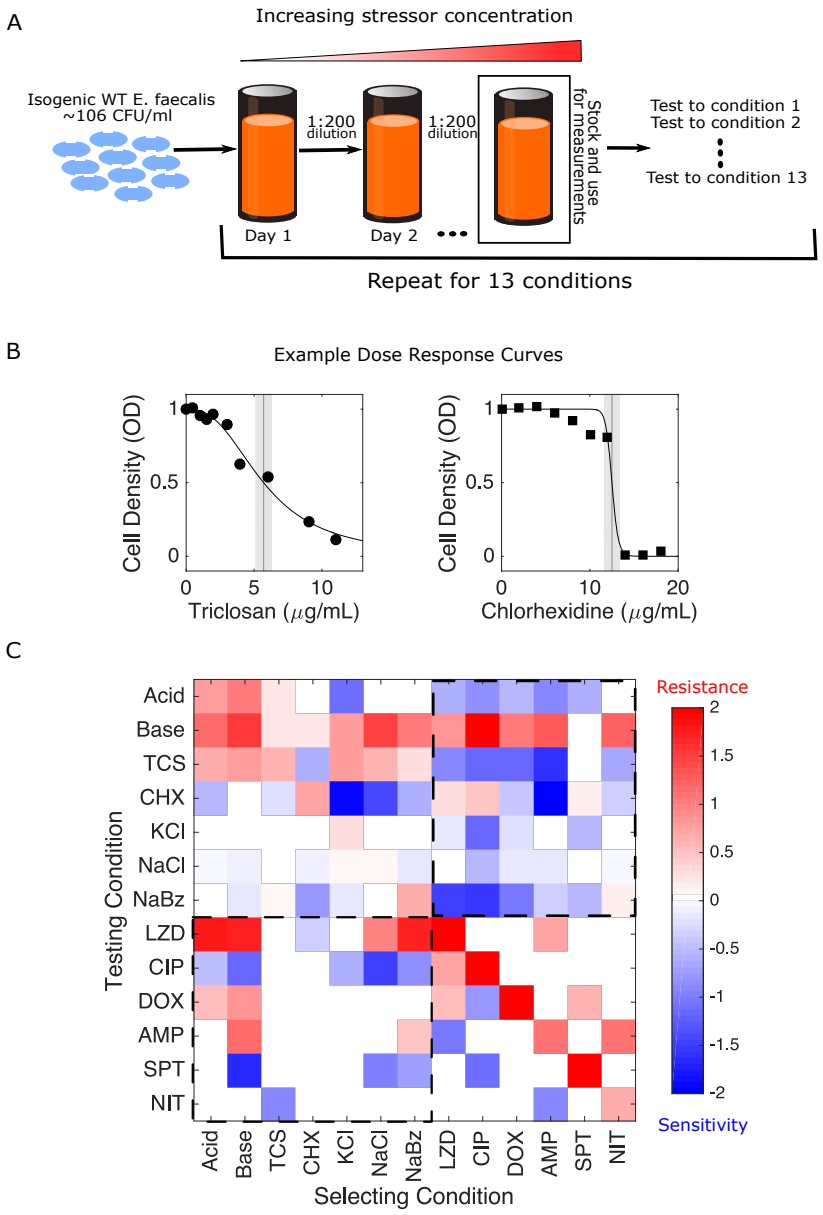

Figure 3.1: **Laboratory evolution reveals collateral sensitivity and cross resistance between antibiotics and environmental stressors in *E. faecalis*.** A. Populations of *E. faecalis* V583 were exposed to increasing concentrations of a single selecting condition over multiple days via serial passage experiments (Methods). The evolution was repeated for 13 different selecting conditions, including six antibiotics and seven non-antibiotic stressors (Table I). At the end of the evolution experiment, a single colony was isolated from each population and tested for modulated sensitivity to each of the 13 environmental conditions.

Figure 3.1: B. Example dose response curves for isolates selected by TCS (left) and chlorhexidine (right). Vertical line represents estimated half-maximal inhibitory concentration (IC_{50}), with shaded regions confidence intervals (95%). C. Resistance (red) or sensitivity (blue) to each condition is quantified using the ($\log_2$-transformed) fold change in the IC_{50} for the selected isolate relative to that of ancestral (V583) cells. Dashed regions correspond to antibiotic susceptibilities of non-antibiotic selected isolates (lower left) and, conversely, non-antibiotic susceptibilities of antibiotic selected isolates (upper right).

(IC_{50}) for all 13 isolates, as well as isolates from the ancestral populations, to each of the 13 conditions (Methods; Figure 3.1B). In total, we estimated the IC_{50} for 170 isolate-condition combinations (each performed in technical replicates of 3). For each isolate-condition combination, we then calculate $c \equiv \log_2 (IC_{50,Mut}/IC_{50,WT})$, the log-scaled fold change in IC_{50} of the mutant (relative to ancestral strains) (Figure 3.1C). Resistance therefore corresponds to $c > 0$ and sensitivity to $c < 0$. To minimize false positives, only c values larger than three σ_{WT} were deemed to have collateral sensitivity or collateral resistance, where σ_{WT} corresponds to the standard error of the mean across three technical replicates of the wild-type.

We find that isolates selected by antibiotics frequently exhibit modulated sensitivity to non-antibiotic conditions, and conversely, isolates selected by non-antibiotics often exhibit modulated sensitivity to antibiotics (Figure 3.1C). Sensitivity was altered in 62 percent (104/169) of condition-mutant pairs, with 58 percent (91/156) corresponding to collateral effects (i.e. modulated resistance to a stressor other than that used for selection). Collateral sensitivity is more common (58 percent, 53/91) than collateral resistance (42 percent, 38/91), though all 13 isolates exhibited both collateral resistance and collateral sensitivity to at least 2 distinct conditions. A histogram of all measured c resistance values (Figure 3.8), as well as the fraction of collaterally sensitive and resistant observations over a wide range of different cut-off values is available in the Supplementary files (Figure 3.8B). NaCl and KCl appear to have only acquired modest resistance. It is possible that resistance acquisition

may be slower to accumulate as *enterococcus* is naturally tolerant to many harsh environments including osmotic stress [28, 29].

We next asked whether the resistance profiles selected by different conditions show statistical similarities. Here, a resistance profile of a selecting condition is defined by a column in Figure 3.1C. One might hypothesize, for example, that profiles selected by chemically similar stressors would be strongly correlated with one another. On the other hand, correlations between profiles could also arise if different stressors are associated with molecularly promiscuous resistance determinants–for example, multidrug efflux pumps [30] that extrude unrelated chemical stressors. Indeed, we found strong correlations between the resistance profiles selected under many different pairs of conditions (Figure 3.2A). For example, profiles selected by NaCl are significantly correlated with those selected by acidic conditions, basic conditions, and NaBz. In addition, profiles selected by doxycycline, a protein synthesis inhibitor, are correlated with those selected by other structurally dissimilar compounds, including two antibiotics (LZD and ciprofloxacin (CIP)) as well as the antiseptic CHX. Overall, correlations between pairs of selecting conditions are dominated by positive correlations (62/78 pairs), including in all 9 pairs eclipsing the significance ($p < 0.01$) threshold. Similarly, we asked whether resistance levels between pairs of different *testing* conditions were correlated across different isolates. Here, a resistance profile of a testing condition is defined as a row in Figure 3.1C. We found positive correlations to also be slightly more common between testing conditions (45/78 pairs), though two of the three pairs eclipsing significance ($p < 0.01$) exhibited negative correlations. Specifically, we found negative correlations between resistance to NaCl and basic conditions and between CIP and TCS, but positive correlations between CIP and spectinomycin (SPT) (See also Figure 3.5 and Figure 3.6 for scatter plots between all pairs of selecting and testing conditions, respectively).

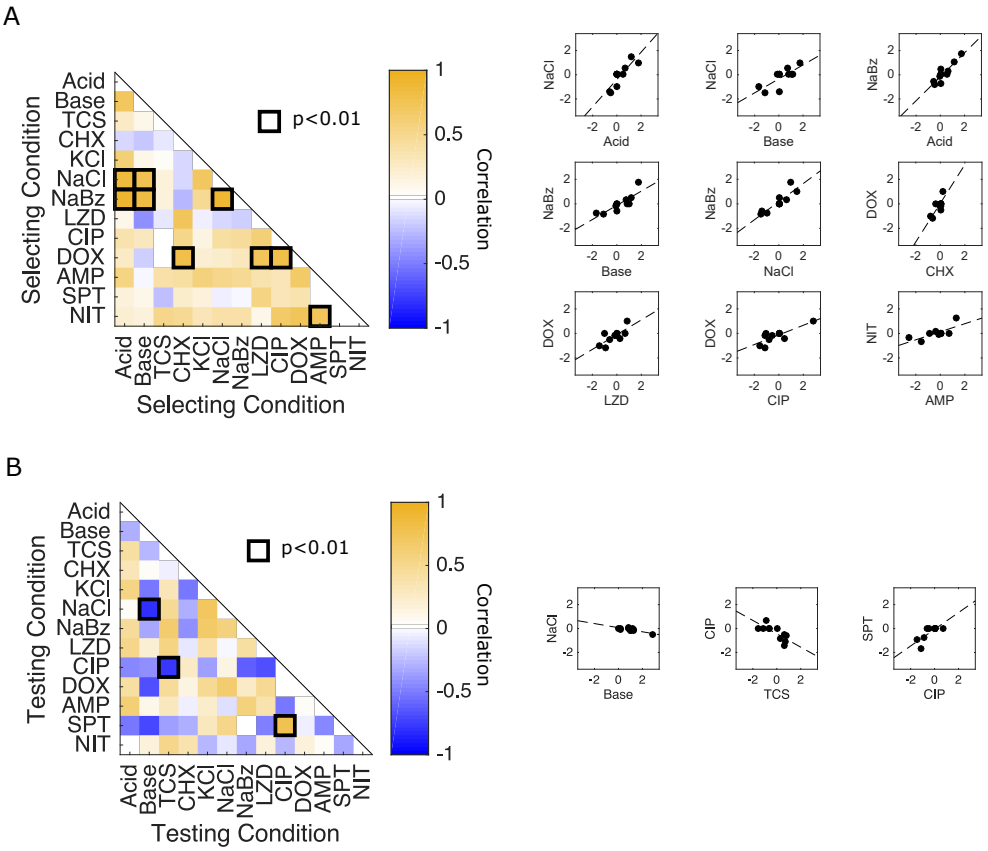

Figure 3.2: **Correlations between collateral effects under different selecting or testing conditions** A. Left panel: Pearson correlation coefficient between collateral profiles (i.e. columns of the matrix in Figure 1C) selected under different conditions. Dark squares highlight significant correlations ($p < 0.01$), which are also shown as scatter plots. Right panels: pairwise scatter plots of resistance profiles selected by different conditions (i.e. scatter plots comparing columns of the matrix in Figure 1C; only pairs with significant correlations, $p < 0.01$, are shown). Each point represents the measured resistance to a single stressor in isolates selected by the conditions on the horizontal and vertical axes. That is, each point is the resistance value c in each of the two conditions labeled by the axis.

Figure 3.2: B. Left panel: Pearson correlation coefficient between resistance levels to a particular testing condition (i.e. rows of the matrix in Figure 1C) across the ensemble of isolates. Dark squares highlight significant correlations ($p < 0.01$). Right panels: pairwise scatter plots of resistance levels to different conditions (i.e. scatter plots comparing rows of the matrix in Figure 1C; only pairs with significant correlations, $p < 0.01$, are shown). Each point represents a single isolate and shows the resistance of that isolate to the pairs of testing conditions on the horizontal and vertical axes. Put another way, each point represents the value c to each condition on the axis. To remove the effects of direct selection, which are typically larger in magnitude and may bias the correlations, the diagonal entries of the collateral sensitivity matrix (corresponding to resistance to the selecting condition) are removed prior to calculating all correlations. In all cases, resistance is measured in units of ($\log_2$-scaled) fold change in IC_{50} relative to ancestral strain. See Figure 3.5 and Figure 3.6 for scatter plots for all pairs.

3.2.2 Strains selected by non-antibiotic pressures often carry mutations in genes known to confer antibiotic resistance or sensitivity.

To identify candidate genes that may underlie changes in sensitivity to one or more environments, we performed whole genome sequencing on both single isolates (a single colony selected from an agar plate) and population samples (well-mixed 200 μL samples) from the evolved populations. Specifically, we sequenced single isolates from each evolved population, an isolate evolved in media (BHI) only for 8 days, and also two individual isolates from the ancestral strains. In addition, we performed population sequencing on a sample from each population, including the media-selected control. Because the number of variant calls rises rapidly for small mutation frequencies (Figure 3.7), we limit our analysis to variants estimated to occur with frequency greater than 30 percent (Methods). Note that samples from four of the antibiotic-selected populations (those selected by AMP, DOX, NIT, SPT) and the BHI-population were sequenced for a previous study [26] and their results are included here for comparison. In addition, we exclude sequencing from the acid-selected population, which was contaminated during preparation for sequencing, and exclude

variants occurring in all sequenced strains. As a final control, we also confirmed a small number of mutations (in *rpsJ* in the DOX-selected isolate and in *parC* in the CIP-selected isolate) via PCR amplification and Sanger sequencing.

Overall, we observe significant agreement between population and single isolate sequencing; every mutation that occurs in the clonal sample also occurs with at least 68 percent frequency in the corresponding population sample (Table 1). Similarly, all mutations occurring at a frequency of at least 90 percent in the population samples also occurs in the clonal sequences. Despite this agreement, we do observe apparent heterogeneity in several populations (e.g. LZD).

This consistency suggests that the phenotypic measurements, performed on single clones isolated from each population, are generally representative of the entire population, though more substantial population heterogeneity is apparent in a several cases (e.g. LZD).

This analysis reveals 54 mutations achieving at least 30 percent frequency in at least one population. All mutations identified were non-synonymous. Using this 30 percent threshold, we see as many as 9 mutations in a strain (KCl) and as few as zero (NIT). While we observe no mutations in the NIT strain, repeated experiments confirm increased resistance. Because the resistance is relatively small (less than a factor two increase), it is possible the observed resistance stems from transient phenotypic resistance related to the post-antibiotic effect or cellular hysteresis observed when rapidly cycling drugs [31]. The control population selected by media alone showed no mutations above 30 percent frequency. 52 of the 54 mutations occurred on the choromosome, while both *prgB* mutations occured on the pTEF2 plasmid. In addition, we see several mutations present in genes known to confer resistance to the selecting drug. For example, the CHX-selected population contains two previously identified mutations responsible for CHX resistance, one in *EF_1608*, a cardiolipin synthetase, and one in EF_2227, an ABC transporter [12, 32]. The TCS isolate con-

Table 3.1: **Mutations identified in selected populations.** Mutations listed in red have been previously linked with resistance to the selecting condition, while genes listed in blue are genes previously identified with resistance to environments other than the selecting condition. Asterisk (*) identifies strains evolved and sequenced for previous work.

Sample	Gene	Pop (%)	Clonal	Description
AMP*	*EF_3191* ← / → *EF_3192*	100	✓	Intergenic
	pyrR ←	43.1		Regulates pyrimidine biosynthesis
	hexA ←	31.7		DNA repair protein
	EF_3290 →	93	✓	Sensor histidine kinase
BASE	*EF_0096* ← / → *EF_0097*	100	✓	Intergenic
	recU ← / → *EF_1150*	100	✓	Intergenic
	EF_1711 ← / ← *pyrE*	100	✓	Intergenic
	ccpA ← / → *pepQ-2*	100	✓	Intergenic
	EF_1204 → / ← *EF_1206*	58.4		Intergenic
	EF_1936 ←	60.6		Conserved hypothetical protein
	EF_3014 ← / ← *EF_3015*	94	✓	Intergenic
CIP	***parC*** ←	100	✓	Topoisomerase IV
	EF_0184 → / → *deoB*	31.9		Intergenic
	[EF_tRNALeu3]–[EF_1076]	100	✓	24-gene deletion
DOX*	*rpsJ* →	100	✓	30S ribosomal protein S10
	rpsJ →	87	✓	30S ribosomal protein S10
	prgB →	100	✓	Surface aggregation protein
CHX	*EF_1608* ←	100	✓	Cardiolipin synthetase
	EF_2227 →	100	✓	ABC transporter
	rpoC ←	100	✓	RNA polymerase
	EF_1187 →	30.6		Conserved hypothetical protein
	EF_1456 →	68.3	✓	Conserved hypothetical protein
	EF_1570 →	38.9		Conserved hypothetical protein
	EF_3114 ←	74.7	✓	Conserved hypothetical protein
KCl	EF_1096 → / → EF_1097	100	✓	Intergenic
	vicK →	100	✓	Sensor histidine kinase
	galU ←	100	✓	UDP-glucose pyrophosphorylase
	EF_1789 ←	100	✓	Conserved hypothetical protein
	EF_2348 ←	100	✓	Conserved hypothetical protein
	EF_2886 ←	100	✓	*marR* family transcriptional regulator
	recA ←	100	✓	DNA repair protein
	EF_0871 → / → *EF_0872*	40.6		Intergenic
	glnA ←	36		Glutamine synthetase
LZD	*EF_1414* ←	100	✓	Conserved hypothetical protein
	EF_0149 → / ← *EF_0150*	34.1		Intergenic
	EF_0797 ←	66.6		Conserved hypothetical protein
	EF_0871 → / → *EF_0872*	33.8		Intergenic
	EF_0871 → / → *EF_0872*	49.4		Intergenic
	prgB →	78.8		Surface aggregation protein
NaBz	***EF_1148*** ←	100	✓	Penicillin binding protein 1A
	atpD ←	100	✓	ATP synthase F1, beta subunit
	EF_0871 → / → *EF_0872*	32.6		Intergenic
	EF_0871 → / → *EF_0872*	31.2		Intergenic
	EF_2604 ←	89.6		Conserved hypothetical protein
NaCl	***vicK*** →	100	✓	Sensor histidine kinase
	codY ←	100	✓	Transcriptional regulator
	EF_2886 ←	100	✓	*marR* family transcriptional regulator
	galU ←	91.8	✓	UDP-glucose pyrophosphorylase
SPT*	*rpsE* →	100	✓	40S ribosomal protein S5
TCS	***EF_0142*** →	100	✓	Multi-drug efflux pump
	fabI ←	100	✓	Triclosan target
	EF_1972 ←	100	✓	Conserved hypothetical protein
	EF_1151 → / → *EF_1152*	37.9		Intergenic
	EF_3074 ←	34		Conserved hypothetical protein

tains a mutation in *fabI*, a common TCS resistance gene and the drug's target [33], as well as *EF_0142*, an efflux multi-drug resistance transporter [34]. We identify a shared mutation between KCl and NaCl in *vicK*, a sensor histidine kinase known to confer resistance to environments such as osmotic stress, pH and temperature [35]. In addition, the DOX-selected population contains two mutations in *rpsJ*, a gene known to confer resistance to the tetracycline class of antibiotics [36], and the CIP-selected population contains a *parC* mutation, a gene known to confer high levels of CIP resistance [37], both of which were reported previously [26].

In addition to mutations present in genes linked with resistance to the selecting condition, we also identified mutations in genes potentially responsible for modulated sensitivity to non-selecting conditions, including mutations to genes known to confer antibiotic resistance in populations selected by non-antibiotic stressors. For example, the NaCl- and KCl-selected populations harbor a mutation in *EF_2886*, a *marR* family transcriptional regulator. The *marR* system is known to regulate efflux pump activity and underlies resistance to a wide range of structurally diverse drugs [38, 39, 40]. Recent work indicates that increased efflux activity comes with a trade-off, as corresponding changes in the proton-motive force can induce sensitivity to aminoglycoside antibiotics [41]. Consistent with these findings, we find that an isolate selected by NaCl exhibited increased sensitivity to the aminoglycoside SPT. The *marR* system is also known to confer resistance to oxidative stress, similar to TCS [42, 40]; it is perhaps not surprising, then, that we observe TCS resistance in populations selected by either NaCl or KCl. We also identify a mutation in EF_1148, a penicillin binding protein (PBP), in isolates selected by NaBz. Mutations in PBPs are known to confer resistance to β-lactam antibiotics [43], and indeed we observe cross-resistance to AMP in isolates from the NaBz-selected population.

Finally, we identify mutations in genes that have been previously linked with collateral sensitivity or resistance to antibiotics, though we observe phenotypes that

differ from those expected. For example, the *marR* mutation in KCl and NaCl, the *EF_2227* mutation in CHX, and the *EF_0142* mutation in TCS are all related to efflux pumps, which are known to confer resistance to a wide array of antibiotics and biocides, especially tetracyclines and quinolones [41, 39]; surprisingly, we see no increased resistance to these antibiotics in the corresponding isolates (Figure 3.1). Additionally, NaCl and KCl share a mutation in *galU* which is known to confer pleiotropic effects [44] and AMP resistance [45], though we see no increase in AMP resistance in isolates from the same population (Figure 3.1). These discrepancies could arise for several reasons. First, while we observe mutations in genes linked with drug resistance, the specific mutations are not necessarily the same. For example, the study of *EF_2227* focuses on the full gene knockout while we observe a single nonsynonymous substitution [32]. On the other hand, the discrepancies could also be explained by epistatic effects that potentially differ in different genetic backgrounds, giving rise to variable phenotypes [46, 47, 48, 49, 50, 51, 52, 53]. It is possible that the isolate selected for phenotyping represents a rare variant of the population and therefore is not well-described by the population sequencing, though the relatively high frequencies estimated for most variants suggests this explanation is unlikely in many cases. A full list of all identified mutations is available with more details in the SI.

3.2.3 Selection by chlorhexidine or triclosan frequently sensitize bacteria to at least one antibiotic.

Previous studies have shown that collateral profiles may be highly variable, even when selection is performed multiple times under the same conditions [54, 26]. To estimate this variability for non-antibiotic stressors, we evolved 32 replicate populations to each of two antimicrobials, TCS and CHX, for a total of 22 days (approximately 170 generations). TCS is an antimicrobial agent found in numerous consumer

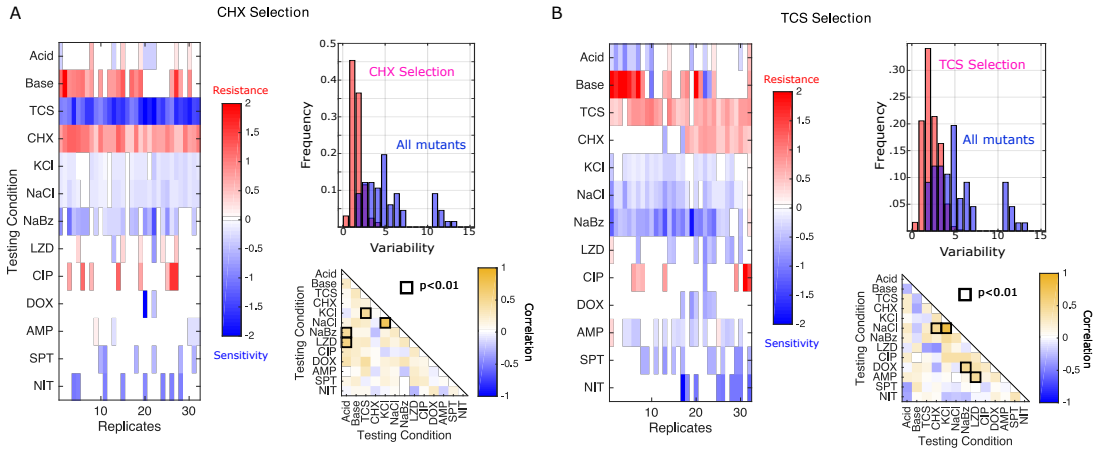

Figure 3.3: **Isolates selected by CHX or TCS are variable but often exhibit increased sensitivity to antibiotics** Collateral resistance profiles for 32 independent populations evolved to either CHX (A) or TCS (B). Left panels: Resistance (red) or sensitivity (blue) to each condition (rows) is quantified using the ($\log_2$-transformed) fold change in the IC_{50} for the selected isolate relative to that of ancestral (V583) cells. Color scale ranges from -2 (4x decrease in IC_{50}, blue) to +2 (4x increase in IC_{50}, red). Top right: Histogram of variability in collateral profiles for isolates selected by CHX / TCS (red) or for the isolates in Figure 3.1 (spanning all conditions, blue). Variability for each collateral profile is defined as the Euclidian distance between that profile and the centroid formed by the relevant ensemble of profiles. Mean variability differs between isolates selected by CHX and all isolated mutants, as well as between isolates selected by TRC and all isolated mutants, each with $p < 0.001$ (t-test with unequal variance). Bottom right: Pearson correlation coefficient between resistance levels to a particular testing condition across the ensemble of isolates.

products, including soaps, body washes, and toothpastes. It has been linked with cross-resistance to antibiotics in multiple species [14] and was recently shown to induce resistance to antibiotics both in vitro and in vivo [55]. CHX is an antimicrobial found in many disinfectants and commonly used as a general antiseptic in hospitals. CHX exposure has been linked with increased resistance to daptomycin in *E. faecium*, a closely related enterococcal species [12]. Following the laboratory evolution to each condition, we measured the resistance profiles for single isolates from each population to all 13 environmental conditions (Figure 3.2.2). Surprisingly, isolates selected by each condition frequently exhibit collateral sensitivity to other agents, with 15/32 CHX isolates and 25/32 TCS isolates showing sensitivity to at least one antibiotic. In addition, all 32 CHX isolates showed strong sensitivity to TCS, while half of the 32 TCS isolates show cross-resistance to CHX.

To quantify variation within an ensemble of collateral profiles, we considered each profile as a 13-dimensional vector, with each component representing resistance to a particular environmental condition. To estimate variability within the ensemble, we calculated the mean pairwise (Euclidean) distance, $\langle d_p \rangle$, across all pairs of profiles in the ensemble. While collateral profiles of isolates selected by TCS ($\langle d_p \rangle = 2.2$) and CHX ($\langle d_p \rangle = 1.6$) both exhibit isolate-to-isolate variability, it is considerably smaller than the variability observed across all conditions ($\langle d_p \rangle = 5.2$). In addition, the distribution of pairwise distances between isolates selected by the same condition (TCS or CHX) is considerably more narrow that the distribution across all isolates (Figure 3.2.2, upper right insets). We also tested for correlations between resistance levels to pairs of stressors across the ensemble of isolates for each condition. Not surprisingly, the correlations between pairs of stressors vary substantially depending on the selecting conditions used to generate the isolates (compare insets in Figure 3.2.2A, Figure 3.2.2B). For example, resistance to KCl is correlated with resistance to TCS following CHX selection (Figure 3.2.2A, lower right) but weakly anticorrelated in

TCS-selected isolates (Figure 3.2.2B, lower right). On the other hand, there are rare pairs of environments–such as NaCl and KCl–where resistance is strongly correlated in all sets of isolates, likely reflecting the extreme chemical similarity between the stressors.

3.2.4 Sequential rounds of antibiotic and non-antibiotic selection can promote sensitivity.

Our results indicate that both collateral sensitivity and cross resistance are surprisingly common in the evolved lineages. Selection by one condition (by definition) leads to resistance to that condition, but it frequently sensitizes the population to multiple other conditions. In fact, our experiments showed that selection by one stressor led to increased sensitivity to between 3 and 7 other conditions (Figure 3.1B). Unfortunately, these increased sensitivities are also accompanied by frequent cross-resistance, placing limits on the number of sensitivities that can be selected by any one condition.

However, we hypothesized that it might be possible to circumvent those limitations by using a sequence of two stressors. While this sequential selection is likely to produce resistance to, at minimum, the two selecting conditions, it's possible that judiciously chosen conditions could lead to more sensitivities than either condition alone–in effect harnessing the orthogonal sensitizing effects of particular pairs of selective forces. To guide our search, we first calculated the expected number of sensitivities following sequential selection by each pair of conditions under the naive assumption that phenotypic effects are purely additive. Because resistance is measured on a log scale, the assumption of additivity means that relative changes in IC_{50} (or similar) are multiplicative; for example, if conditions 1 and 2 each reduce IC_{50} to 40 percent of the value in ancestral cells, their sequential application would reduce IC_{50} to 16 percent. We note that such null models are imperfect, as they fail

to capture epistasis and known hysteresis in evolutionary trajectories (see, for example, [56]). Here we use the null model only to identify candidate condition pairs for further experimental investigation. Under these additivity assumptions, the number of sensitivities is expected to increase for most pairs of stressors; that is, assuming additivity of the measured sensitivity profiles, sequential exposure to pairs of stressors is often predicted to sensitize the population to more stressors than exposure to either single agent alone (Figure 3.2.4A). In three cases (LZD-NaCl, LZD-NaBz, and NIT-SPT), the number of sensitivities is expected to increase by three or more, providing a substantial benefit over the single agent selecting conditions.

To test these predictions experimentally, we focused on the pair LZD, a protein synthesis inhibitor, and NaBz, a commonly used food preservative. Our original selection experiments showed that selection in LZD led to 5 sensitivities and NaBz led to 4 sensitivities; the sensitivities are largely non-overlapping, and sequential selection is therefore predicted to an increase in the number of sensitivities. To test this prediction, we performed experimental evolution on eight replicate populations to each of 3 conditions: LZD alone, NaBz alone, and a two-phase sequence consisting of LZD evolution followed by NaBz evolution. For convenience, we limited each evolution phase to 10 days (70-80 generations), making this considerably shorter than the original adaption in Figure 3.1. We then tested an isolate from each population for modulated resistance to each of the 13 environmental conditions (Figure 3.2.4B).

The isolates selected by LZD or NaBz alone had sensitivity profiles that are similar, but not identical, to those selected in the original experiment (Figure 3.1). For both conditions, the single agent evolution led to increased sensitivity to an average of approximately 4 conditions (Figure 3.2.4C). Strikingly, however, evolution in the LZD-NaBz sequence ("switch") sensitized the isolates to more than 6 conditions on average, with some isolates exhibiting sensitivity to eight conditions.

To test the quantitative accuracy of the null model, we generated an ensemble

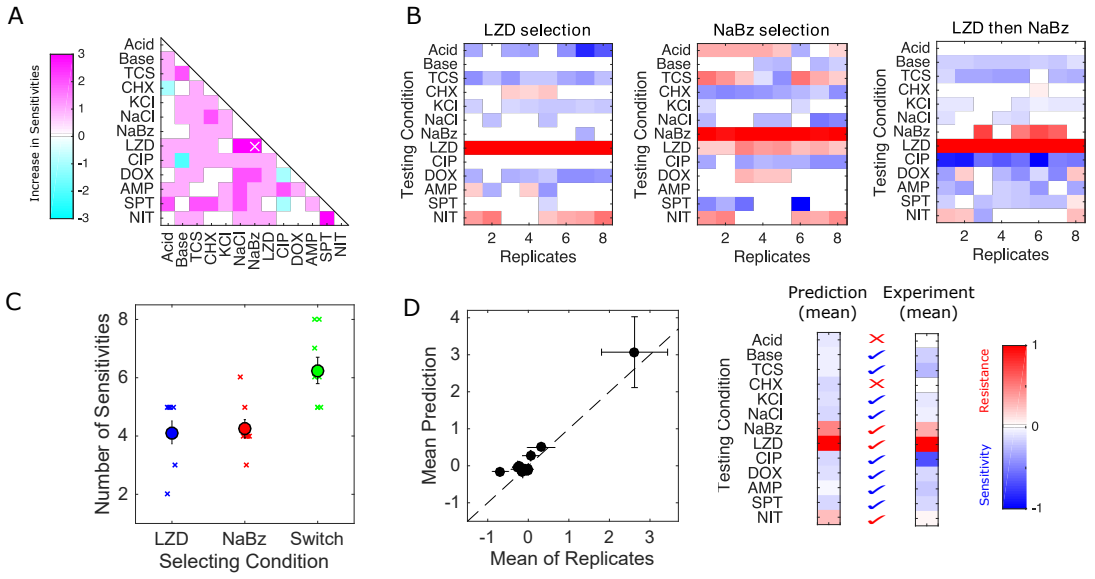

Figure 3.4: **Selection in alternating environments can induce sensitivity to more stressors than selection in single environments** A. Predicted change in number of sensitivities following sequential evolution using pairs of conditions. Change is positive if sequential evolution is predicted to result in more sensitivities than evolution in either component alone. Predictions assume additivity of (log-scaled) resistance profiles. A sequence of LZD and NaBz (white x) is predicted to give the maximum increase in sensitivities. B. Resistance profiles for replicate evolution experiments (8 per condition) in LZD only, NaBz only, or a two-step sequence consisting of LZD selection followed by NaBz selection. Resistance (red) or sensitivity (blue) to each condition (rows) is quantified using the ($\log_2$-transformed) fold change in the half-maximal inhibitory concentration (IC_{50}) for the selected isolate relative to that of ancestral (V583) cells. C. Left panel: Isolates evolved in the alternating environment ("switch" between LZD then NaBz, green) exhibit sensitivity to more environments than isolates selected in each environment alone (blue and red; $p < 0.01$, Wilcoxon rank sum test for pairwise comparisons between LZD and switch and between NaBz and switch. D. Left: scatter plot comparing the mean collateral profile of isolates from the alternating selection ("experiment") and mean collateral profiles predicted by an average (linear sum) of profiles generated in the single environments ("prediction"). Right panel: heat maps (color scale same as for panel A). Check marks indicate correctly predicted sensitivity (blue) or resistance (red). X indicates incorrect prediction.

of plausible resistance profiles for the sequential selection experiment. Each profile in the predicted ensemble corresponds to the mean of one pair of profiles, with one member of the pair drawn from the LZD only selection (Figure 3.2.4B, left) and one drawn from the NaBz only selection (Figure 3.2.4B, middle). The mean profile in this ensemble agrees surprisingly well with the mean profile measured in the LZD-NaBz evolution (Figure 3.2.4D).

3.3 Discussion

These results provide a systems-level picture of the phenotypic trade-offs accompanying evolved resistance to antibiotic and non-antibiotic stressors in an opportunistic pathogen. We find that collateral resistance and collateral sensitivity are surprisingly pervasive across conditions, underscoring the need to better understand how adaptation to non-antibiotic environments may contribute to drug resistance. These widespread collateral effects raise the question of whether frequently encountered stressors–food additives, preservatives, biocides, or simply common elements of natural environments–may steer bacteria toward multidrug resistance, and in turn, whether there may be an unappreciated role for these agents in slowing or reversing resistance. As proof-of-principle, we showed experimentally that sequential adaptation to different environments can be used to sensitize bacterial to antibiotics, a consequence of the largely non-overlapping sensitivities induced by each agent alone.

The goal of this study was to investigate patterns of resistance between antibiotics and non-drug stressors at a phenotypic level. By taking a systems-level view, we hoped to gauge the prevalence of collateral sensitivity and assess the potential of non-antibiotic agents for modulating resistance. As the drawbacks of this study are the same as the previous chapter, they will not be re-stated here. There are many well-known examples of molecular mechanisms that confer non-specific collateral resistance to structurally unrelated compounds in bacteria, including a number

of multidrug resistance transporters and efflux pumps [38, 34, 57, 30]. Collateral sensitivity, on the other hand, remains much less understood, even simply between antibiotics. Recent evidence suggests these sensitivities may be governed by target mutations that induce global changes in gene regulation or by mutations altering drug uptake and efflux [58]. Similar mutations appear in our evolved mutations, suggesting that these mechanisms may also underlie many of the observed collateral effects between antibiotic and non-antibiotic stressors. However, definitely linking particular mutations with phenotypic effects will require considerable follow-up work to disentangle, for example, the potential effects of mutational epistasis and genetic background on drug resistance phenotypes. In addition, while we used standard alignment protocols, identifying repeat sequences or mobile element mutations such as insertion sequences remains a challenge. Because mobile elements play an important role in V583 evolution, it is likely we were unable to identify some important mutations.

Additionally, it is not clear how these results might change if experiments were performed in a different ancestral strain. Most notably, strain V583 is highly resistant to multiple antibiotics,; adaptation dynamics in strains without high level multidrug resistance could differ substantially. Indeed, recent work underscores the notion that the ability to evolve antibiotic resistance depends on genotype (and therefore potentially history) [48]. Finally, we note that because we have limited the sequencing analysis to mutations that appear relatively frequently (>30 percent), our analysis omits some features of population heterogeneity that may play an important role in the evolution of collateral sensitivity. Future work may aim to further investigate links between this heterogeneity and the potential for gene-specific variations in mutation rates and selection.

We have shown experimentally that sequential adaptation to antibiotic and non-antibiotic conditions can sensitize bacteria to more environments than either agent

alone. While we focus here on a clinically relevant bacterial species, it is not clear that these results will generalize to other species. We used a simple additive model to identify candidate environmental pairs for sequential selection. While the model gave surprisingly accurate predictions in these experiments, it will clearly fail when effects of epistasis or evolutionary hysteresis are strong [59]. On the other hand, if epistasis effects are approximately symmetric about zero or typically small, additive null models–similar, in spirit, to those developed for drug combination effects [60]–may still prove useful for finding environmental pairs that increase the number of sensitivities, though the predictions of specific profiles are likely to become increasingly inaccurate. Long-term application will therefore require continued experimental mapping of the collateral sensitivity profiles selected by increasingly complex and realistic environmental conditions.

Table 3.2: **Table of antibiotics used in this study and their targets.**

Condition (abbreviation)	**Class**	**Mechanism of Action**
Ampicillin (AMP)	β-lactam	Inhibits cell wall synthesis
Doxycycline (DOX)	Tetracycline	30S protein synthesis inhibitor
Spectinomycin (SPT)	Aminoglycosides	30S protein synthesis inhibitor
Linezolid (LZD)	Oxazolidinone	50S protein synthesis inhibitor
Ciprofloxacin (CIP)	Quinolone	DNA gyrase inhibitor
Nitrofurantoin (NIT)	Nitrofuran	Multiple mechanisms
Chlorhexidine (CHX)	Biocide	Disrupts the cell membrane
Triclosan (TRC)	Biocide	Inhibits fatty acid synthesis
Sodium Benzoate (NaBz)	Preservative	Decreases intracellular pH
Alkaline pH (Base)	N/A	N/A
Acidic pH (Acid)	N/A	N/A
Potassium Chloride (KCl)	N/A	N/A
Sodium Chloride (NaCl)	N/A	N/A

3.4 Materials and Methods

3.4.1 Strains, antibiotics, non-antibiotics and media.

All mutants were derived from *E. faecalis* V583, a fully sequenced vancomycin-resistant clinical isolate [61]. The 13 conditions used to select mutants are listed in Table 1. Antibiotics were prepared from powder stock and stored at -20C with the exception of ampicillin, which was stored at -80C. TCS, CHX and NaBz were prepared from powder stock and stored at -20C. Acid (pH≈1.5) and Base (pH> 10.5) stock solutions were prepared by titrating HCl and NaOH, respectively, into BHI medium. These stock solutions were mixed in appropriate volumes with standard BHI (pH≈7) to create selecting media for evolution experiments. Saturated KCl and NaCl stock solutions were prepared by dissolving KCl and NaCl into BHI medium. As with acid and base, appropriate mixtures of saturated KCl and NaCl solutions were mixed with standard BHI medium. Evolution and IC_{50} measurements were conducted in

BHI medium alone.

3.4.2 Laboratory evolution experiments

Evolution experiments were performed in 96-well plates with a maximum volume of 2 mL and a working volume of 1 mL BHI. Each day, at least three replicate populations were each grown in a different concentrations of the selecting agent. The concentrations were chosen to include both sub- and super-inhibitory concentrations. After 20-23 hours of incubation at 37C, aliquots (5 μL) from the population that survived (OD>0.3) the highest concentration were added to a new series of wells and the procedure was repeated for 30-60 days (maximum of about 450 generations). Note that isolates from antibiotic selection experiments were evolved for only 8 days (maximum of 60 generations), because resistance to antibiotics increased much more rapidly than resistance to other agents (see [26]). To achieve roughly similar levels of resistance to the non-antibiotic conditions, we extended the selection time window until either 1) we observed 2-3 days of growth in a concentration at least two times the ancestral MIC or 2) until the resistance appeared to plateu. Adaptation experiments to CHX and TRC lasted for 30 and 50 days respectively, while NaCl, KCl, acid, base and NaBz experiments continued for a total of 60 days. On the final day of selection, we plated a sample from each population on BHI agar plates, isolated a single colony from each plate, and stored the remaining population volume at -80C in 30 percent glycerol.

3.4.3 Measuring drug resistance and sensitivity

IC_{50} measurements for each condition/drug were performed in triplicate for each isolate (except in the case of the ancestral wild-type strain, which was performed in replicates of 8) in 96-well plates by exposing mutants in different wells to 6-10 concentrations of drug, typically in a linear dilution series prepared in BHI medium.

After 12 hours of growth at 37C, the optical density at 600 nm (OD) was measured using an Enspire Multimodal Plate Reader (Perkin Elmer) with an automated 20-plate stacker assembly.

Each OD reading was normalized to the OD reading for the same isolate in the absence of drug. To quantify resistance, the resulting dose response curve was fit to a Hill-like function $f(x) = (1 + (x/K)^h)^{-1}$ using nonlinear least squares fitting, where K is the half-maximal inhibitory concentration (IC_{50}) and h is a Hill coefficient describing the steepness of the dose-response relationship. A mutant strain was deemed collaterally sensitive (resistant) if its IC_{50} varied by more than $3\sigma_{WT}$ from that of the ancestral strain, where σ_{WT} is the uncertainty (standard error across 8 replicates) of the IC_{50} measured in the ancestral strain. Note that all estimates of IC_{50} in the ancestral ("wild-type") strain, across all replicates and for all conditions, are contained in this $\pm 3\sigma_{wT}$ range, which suggests that there are unlikely to be false positives in designating isolates as sensitive or resistant.

3.4.4 Whole-genome sequencing

We sequenced single isolates and population samples from the 13 evolved populations and a control V583 strain propagated in BHI for 8 days. We also sequenced single isolates from two (ancestral) V583 frozen stocks. Samples from each population were streaked from a frozen stock, grown overnight in BHI, and triple washed in PBS. DNA was isolated using a Quick-DNA Fungal/Bacterial Kit (Zymo Reserach) according to manufacturer's instructions. The clonal samples were sequenced at the University of Michigan sequencing core using an Illumina MiSeq system, and the population samples were sequenced at the Microbial Genome Sequencing Center (MiGS) at University of Pittsburgh using a NextSeq 550 system.

The resulting genomic data was analyzed using the high-throughput computational pipeline breseq [62], with default settings. Average read coverage depth was

about 150 for single colony sequencing and 200 on the population sequencing batch. Briefly, genomes were trimmed and subsequently aligned to E. faecalis strain V583 (Accession numbers: AE016830 - AE016833; see [27]) via Bowtie 2 [63]. A sequence read was discarded if less than 90 percent of the length of the read did not match the reference genome or a predicted candidate junction. At each position a Bayesian posterior probability is calculated and the log10 ratio of that probability versus the probability of another base (A, T, C, G, gap) is calculated. Sufficiently high consensus scores are marked as read alignment evidence (in our case a consensus score of 10). Any mutation that occurred in either of the 2 control V583 strains was filtered from the results.

For population sequencing, we limit our analysis to mutations that occur at a frequency of greater than 30 percent. The choice of a cutoff percentage will always be slightly arbitrary. Our goal was to minimize false positives while maintaining the ability to identify mutations that occur at less than 100 percent. Our choice of 30 percent stems from the distribution of mutation frequencies from our population sequencing sample (See Figure 3.7); below 30 percent, the number of variant calls rises rapidly. While it is possible, and perhaps likely, that lower frequency mutations may play a significant role in the evolution and observed phenotypes, additional experiments would be needed to distinguish true variants from false positives.

3.5 Appendix

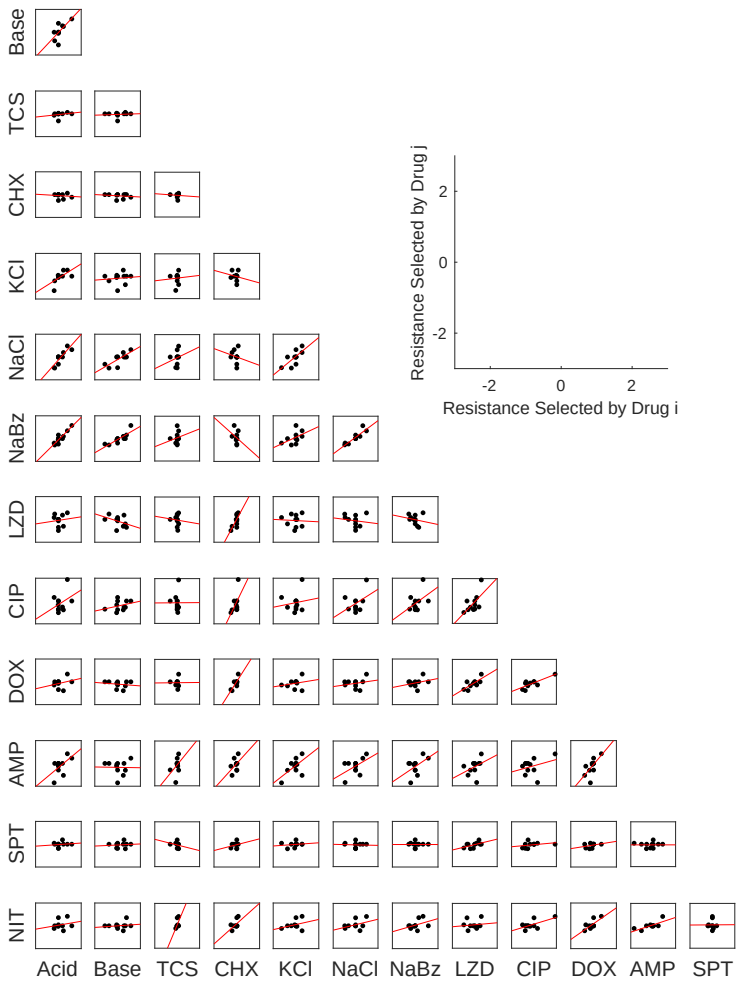

Figure 3.5: **Scatter plots for resistance levels selected by different pairs of conditions.** Pairwise scatter plots of resistance profiles selected by different conditions (that is, scatter plots comparing pairs of columns of the collateral sensitivity matrix). Each point represents the measured resistance to a single stressor in isolates selected by the pairs of conditions on the horizontal and vertical axes. To remove the effects of direct selection, which are typically larger in magnitude and may bias the correlations, the diagonal entries of the collateral sensitivity matrix (corresponding to resistance to the selecting condition) are removed. In all cases, resistance is measured in units of ($\log_2$-scaled) fold change in IC_{50} relative to ancestral strain.

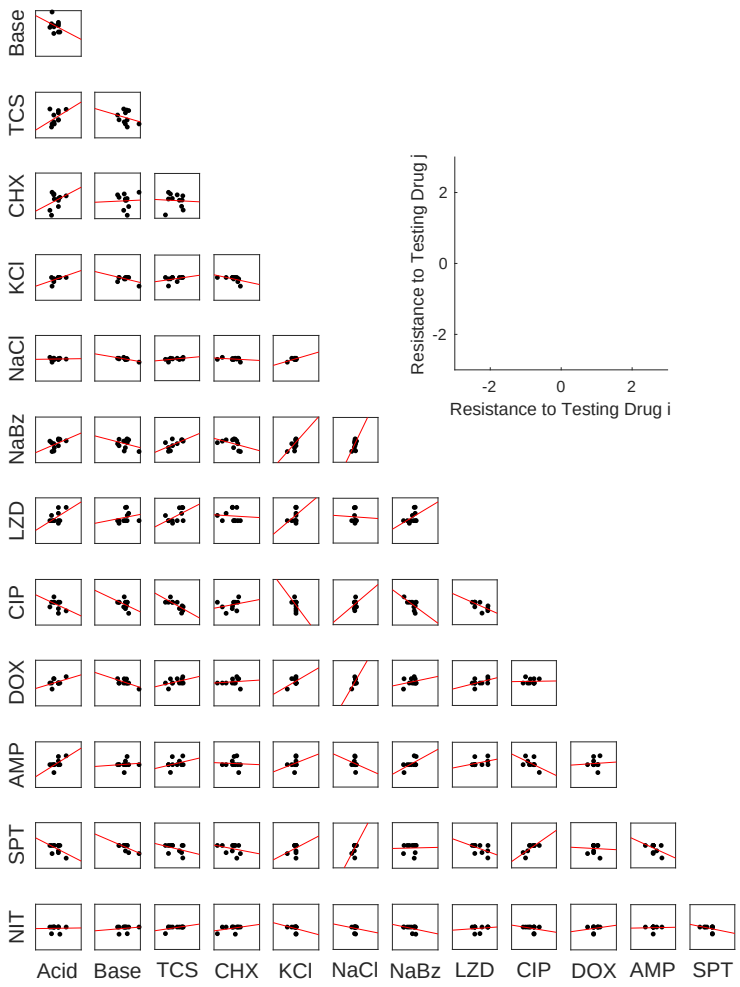

Figure 3.6: **Scatter plots for resistance levels to different pairs of testing conditions.** Pairwise scatter plots of resistance levels to different conditions (that is, scatter plots comparing pairs of rows of the collateral sensitivity matrix). Each point represents resistance to each of the paired testing conditions (on the horizontal and vertical axes) in a single isolate. To remove the effects of direct selection, which are typically larger in magnitude and may bias the correlations, the diagonal entries of the collateral sensitivity matrix (corresponding to resistance to the selecting condition) are removed. In all cases, resistance is measured in units of ($\log_2$-scaled) fold change in IC_{50} relative to ancestral strain.

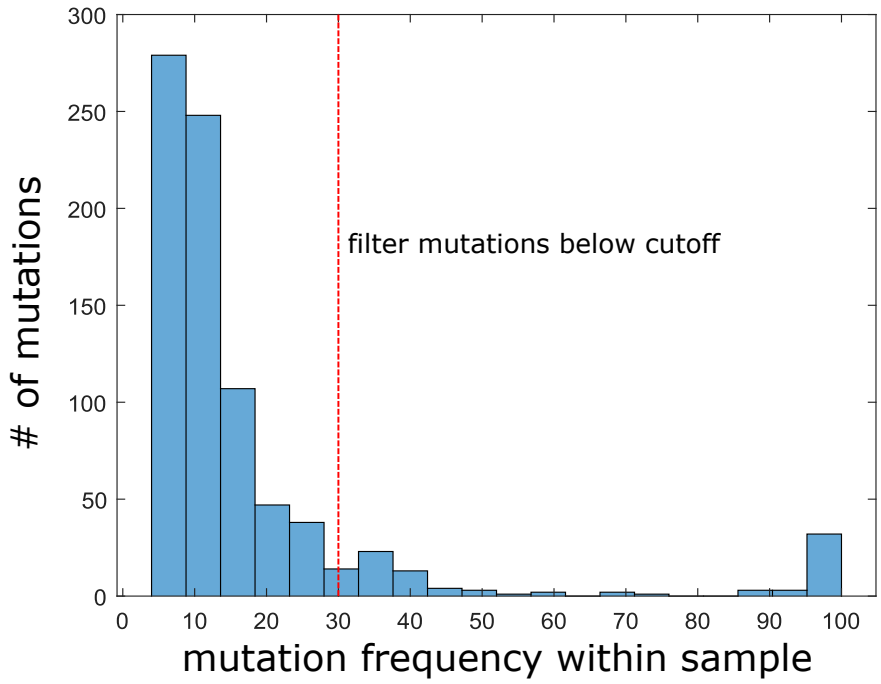

Figure 3.7: **Distribution of frequencies from identified mutations via population sequencing.** A histogram revealing the sample frequency of each mutation identified via population sequencing. The dotted red lines denotes the semi-arbitrary cutoff we have chosen where any mutation with a frequency below 30 percent is filtered from analysis.

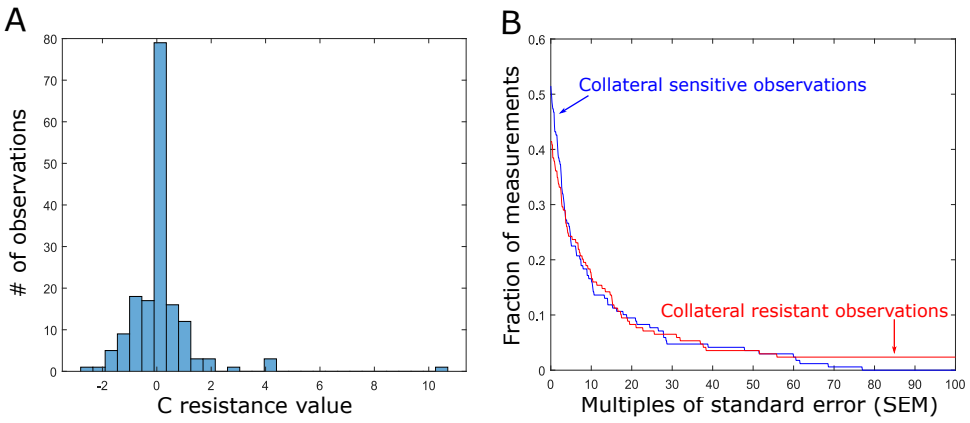

Figure 3.8: **Distribution of collateral observations across all testing conditions.** A. Histogram revealing the frequency of measured resistance values, c, across all 13 mutants where $c \equiv \log_2 (\mathrm{IC}_{50,Mut}/\mathrm{IC}_{50,WT})$. B. Fraction of measured IC_{50} values that qualify as collaterally sensitive (blue) or collaterally resistant (red), as the increase or decrease in IC_{50} required to qualify as resistant or sensitive increases. The x-axis represents multiples of the standard error of the mean across three technical replicates of the wild-type to each condition. Fraction sensitive and fraction resistant remain similar despite large changes in cutoff value.

3.6 References

1 S. B. Levy and B. Marshall, "Antibacterial resistance worldwide: causes, challenges and responses," *Nature medicine* **10**(12), S122–S129 (2004).

2 H. W. Boucher, G. H. Talbot, J. Bradley, *et al.*, "Bad bugs, no drugs; no esape! an update from the infections diseases society of america.," *Clin. Infect. Dis.* **48**, 1–12 (2009).

3 D. E. Goldberg, R. Siliciana, and W. R. J. Jr, "Outwitting evolution: Fighting drug-resistant tb, malaria, and hiv.," *Cell* **148**, 1271–1283 (2012).

4 A. Pfaller, "Antifungal drug resistance: Mechanisms, epidemiology, and consequences for treatment.," *Am. J. Med.* **125**, S3–S13 (2012).

5 M. Raviglione, B. Marais, K. Floyd, *et al.*, "Scaling up interentions to achieve global tuberculosis control: Progress and new developments.," *Lancet* **379**, 1902–1913 (2012).

6 P. Borst, "Cancer drug pan-resistance: Pumps, cancer stem cells, quiescence, epithelial to mesenchymal transition, blocked cell death pathways, persister or what?.," *Open Biol.* **2** (2012).

7 K. M. Pluchino, M. D. Hall, A. S. Goldsborough, *et al.*, "Collateral sensitivity as a strategy against cancer multidrug resistance.," *Drug Resis. Updat.* **15**, 98–105 (2012).

8 C. Seiler and T. U. Berendonk, "Heavy metal driven co-selection of antibiotic resistance in soil and water bodies impacted by agriculture and aquaculture.," *Front Microbiol.* **3** (2012).

9 A. Hassen, N. Saidi, M. Cherif, *et al.*, "Resistance of environmental bacteria to heavy metals.," *Bioresource Technology* **64**, 7–15 (1998).

10 C. Baker-Austin, M. S. Wright, R. Stepanauskas, *et al.*, "Co-selection of antibiotic and metal resistance.," *Trends in Microbiology* **14**, 176–182 (2006).

11 X. Ji, Q. Shen, F. Liu, *et al.*, "Antibiotic resistance gene abundances associated with antibiotics and heavy metals in animal manures and agricultural soils adjacent to feedlots in shanghai; china.," *Journal of Hazardous Materials* **235-236**, 178–185 (2012).

12 P. Bhardwaj, A. Hans, K. Ruikar, *et al.*, "Reduced chlorhexidine and daptomycin susceptibility in vancomycin-resistant enterococcus faecium after serial chlorhexidine exposure," *Antimicrobial agents and chemotherapy* **62**(1), e01235–17 (2018).

13 D. E. Carey and P. J. McNamara, "The impact of triclosan on the spread of antibiotic resistance in the environment.," *Frontiers in Microbiology* **5** (2015).

14 S. P. Yazdankhah, A. A. Scheie, E. A. Høiby, *et al.*, "Triclosan and antimicrobial resistance in bacteria: an overview," *Microbial drug resistance* **12**(2), 83–90 (2006).

15 M. E. Wand, L. J. Bock, L. C. Bonney, *et al.*, "Mechanisms of increased resistance to chlorhexidine and cross-resistance to colistin following exposure of klebsiella pneumoniae clinical isolates to chlorhexidine.," *Antimicrobial agents and chemotherapy* **61** (2017).

16 C. Horner, D. Mawer, and M. Wilcox, "Reduced susceptibility to chlorhexidine in staphylococci: is it increasing and does it matter?," *Journal of antimicrobial chemotherapy* **67**, 2547–2559 (2012).

17 A. Knöppel, J. Näsvall, and D. I. Andersson, "Evolution of antibiotic resistance without antibiotic exposure," *Antimicrobial agents and chemotherapy* **61**(11), e01495–17 (2017).

18 V. Lázár, A. Martins, R. Spohn, *et al.*, "Antibiotic-resistant bacteria show widespread collateral sensitivity to antimicrobial peptides," *Nature Microbiology* **3**(6), 718 (2018).

19 O. Lamrabet, M. Martin, R. E. Lenski, *et al.*, "Changes in intrinsic antibiotic susceptibility during a long-term evolution experiment with escherichia coli," *mBio* **10**(2), e00189–19 (2019).

20 D. Nichol, P. Jeavons, A. G. Fletcher, *et al.*, "Steering evolution with sequential therapy to prevent the emergence of bacterial antibiotic resistance," *PLoS computational biology* **11**(9), e1004493 (2015).

21 M. Baym, L. K. Stone, and R. Kishony, "Multidrug evolutionary strategies to reverse antibiotic resistance," *Science* **351**(6268), aad3292 (2016).

22 D. B. Clewell, M. S. Gilmore, Y. Ike, *et al.*, *Enterococci: from commensals to leading causes of drug resistant infection*, Massachusetts Eye and Ear Infirmary (2014).

23 R. M. Donlan, "Biofilms and device-associated infections.," *Emerging infectious diseases* **7**(2), 277 (2001).

24 T. O'Driscoll and C. W. Crank, "Vancomycin-resistant enterococcal infections: epidemiology, clinical manifestations and optimal management.," *Drug Resis. Updat.* **8**, 217–230 (2015).

25 Y. Cetinkaya, P. Falk, and C. G. Mayhall, "Vancomycin resistant enterococci.," *Clin. Microbiol. Rev.* **13**, 686–707 (2000).

26 J. Maltas and K. B. Wood, "Pervasive and diverse collateral sensitivity profiles inform optimal strategies to limit antibiotic resistance," *PLOS Biology* **17**, e3000515 (2019).

27 I. T. Paulsen, L. Banerjei, G. Myers, *et al.*, "Role of mobile dna in the evolution of vancomycin-resistant enterococcus faecalis," *Science* **299**(5615), 2071–2074 (2003).

28 M. Solheim, S. L. La Rosa, T. Mathisen, *et al.*, "Transcriptomic and functional analysis of nacl-induced stress in enterococcus faecalis," *PLoS One* **9**(4), e94571 (2014).

29 M. S. Gilmore, D. B. Clewell, P. Courvalin, *et al.*, "The enterococci: pathogenesis, molecular biology, and antibiotic resistance," (2002).

30 E.-W. Lee, M. N. Huda, T. Kuroda, *et al.*, "Efrab, an abc multidrug efflux pump in enterococcus faecalis," *Antimicrobial Agents and Chemotherapy* **47**(12), 3733–3738 (2003).

31 R. Roemhild, C. S. Gokhale, P. Dirksen, *et al.*, "Cellular hysteresis as a principle to maximize the efficacy of antibiotic therapy," *Proceedings of the National Academy of Sciences* **115**(39), 9767–9772 (2018).

32 F. J. Li and K. L. Palmer, "Efref and the transcription regulator chlr are required for chlorhexidine stress response in enterococcus faecalis v583," *Antimicrobial Agents and Chemotherapy* **62**(6) (2018).

33 R. J. Heath, J. R. Rubin, D. R. Holland, *et al.*, "Mechanism of triclosan inhibition of bacterial fatty acid synthesis," *Journal of Biological Chemistry* **274**(16), 11110–11114 (1999).

34 S. Kumar, M. M. Mukherjee, and M. F. Varela, "Modulation of bacterial multidrug resistance efflux pumps of the major facilitator superfamily.," *International Journal of Bacteriology* **2013** (2013).

35 D. Senadheera, K. Krastel, R. Mair, *et al.*, "Inactivation of vick affects acid production and acid survival of streptococcus mutans," *Journal of Bacteriology* **191**(20), 6415–6424 (2009).

36 K. Beabout, T. G. Hammerstrom, A. M. Perez, *et al.*, "The ribosomal s10 protein is a general target for decreased tigecycline susceptibility," *Antimicrobial Agents and Chemotherapy* **59**(9), 5561–5566 (2015).

37 R. J. Belland, S. G. Morrison, C. Ison, *et al.*, "Neisseria gonorrhoeae acquires mutations in analogous regions of gyra and parc in fluoroquinolone-resistant isolates," *Molecular Microbiology* **14**(2), 371–380 (1994).

38 S. B. Levy, "Active efflux mechanisms for antimicrobial resistance.," *Antimicrobial agents and chemotherapy* **36**(4), 695 (1992).

39 P. Sharma, J. R. J. Haycocks, A. D. Middlemiss, *et al.*, "The multiple antibiotic resistance operon of enteric bacteria controls dna repair and outer membrane integrity," *Nature communications.* **8** (2017).

40 Z. Hao, H. Lou, Z. Rongfeng, *et al.*, "The multiple antibiotic resistance regulator marr is a copper sensor in escherichia coli," *Nature chemical biology.* **10**, 21–28 (2014).

41 V. Lazar, I. Nagy, R. Spohn, *et al.*, "Genome-wide analysis captures the determinants of the antibiotic cross-resistance interaction network.," *Nat. Commun.* **5** (2014).

42 J. Lu, M. Jin, S. H. Nguyen, *et al.*, "Non-antibiotic antimicrobial triclosan induces multiple antibiotic resistane through genetic mutation," *Environment International* **118**, 257–265 (2018).

43 A. Arbeloa, H. Segal, J.-E. Hugonnet, *et al.*, "Role of class a penicillin-binding proteins in pbp5-mediated β-lactam resistance in enterococcus faecalis," *Journal of Bacteriology* **186**(5), 1221–1228 (2004).

44 L. Rigottier-Gois, A. Alberti, A. Houel, *et al.*, "Large-scale screening of a targeted enterococcus faecalis mutant library identifies envelope fitness factors," *PLoS One* **6**(12), e29023 (2011).

45 K. G. Eriksson-Grennberg, K. Nordström, and P. Englund, "Resistance of escherichia coli to penicillins ix. genetics and physiology of class ii ampicillin-resistant mutants that are galactose negative or sensitive to bacteriophage c21, or both," *Journal of Bacteriology* **108**(3), 1210–1223 (1971).

46 R. F. Guerrero, S. V. Scarpino, J. V. Rodrigues, *et al.*, "Proteostasis environment shapes higher-order epistasis operating on antibiotic resistance," *Genetics* **212**(2), 565–575 (2019).

47 D. M. Weinreich, Y. Lan, C. S. Wylie, *et al.*, "Should evolutionary geneticists worry about higher-order epistasis?," *Current opinion in genetics & development* **23**(6), 700–707 (2013).

48 K. J. Card, T. LaBar, J. B. Gomez, *et al.*, "Historical contingency in the evolution of antibiotic resistance after decades of relaxed selection," *PLOS Biology* **17**, 1–18 (2019).

49 C. B. Ogbunugafor, C. S. Wylie, I. Diakite, *et al.*, "Adaptive landscape by environment interactions dictate evolutionary dynamics in models of drug resistance," *PLoS computational biology* **12**(1), e1004710 (2016).

50 M. C. Whitlock, P. C. Phillips, F. B.-G. Moore, *et al.*, "Multiple fitness peaks and epistasis," *Annual review of ecology and systematics* **26**(1), 601–629 (1995).

51 S. Trindade, A. Sousa, K. B. Xavier, *et al.*, "Positive epistasis drives the acquisition of multidrug resistance," *PLoS genetics* **5**(7), e1000578 (2009).

52 M. O. Sommer, C. Munck, R. V. Toft-Kehler, *et al.*, "Prediction of antibiotic resistance: time for a new preclinical paradigm?," *Nature Reviews Microbiology* **15**(11), 689–696 (2017).

53 M. F. Schenk, I. G. Szendro, M. L. Salverda, *et al.*, "Patterns of epistasis between beneficial mutations in an antibiotic resistance gene," *Molecular biology and evolution* **30**(8), 1779–1787 (2013).

54 D. Nichol, J. Rutter, C. Bryant, *et al.*, "Antibiotic collateral sensitivity is contingent on the repeatability of evolution," *Nature communications* **10**(1), 334 (2019).

55 C. Westfall, A. L. Flores-Mireles, J. I. Robinson, *et al.*, "The widely used antimicrobial triclosan induces high levels of antibiotic tolerance in vitro and reduces antibiotic efficacy up to 100-fold in vivo," *Antimicrobial agents and chemotherapy* , AAC–02312 (2019).

56 C. Barbosa, V. Trebosc, C. Kemmer, *et al.*, "Alternative evolutionary paths to bacterial antibiotic resistance cause distinct collateral effects.," *Mol. Biol. Evol.* **34**, 2229–2244 (2017).

57 B. D. Schindler and G. W. Kaatz, "Multidrug efflux pumps of gram-positive bacteria," *Drug Resistance Updates* **27**, 1–13 (2016).

58 C. Pál, B. Papp, and V. Lázár, "Collateral sensitivity of antibiotic-resistant microbes," *Trends in microbiology* **23**(7), 401–407 (2015).

59 R. Roemhild, C. S. Gokhale, P. Dirksen, *et al.*, "Cellular hysteresis as a principle to maximize the efficacy of antibiotic therapy," *Proceedings of the National Academy of Sciences* **115**(39), 9767–9772 (2018).

60 D. Russ and R. Kishony, "Additivity of inhibitory effects in multidrug combinations," *Nature microbiology* **3**(12), 1339 (2018).

61 D. F. Sahm, J. Kissinger, M. S. Gilmore, *et al.*, "In vitro susceptibility studies of vancomycin-resistant enterococcus faecalis," *Antimicrobial Agents and Chemotherapy* **33**, 1588–1591 (1989).

62 D. E. Deatherage and J. E. Barrick, "Identification of mutations in laboratory-evolved microbes from next-generation sequencing data using breseq," in *Engineering and analyzing multicellular systems*, 165–188, Springer (2014).

63 B. Langmead and S. L. Salzberg, "Fast gapped-read alignment with bowtie 2," *Nature methods* **9**(4), 357 (2012).

CHAPTER IV

Evolution in Alternating Environments With Tunable Inter-landscape Correlations

This chapter was amended from: Jeff Maltas, Douglas M. McNally, and Kevin B. Wood. 'Evolution in alternating environments with tunable inter-landscape correlations' bioRxiv, doi: 10.1101/803619 (2019).

4.1 Introduction

In this chapter we turn from the experimentally-based studies on collateral evolution of the previous two chapters, to a more abstract investigation of collateral sensitivity based on evolution in fluctuating environments. Natural populations experience tremendous environmental diversity, and understanding how this spatiotemporal diversity influences evolutionary dynamics is a long-standing challenge. A great deal of work, both theoretical and experimental, has shown that spatial [1, 2, 3, 4, 5, 6, 7, 8, 9, 10] and temporal [11, 12, 13, 14, 15, 16, 17, 18, 19, 20, 21, 22, 23, 24, 25, 26, 27, 28, 29, 30, 31] heterogeneity play an important role in adaptation of asexual communities. For example, temporal or spatial fluctuations may lead to increased fixation probability and adaptation rates [26, 18, 11, 2, 5, 1, 17], a phenomenon that is also exploited in genetic programming algorithms [32]. In addition, environments that change in systematic ways may promote facilitated variation [33, 34], allowing organisms to preferentially harness the beneficial effects of random genetic changes and rapidly adapt to future perturbations. And when phenotypes themselves fluctuate over time, the frequency of inter-phenotype switching can evolve to match the timescale of environmental fluctuations [16, 15, 19, 20].

It is increasingly clear that these evolutionary dynamics have practical consequences for human health. The rise of drug resistance, which threatens the efficacy of treatments for bacterial infections, cancer, and viruses, is driven–at least in part–by evolutionary adaption occurring in complex, heterogeneous environments. Spatial heterogeneity in drug concentration has been shown to accelerate the evolution of resistance [35, 36, 37, 38, 39, 40], though adaptation may also be slowed when fitness

landscapes [37] or drug profiles [41] are judiciously tuned. Similarly, temporal variations in drug exposure–for example, drug cycling–can slow resistance under some conditions, though hospital-level strategies such as mixing may be more effective at generating the requisite environmental heterogeneity [42, 43]. Our last two chapters showed how collateral effects can influence evolution. In essence, these strategies force populations to simultaneously adapt to incompatible evolutionary tasks [44, 45].

Evolutionary adaptation is often modeled as a biased random walk on a high-dimensional landscape that links each specific genotype with a particular fitness [46, 47, 48]. In the simplest scenario, these landscapes represent evolution in the strong selection weak mutation (SSWM) limit, where isogenic populations evolve step-wise as the current genotype is replaced by that of a fitter descendant. While these idealized models are strictly valid only under certain conditions–for example, SSWM typically holds when mutation rate and effective population size are small–simple models have contributed significantly to our understanding of evolution [47, 48, 49, 12, 13, 50, 51]. In the context of fitness landscape models, control strategies that exploit collateral effects force the population to adapt to sequences of distinct, but statistically related, landscapes. For example, alternating between two drugs that induce mutual collateral sensitivity corresponds to landscapes with anti-correlated fitness peaks. When environments change in systematic ways–for example, by forcing the population to adapt to modular tasks comprised of related sub-goals–adaptation may select for generalists, genotypes that are fit in a wide range of environments at the cost of suboptimal specialization for any particular task [34, 52]. Relatively recent theoretical work also shows that conditional effects of evolutionary history can be captured by slowly changing landscapes–*seascapes*–which allow for the incorporation of time-dependent correlations [21, 10]. In general, however, understanding evolution in correlated landscapes–and in particular, how the choice of that correlation impacts fitness adaptation–remains challenging.

In this work, we investigate evolutionary dynamics of asexual populations in rapidly alternating environments described by pairs of (potentially rugged) fitness landscapes with tunable inter-landscape correlations (Fig 4.1). This problem is loosely inspired by adaptation of microbial communities to 2-drug cycles in which each drug induces collateral resistance or sensitivity to the other, though the scenario in question may arise in many different contexts, including evolution in antibodies [53] and viruses [54]. Our goal is to understand how the interplay between intra-landscape disorder (ruggedness) and inter-landscape fitness correlations impact fitness. By formulating the evolutionary dynamics as a simple Markov chain [55, 56], we are able to efficiently calculate time-dependent genotype distributions and investigate adaptation to ensembles of landscape pairs with various levels of epistasis and fitness correlations–results that would be more difficult to achieve from stochastic simulations alone. We find that rapid switching can either increase or decrease the steady state fitness of the population, depending on both the correlation between landscapes and level of intra-landscape ruggedness (i.e. epistasis). On short timescales, mean fitness is generally highest in static landscapes, but rapid switching between correlated environments can produce fitness gains for sufficiently rugged landscapes on longer timescales. Surprisingly, longer periods of rapid switching can also produce a genotype distribution whose fitness is, on average, larger than that of the ancestor population in both environments, even when the landscapes themselves are anti-correlated. To intuitively understand these results, we visualized genotype distributions and inter-genotype transitions as network diagrams, revealing that rapid switching in highly correlated environments frequently shepherds the population to genotypes that are locally optimal in both landscapes and, in doing so, fosters escape from the locally optimal but globally suboptimal fitness peaks that limit adaptation in static environments. The dynamics arise, in part, from the fact that rugged landscape pairs are increasingly likely to exhibit shared maxima as they become more positively cor-

related, and in turn, for landscapes with positive correlations, the mean fitness of these shared peaks is higher than that of non-shared peaks. By contrast, evolution in anti-correlated landscape pairs sample large regions of genotype space, exhibiting ergodic-like steady-state behavior that results in decreased average fitness.

4.2 Results

4.2.1 Markov chain model of evolution in alternating landscape pairs with tunable correlations

We consider evolution of an asexual haploid genome with N mutational sites. Each mutational site can have one of two alleles (labeled 0 or 1), and a single genotype can therefore be represented by one of the 2^N possible binary sequences of length N. The fitness of each genotype depends on the specific environment in which evolution takes place. We consider two different environments ("A" and "B"), and in each environment, every genotype is assigned a fixed fitness value, which defines the corresponding fitness landscapes (landscape A and landscape B) in each environment. Each fitness landscape is therefore defined on an N-dimensional hypercubic graph, with the nodes corresponding to specific genotypes.

To construct the landscape for a given environment, we use a many-peaked "rough Mt. Fuji" landscape [57, 25, 58]. Specifically, we assume that the fitness of the ancestor genotype (0,0,0...0) is zero and that the fitness f_i associated with a single mutation at mutational site i is drawn from a uniform distribution on the interval [-1,1]. Single mutations can therefore lead to increases ($f_i > 0$) or decreases ($f_i < 0$) in fitness. To fully specify the base landscape (i.e. the smooth landscape in the absence of epistasis), we then assume fitness associated with multiple mutations is additive. Finally, landscape ruggedness is incorporated by adding to the fitness of each genotype j a fixed, random variable ξ_j drawn from a zero-mean normal distribution with variance

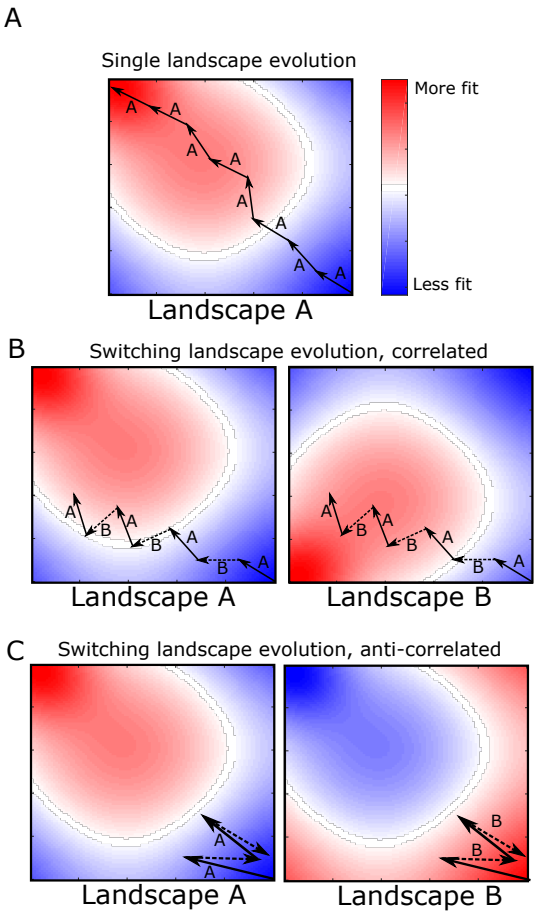

Figure 4.1: **Adaptation to alternating landscapes may depend on inter-landscape correlations** A. Schematic fitness landscape, with fitness varying from less fit (blue) to more fit (red) over the two dimensional genotype space. Starting from a single genotype (lower right hand corner), adaptation follows a biased random walk (arrows) toward local fitness maxima (in this case, in the upper left side of the landscape). B and C. Fitness landscapes A and B are positively (B) or negatively (C) correlated and do not share a global fitness maximum. Adaptation under rapid alternation of landscapes A and B leads to an altered evolutionary trajectory (represented as arrows, with solid arrows indicating steps in A and dashed arrows steps in B). In this example, the final fitness achieved in both correlated (panel B) and anti-correlated (panel C) landscapes is lower than that of static landscape evolution (panel A). Adaptation to anti-correlated landscapes leads to a particularly significant decrease in final fitness, as each step in B effectively reverses the progress made the previous step in A.

σ^2. The variable σ–the amplitude of the noise–determines the level of ruggedness of the landscape, which simulates epistasis [59, 60, 61, 62, 63, 64, 65]. In what follows, we focus on landscapes of size $N = 7$ (128 total genotypes) for computational convenience and limit ourselves primarily to $\sigma = 0$ (smooth landscapes) or σ=1 (rugged landscapes).

Our goal is to investigate evolution in rapidly changing environments that correspond to landscape pairs with correlated fitness peaks. To do so, we generate for each landscape A a "paired" landscape B with similar statistical properties (identical fitness mean and variance) but fitness peaks that are, on average, correlated with those of landscape A in a tunable way. To do so, we represent each landscape A as a vector $\bar{A}$ of length 2^N and use simple matrix algebra to generate a random vector $\bar{A}_\perp$ orthogonal to $\bar{A}$; by construction, then, this vector corresponds to a landscape whose fitness values are, on average, uncorrelated with those of landscape A. It is then straightforward to generate a vector $\bar{B}$, a linear combination of $\bar{A}$ and $\bar{A}_\perp$, such that the fitness values of landscapes A and B are correlated to a tunable degree $-1 \leq \rho \leq 1$, where ρ is the Pearson correlation coefficient between the two vectors $\bar{A}$ and $\bar{B}$. (see Methods).

With the landscapes specified, we then model adaptation in the well-characterized Strong Selection Weak Mutation (SSWM) limit [46, 47, 48], which can be formally described by a Markov chain [56, 55]. During each time step, the population transitions with uniform probability to one of the neighboring genotypes with a higher fitness in the current environment. We compare adaptation on a single landscape (single landscape evolution, SLE) with adaptation to rapid alternation of the two correlated landscapes A and B, which we refer to as paired landscape evolution (PLE). We focus here on the limit of rapid environmental switching, where the fitness landscape changes (A-B-A-B...) at each time step. This corresponds loosely to the rapid environmental switching seen in many laboratory experiments [66, 67, 68, 69].

We are primarily interested in comparing the (average) steady-state fitness of populations undergoing SLE to that of populations undergoing PLE. The average fitness, $\bar{F_X}(\bar{p})$, in environment X can be calculated at any time step t using $\bar{F}_X(\bar{p}) = \bar{X} \cdot \bar{p}(t)$, where $\bar{p}(t)$ is the vector whose i^{th} component is the probability to be in genotype i at time t and $\bar{X}$ is the landscape vector for environment X. Because the process can be described by a Markov chain, the vector $\bar{p}(t)$ is given by $\bar{p}(t) = T_M \bar{p}(0)$, where the matrix T_M describes the sequence of environments over time (e.g. $T_M = T_A^M$ for M steps in environment A, or $T_M = (T_B T_A)^{M/2}$ for M consecutive A-B cycles, with T_A and T_B the transition matrices corresponding to single steps in environment A and B, respectively). In what follows, we focus primarily on the mean fitness difference between the SLE and PLE adaptation, which is given by $\bar{F}_\Delta^A \equiv \bar{F}_A(\bar{p}_A) - \bar{F}_A(\bar{p}_{AB})$, where $\bar{p}_A$ is the steady state genotype distribution following adaptation to environment A, and $\bar{p}_{AB}$ is the steady state genotype distribution following adaptation to alternating A-B environments. Note that we define this fitness difference, $\bar{F}_\Delta^A$, with respect to landscape $\bar{A}$ (noted by superscript), which allows us to compare adaptation in environment A with adaptation in the alternating A-B environments. In the drug cycling analogy, we are measuring the average fitness in the drug A environment–essentially a measure of resistance to that drug. In all calculations, we consider an ensemble of 1000 landscapes pairs–with each pair sharing the same mean and variance in fitness and the same inter-landscape correlations–and we average the results over this ensemble.

4.2.2 Adaptation in rugged landscapes frequently ends in local, sub-optimal fitness maxima

While adaptation to static, rugged landscapes is well-understood, we first briefly discuss the effects of landscape ruggedness in the context of the current model. In static landscapes, steady state is reached when the genotype corresponds to a lo-

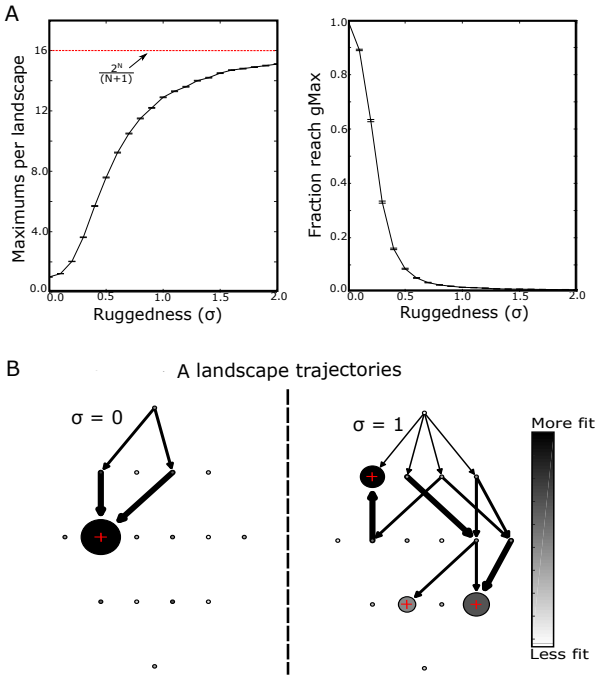

Figure 4.2: **Rugged landscapes trap populations in non-optimal fitness maxima** A. Left panel: average number of local fitness maxima per landscape as a function of increasing ruggedness (epistasis, σ). Dotted red line is the theoretical maximum ($2^N/(N+1) = 16$). Right panel: fraction of adapted populations that reach the global fitness maximum value as a function of ruggedness. Error bars are $\pm$ standard error of the mean in the ensemble of landscapes. B. Sample adaptive trajectories for small landscapes ($N = 4$) and $\sigma = 0$ (left) or $\sigma = 1$ (right). Each circle represents a genotype, with the ancestral genotype at the top. The shading of the circle represents the relative fitness of that genotype (ranging from less fit, white, to more fit, black) and the size of the circle indicates occupation probability in the steady state. Red + symbols mark genotypes corresponding to local fitness maxima. Arrows represent transitions between genotypes that occur with nonzero probability given that adaptation begins in the ancestral genotype.. The width of the arrow represents the magnitude of the transition probability.

cal fitness maximum. In the case of smooth, purely additive landscapes ($\sigma = 0$), there is a single fitness peak that corresponds to the global maximum, which we call gMax. However, as the landscape becomes more rugged ($\sigma > 0$), the average number of local maxima increases, eventually reaching the theoretical maximum of $2^N/(N+1)$ (Fig 4.2A). In turn, the fraction of adaptation trajectories that reach the global maximum decreases, reflecting the propensity of rugged landscapes to trap evolution in globally sub-optimal genotypes. To visualize these results, we represented the steady state genotype distributions and inter-genotype transitions as a network diagram (Fig 4.2B), with each node (circle) representing a genotype. The shading of each circle represents the relative fitness of that genotype (ranging from less fit, white, to more fit, black) and the size of the circle indicates occupation probability in the steady state. Arrows connecting different genotypes indicate nonzero transition probabilities, with the thickness of the arrow corresponding to its magnitude. We show only those transitions that can occur when adaptation starts in the ancestor genotype (top of diagram). In the case of evolution on a smooth landscape ($\sigma = 0$, Fig 4.2B, left panel), all trajectories lead to the single global maximum (indicated by red "+"). However, in the rugged landscape ($\sigma = 1$, Fig 4.2B, right panel), there is a nonzero probability of settling in each of three local maxima, and the population frequently ends in a non-optimal genotype. Increasing ruggedness would therefore be expected to lower the average fitness achieved in an ensemble of landscapes.

4.2.3 Switching between positively correlated landscapes can produce higher average fitness than adaptation to a static environment

Next, we set out to compare adaptation to landscape A with adaptation to alternating landscapes (A, B) with a tunable level of correlation, ρ, in the absence of epistasis ($\sigma = 0$, Fig 4.3A, blue). On these smooth landscapes, the fitness is single-peaked [25], and in the absence of switching, the population always reaches this global

maximum. In alternating environments, adaptation approaches the same average fitness as in static environments (i.e. $\bar{F}_{\Delta}^{A} \approx 0$)–implying that it finds the global fitness maximum–for all but the most negatively correlated landscapes ($\rho < -0.85$), where switching leads to steep decreases in fitness. By contrast, when landscapes are rugged ($\sigma = 1$), we find a range of correlations for which switching (PLE) increases the mean fitness ($\bar{F}_{\Delta}^{A} < 0$, Fig 4.3A, orange). Furthermore, as ruggedness increases, the range of correlations leading to increased fitness grows (Fig 4.3B).

4.2.4 Fitness can be maximally increased in either static or alternating environments depending on the timescale

We find that adaptation to static environments typically occurs on a faster timescale than adaptation to alternating environments (Fig 4.8). As a result, the protocol yielding the highest average fitness may differ depending on the timescale over which the comparison is made. For example, on short timescales (5 evolutionary steps, (Fig 4.3C, blue), adaptation to static environments always leads to greater fitness gain, regardless of the correlation between landscapes. On moderate (11 evolutionary steps, Fig 4.3C, red) to long (Fig 4.3C, black) timescales, however, we again see a range of positive correlations for which switching improves fitness–first only for highly correlated landscapes, and then eventually for a wider range of positively correlated landscapes. This result indicates that the optimal protocol for increasing fitness may depend on the chosen timescale. In the context of drug cycling, these results suggest that different strategies may be called for in scenarios that heavily weight short-term evolutionary dynamics–for example, the treatment regime for a single patient–and those associated with long evolutionary time-scales, such as the emergence of hospital-wide antibiotic resistance over the course of years.

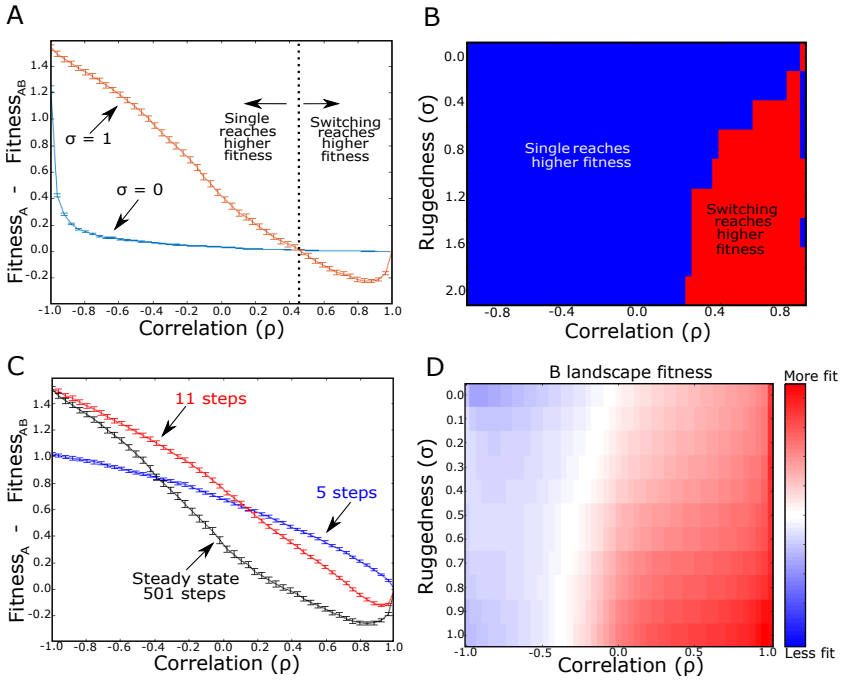

Figure 4.3: **Modulated fitness in alternating landscapes depends on intra-landscape ruggedness and inter-landscape correlations.** A. Difference in average fitness (at steady state) between populations adapted to a single static landscape (A) or rapidly alternating landscape pairs (A-B) as a function of correlation between landscapes A and B. Average fitness is defined as the mean fitness of the steady state genotypte distribution (which arises following adaptation to either static or switching protocols) measured in landscape A. Blue curve: $\sigma = 0$ (no epistasis; smooth); Orange curve: $\sigma = 1$ (orange; rugged). Dotted vertical line (corresponding to zero fitness difference) indicates critical value of correlation; above this critical value, switching between rugged landscape pairs ($\sigma = 1$) leads to larger fitness gains than evolution in a static landscape. B. Heatmap showing regions of parameter space (ruggedness σ, inter-landscape correlation) where switching leads to higher (red) or lower (blue) fitness than evolution in a static landscape. C. Identical to panel A, but curves are shown for 5 (blue), 11 (red) and 501 (black) evolutionary steps. σ=1 for all curves. D. Collateral fitness change, ranging from blue (less fit) to red (more fit), for populations adapted to alternating environments A and B as a function of ruggedness (σ) and inter-landscape correlation. Collateral fitness change is defined as the increase in average fitness in landscape B (relative to ancestor) associated with the steady state genotype distribution arising from adaptation to alternating A-B landscapes. $N = 7$ in all panels, but see also Figure 4.7. Error bars in panels A and C are $\pm$ standard error of the mean in the ensemble of landscapes.

4.2.5 Adaptation to alternating landscapes can lead to increased mean fitness in both landscapes, even when they are anticorrelated

While we have so far focused on mean fitness defined in landscape A, either due to static ($\bar{F}_A(\bar{p}_A)$) or alternating ($\bar{F}_A(\bar{p}_A)$) environments, we also asked how fitness in landscape B was modulated during adaptation. If adaptation occurs to a static landscape (A), the results are simple: the genotype adapted to A will on average exhibit increased (decreased) fitness in B when landscape B is positively (negatively) correlated with A. This scenario is reminiscent of collateral effects between different drugs, where increased resistance to one drug may be associated with either increased (cross resistance) or decreased (collateral sensitivity) resistance to a different (unseen) drug. In the case of alternating environments, however, the outcome is less clear *a priori*.

For smooth landscapes ($\sigma = 0$), we find that adaptation to the alternating landscapes leads to increased fitness in B ($\bar{F}_B(\bar{p}_{AB}) > 0$) when the landscapes are positively correlated and decreased fitness when they are negatively correlated (Fig 4.3D). Nonzero epistasis shifts the boundary separating increased and decreased fitness toward negative correlations. As a result, switching leads to increased fitness in both landscapes for a wider range of correlations–even, counterintuitively, in cases where the landscapes are (weakly) anti-correlated. In the context of drug cycling, this result suggests that cross resistance is likely to arise following repeated cycling of two drugs, even when their fitness landscapes are anti-correlated (i.e. drugs induce mutual collateral sensitivity).

4.2.6 Alternating between highly-correlated landscapes promotes escape from local fitness optima

To understand why switching between highly correlated landscapes can increase fitness relative to single landscape adaptation, we again represented adaptation on a

simple ($N = 4$) network representing a particular pair of fitness landscapes (Fig 4.12). The choice of N=4 allows for a simpler visual interpretation of the results, and the relevant dynamics are qualitatively similar for a broad range of landscape sizes (Fig 4.7). The landscape for environment A is characterized by multiple local maxima (Fig 4.12A, left panel), and in this example, the adaptation dynamics starting from the ancestral genotype are relatively simple, with only two paths possible (Fig 4.12A, right panel). With equal probability, the trajectory ends in one of two possible states, one of which is the global maximum.

If we now introduce rapid alternation with a second, positively correlated landscape ($\rho = 0.8$), the dynamics are much richer (Fig 4.12B). In this example, there is a single shared (local) maximum between the two landscapes (marked with red "+"), and adaptation to alternating environments eventually shepherds all trajectories to this shared maximum, which also happens to be the global maximum. As a result, alternating between landscapes leads to (on average) greater fitness increases than that achieved in static landscapes, where trajectories are split between local and global maxima. Intuitively, this example suggests that one advantage of rapid switching is that it dislodges trajectories from suboptimal local maxima–that is, switching between highly (but not perfectly) correlated landscapes provides a source of fluctuations that maximize the likelihood of finding globally optimal genotypes. This result is reminiscent of the observed "ratchet-like" mechanism of the *lac* operon in *Escherichia coli* [31].

4.2.7 Evolution in highly anti-correlated paired landscapes broadly samples genotype space resulting in reduced average fitness

We now return to dynamics in strongly anti-correlated landscapes, where shared maxima may be less likely to occur. To intuitively understand dynamics in this regime, we visualized the fitness landscape and evolutionary trajectories for a pair of

simple ($N = 4$) anticorrelated landscapes (Fig 4.13). In this example, adaptation to the static landscape leads to considerably higher fitness than adaptation to alternating landscapes. Interestingly, we see that the genotype distribution remains broad, even for long times. In fact, the only genotypes that remain unoccupied ($p_i = 0$) are those five that correspond to local minima in the A landscape. Including an additional step in landscape B leads to a similarly broad distribution, now with unoccupied genotypes corresponding to local minima of landscape B (Figure 4.10). In contrast to adaptation to single landscapes or alternating, positively correlated landscapes, the steady state distribution is not dominated by local fitness maxima but instead corresponds to broad genotype distribution and an associated decrease in average fitness.

4.2.8 Adaptation to alternating landscapes is frequently dominated by presence or absence of shared fitness maxima

We hypothesized that the increased fitness in alternating landscapes is closely linked to the expected number of shared maxima between paired landscapes. To probe this hypothesis, we first estimated what fraction of the local maxima in a given fitness landscape would (on average) also correspond to local maxima in a second (correlated) landscape. As intuition suggests, the fraction of shared maxima increases with correlation, both for smooth and rugged landscapes (Fig 4.4A). In addition, we estimated the fraction of landscape pairs in the entire ensemble that share at least one shared maximum (Fig 4.4B). Again we find that this quantity increases with correlation, but it does so much more rapidly for rugged landscapes. For smooth landscapes, the latter fraction increases gradually–and the curve is identical to that in (Fig 4.4A), a result of the fact that smooth landscapes have only a single (global) maximum.

To link these architectural properties of the landscapes with dynamics, we calcu-

lated adaptation trajectories under rapid switching of all paired landscapes in these ensembles (Fig 4.4C). For both smooth landscapes and negatively correlated rugged landscapes, the fraction of trajectories ending in a shared maximum closely mirrors the fraction of landscapes pairs that share a maximum. This correspondence suggests that under these conditions, when landscapes share a local maximum, the adapting system is likely to settle there. On the other hand, for positively correlated rugged landscapes, the likelihood of finding a shared maximum is relatively insensitive to correlation until ρ becomes quite large ($> .80$), when it rapidly increases (Fig 4.4C).

The further clarify the connection between fitness and shared maxima, we divided the local fitness maxima from landscape A into one of two categories: those that also correspond to a local maximum in landscape B, and those that do not. We found, somewhat counter-intuitively, that the mean fitness differs for the two categories (Fig 4.4D). For negatively correlated landscape pairs, the fitness of shared maxima is less than that of non-shared maxima. By contrast, shared maxima in highly (positively) correlated landscapes have a higher mean fitness than non-shared maxima. In addition, there is a range of positive ρ where the fitness of shared maxima is also greater than the average fitness of maxima in a single A landscape (which corresponds to the $\rho \to 1$ limit of the curve), offering an explanation for the fitness increase induced by alternating between highly correlated landscapes. Specifically, evolutionary trajectories typically settle into a single local maxima for adaptation to both static and positively correlated, alternating environments; however, for a range of highly (but not perfectly) correlated landscape pairs, the mean fitness of those shared maxima is greater than the mean fitness of local maxima in a single A landscape.

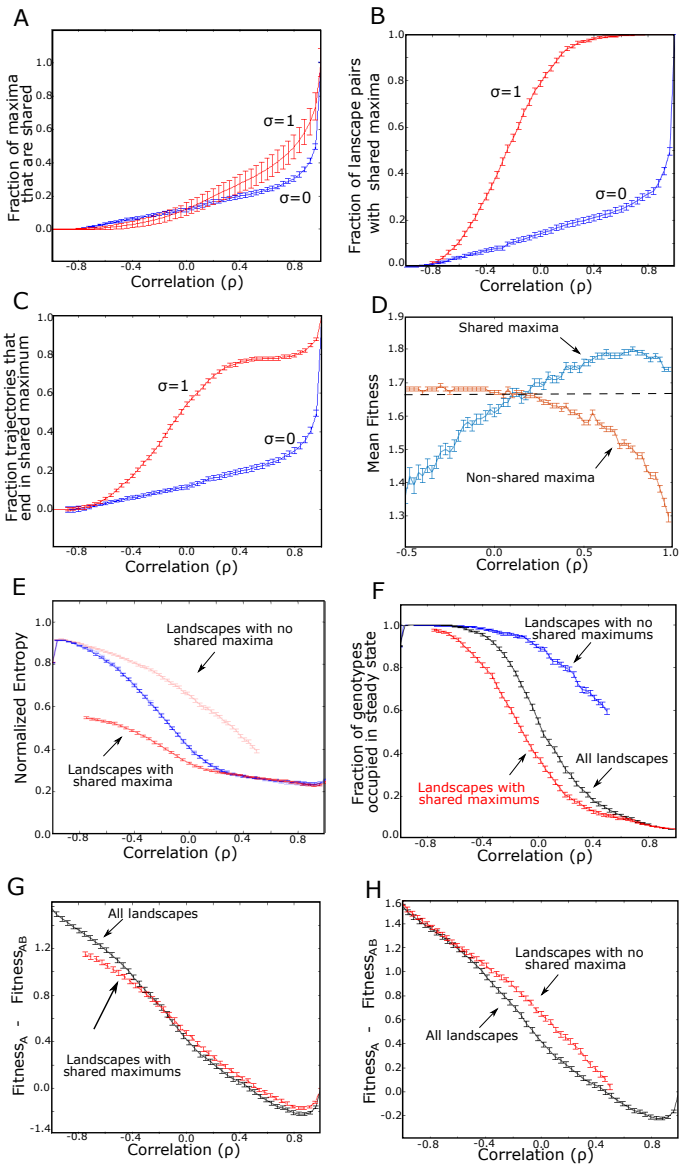

Figure 4.4: **Evolution in alternating landscapes is frequently dominated by presence or absence of shared fitness maxima.** A. Fraction of local maxima in landscape A that also correspond to a shared maxima in landscape B ($\sigma = 0$, blue; and $\sigma = 1$, red). B. Fraction of landscape pairs share at least one maximum. C. Fraction of trajectories ending in a shared maximum as a function of correlation. D. Average fitness of shared maxima (blue) and average fitness of non-shared maxima (orange). Dashed line is average fitness of all local maxima in landscape A. E. Normalized entropy of the steady state genotype distribution following adaptation to alternating landscapes. Curves correspond to the full landscape pair ensemble (blue) and a reduced ensemble consisting only of landscapes that contain a shared maximum (red), bottom, and a reduced ensemble consisting only of landscapes with no shared maxima (red, top).

Figure 4.4: The relative entropy is defined as $S(p)/S_{max} \equiv -\sum_i p_i \ln p_i$, where p_i is the steady state probability of being in genotype i and S_{max} is the entropy of a uniform distribution. F. Fraction of genotypes that have a nonzero probability of occupation in either the last A step or last B step at steady-state. Curves represent the paired landscape ensemble with no shared maxima (blue), the ensemble where every pair has at least one shared maximum (red), and the full ensemble (black). G. Difference in average fitness achieved in static and switching landscapes. Curves correspond to the full ensemble of paired landscapes (black) or a restricted ensemble that includes on those pairs that share a fitness maximum (red). H. Similar to panel F, with curves corresponding to the full ensemble (black) or a restricted ensemble that includes only those pairs with no shared fitness maxima (red). Error bars are ± standard error of the mean in the ensemble of landscapes. Error bars are ± standard error of the mean in the ensemble of landscapes. $N = 7$ for all curves, and $\sigma = 1$ for all curves in panels D-H.

4.2.9 Steady-state genotype distributions transition from narrow to broad as correlation is decreased

To further characterize steady state dynamics, we calculated the entropy of the steady state genotype distribution, defined as $S(p)/S_{max} \equiv -\sum_i p_i \ln p_i$, where p_i is the steady state probability of being in genotype i and S_{max} is the entropy of a uniform distribution (Fig 4.4E)–that is, a state where every genotype is equally probable. To capture dynamics associated with potential non-fixed point behavior, for this analysis we slightly modify the definition of steady state to be $p_i = (p_A + p_B)/2$, where p_A is the steady state fitness following a step in landscape A (the previously used definition) and p_B the fitness in the same steady state regime but following a step in landscape B (in words, we average over a full A-B cycle in the steady state). We find that as correlation (ρ) increases, the entropy of the system decreases, indicating that the dynamics are confined to an ever smaller set of genotypes–presumably those corresponding to shared maxima. Indeed, if we restrict the ensemble to only those landscape pairs that share a maximum, the entropy of the distribution is unchanged for highly correlated landscapes, suggesting that shared maxima dominate the steady

state dynamics. By contrast, when landscape pairs are anticorrelated, restricting the ensemble to pairs *without* shared maxima closely approximates the results of the full ensemble, suggesting that dynamics in this regime are dominated by qualitatively different behavior. Consistent with changes in the entropy of the genotype distribution, we also find that correlation dramatically changes the fraction of genotype space occupied (with nonzero probability) in the steady state (Fig 4.4F). For highly correlated landscapes, only a small fraction of the total genotype space is occupied. By contrast, highly anti-correlated landscapes produce steady state distributions wherein all states are occupied with non-zero probability, suggesting ergodic-like behavior, consistent with the example in Fig 4.13. The fact that relative entropy remains less than 1 in this regime does indicate, however, that the distribution is not fully uniform.

Finally, in Fig 4.4G, we plot the difference in steady state fitness achieved in static vs alternating environments for both the full landscape pair ensemble (black) and for a reduced ensemble consisting only of landscapes with shared maxima (red). We find that the curves are nearly identical over a wide range of correlations $\sigma > -0.4$. Similarly, when correlation is strongly anticorrelated, fitness differences are similar between the full ensemble and the reduced ensemble with no shared maxima (Fig 4.4H). Taken together, these results provide evidence that adaptation is frequently dominated by the presence or absence of shared fitness maxima, which in turn depends on the correlation between landscapes and landscape ruggedness.

4.2.10 A simple phenomenological model suggests these results are robust to small and moderate clonal interference

We now consider the role of clonal interference. Traditional descriptions of clonal interference still allow mutations to fix sequentially, however the probability of fixation is increasingly related to the fitness advantage of the mutant [49]. In order to investigate the effect of this classical clonal interference we borrow a phenomenolog-

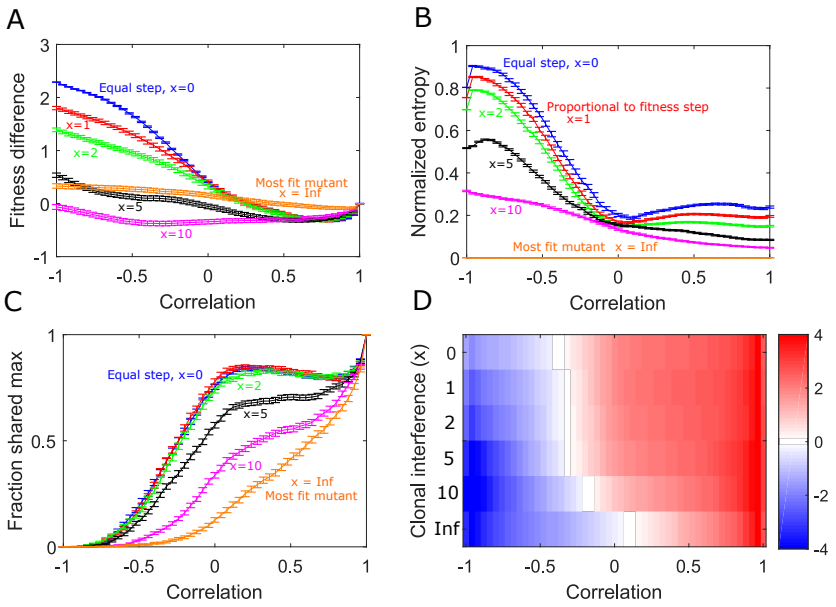

Figure 4.5: **Small and moderate clonal interference slightly reduce the effects of alternating landscape evolution.** A. Difference in average fitness achieved in static and switching landscapes. Curves correspond to different strengths of clonal interference (blue: random walker, $x = 0$, red: proportional walker, $x = 1$, green: $x = 2$, black: $x = 5$, magenta: $x = 10$, orange: $x\ infinite$, always steps to largest fitness neighbor). B. Normalized entropy of the steady state genotype distribution following adaption to alternating landscapes with different clonal interference. C. Fraction of trajectories ending in a shared maximum as a function of correlation with different clonal interference. D. Collateral fitness change, ranging from blue (less fit) to red (more fit), for populations adapted to alternating environments A and B as a function of clonal interference (x).

ical model developed by Tan and Gore [25]. In our current model, the population is treated as a *random walker* that steps to any nearby genotype with a higher fitness with equal probability. In the phenomenological model, the population is treated as a homogeneous *greedy walker*, where as x becomes larger, the probability of stepping to the more fit neighbors increases dramatically.

Using this phenomenological model, we observe for small and moderate population sizes ($x \sim 5$, 10^5 cells) our results remain qualitatively unchanged (Fig 4.5). However, as the population size gets large ($x > 5$, $> 10^5$ cells) the fitness difference, genetic

diversity and collateral effects due to switching disappear. These difference can be seen most dramatically in anti-correlated landscape pairs.

Of course, this classical model of clonal interference has limitations. It assumes a homogeneous population, thus ignoring the genetic diversity necessary of clonal interference. In addition, it neglects the possibility for deleterious or multiple simultaneous mutations to fix. Still, this model provides insight into a critical aspect of clonal interference where more fit mutants are more likely to fix.

4.2.11 Consecutive steps in the same landscape before switching changes the quantitative, but not qualitative results

We now consider how the period of switching may impact our results. To do this, we varied the amount of consecutive steps in the same landscape before switching from a single step (identical to the original model) to twenty steps (Fig 4.6). Similar to the addition of clonal interference, we see a quantitative shift to smaller fitness differences (Fig 4.6A), however the qualitative behavior, including switching leading to an increase in fitness at high correlation remains the same.

As with clonal interference, the largest difference occur in anti-correlated landscape pairs. As the the number of consecutive mutations in a single environment grows, the probability of ending in a genotype that is not a maximum in A or B necessarily shrinks, as evidence by the smaller entropy (Fig 4.6B). Interestingly, observing collateral resistance in anti-correlated landscapes is robust to period selection (Fig 4.6D). Importantly, the fitness advantage conferred by switching between correlated landscape pairs is robust to period choice.

4.3 Discussion

Our results indicate that both intra-landscape disorder (ruggedness) and inter-landscape fitness correlations impact fitness in rapidly alternating fitness landscapes.

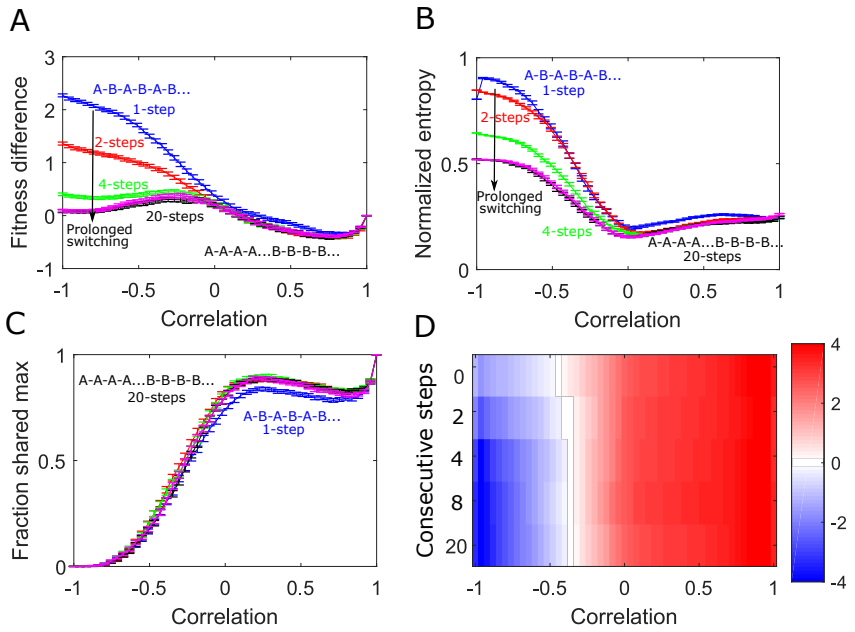

Figure 4.6: **Consecutive steps in the same landscape before switching lessens the effects of alternating landscape evolution.** A. Difference in average fitness achieved in static and switching landscapes. Curves correspond to different evolutionary steps taken in a landscape before switching (blue: 1 step, red: 2 steps, green: 4 steps, magenta: 8 steps, black: 20 steps). B. Normalized entropy of the steady state genotype distribution following adaption to alternating in landscapes with different switching periods. C. Fraction of trajectories ending in a shared maximum as a function of correlation with different switching periods. D. Collateral fitness change, ranging from blue (less fit) to red (more fit), for populations adapted to alternating environments A and B as a function of switching period.

Compared with static adaptation, rapid switching can lead to increased or decreased fitness, depending on both the correlation between landscapes and level of intra-landscape ruggedness (i.e. epistasis). Perhaps most strikingly, switching between highly, but not perfectly, correlated rugged landscapes can increase fitness by promoting escape from local fitness maxima, increasing the likelihood of finding global fitness optima. Furthermore, rapid switching can also produce a genotype distribution whose fitness is, on average, larger than that of the ancestor population in both environments, even when the landscapes themselves are anti-correlated. Adaptation dynamics are often dominated by the presence or absence of shared maxima between landscapes. Rugged landscape pairs are increasingly likely to exhibit shared maxima as they become more positively correlated, and in turn, for landscapes with positive correlations, the mean fitness of these shared peaks is higher than that of non-shared peaks. By contrast, evolution in anti-correlated landscape pairs samples large regions of genotype space, exhibiting ergodic-like steady-state behavior that results in decreased average fitness. A simple phenomenological model suggests these results are robust to competition due to small and moderate clonal interference, however they disappear as population sizes grow excessively large. In addition, while prolonging the period of switching can alter the dynamics in anti-correlated landscape evolution, the fitness advantage conferred by alternating evolution in correlated landscape pairs is robust to the period of switching.

While our results are loosely inspired by antibiotic cycling, the model is highly idealized and certainly cannot make predictions that apply directly to clinical scenarios. At the same time, the simplicity and relative generality of the model means that it may be relevant for understanding the qualitative behavior of a wide range of systems, including evolution in antibodies [53], viruses [54], and bacteria, where ratchet-like mechanisms for rapid adaptation have been observed experimentally [31]. Our model relies on the Strong Selection Weak Mutation (SSWM) limit and also

neglects potentially relevant dynamics that could arise due to clonal interference, horizontal gene transfer, and fixation of deleterious mutations. In addition, we focus on small ($N = 7$) genotype for tractability, and dynamics could differ for genotypes of drastically different sizes.

It is important to note that the paired landscapes in our ensembles are constructed to share certain global features–like mean fitness–and are related by a prescribed inter-landscape correlation, but they are not statistically identical. For example, the average number of local maxima can differ between landscape A and B, leading to different levels of evolved fitness for each landscape individually (Figure 4.11). This indicates that landscapes A and B have effectively different levels of epistasis, depending on the desired value of ρ, though these differences are most pronounced when A landscapes are very smooth ($\sigma \approx 0$). These differences do not seem to be appreciably impacting fitness dynamics, as removing them by choosing a reduced ensemble (keeping only the B landscapes the exhibit similar fitness gains as A under static adaptation) does not appreciably modify the results (Figure 4.11). Nevertheless, it may be interesting to investigate switching dynamics using landscapes with different types of statistical similarities–for example, those that differ only in higher-order moments, or those that fully decouple landscape ruggedness and correlation [52]). In fact, the results presented here are complementary to recent findings showing that environmental switching can enhance the basin of attraction for generalists, which are genotypes that are fit in multiple environments [52]. While the focus of the work is different–and the timescale of environmental switching and the statistical relationships between landscape pairs differ in their model–our results similarly highlight the importance of shared landscape maxima in determining adaptation dynamics. Future work may aim to further elucidate the evolutionary impacts of varying timescale, ordering, and temporal correlations in landscape dynamics. In the long run, we hope results from idealized models like these offer increased conceptual clarity to comple-

ment the rapidly evolving experimental approaches for mapping landscape dynamics in living organisms.

4.4 Methods

4.4.1 Construction of the landscapes

We consider evolution of an asexual haploid genome with N mutational sites. Each mutational site can have one of two alleles (labeled 0 or 1), and a single genotype can therefore be represented by one of the 2^N possible binary sequences of length N. To construct the landscape for a given environment, we use a many-peaked "rough Mt. Fuji" landscape [57, 25, 58]. Specifically, we assume that the fitness of the ancestor genotype (0,0,0...0) is zero and that the fitness f_i associated with a single mutation at mutational site i is drawn from a uniform distribution on the interval [-1,1]. We then assume fitness associated with multiple mutations is additive, and landscape ruggedness is incorporated by adding to the fitness of each genotype j a fixed, random variable ξ_j drawn from a zero-mean normal distribution with variance σ^2.

To create paired fitness landscapes, we represent each landscape A as a vector $\bar{A}$ of length 2^N, which we center and rescale to achieve a zero mean, unit variance vector. Then, we generate a Gaussian random vector $\bar{A}_\perp$ (also with zero mean and unit variance) and subtract from $\bar{A}_\perp$ its projection onto $\bar{A}$, making $\bar{A}_\perp$ orthogonal to $\bar{A}$; by construction, this vector corresponds to a landscape whose fitness values are, on average, uncorrelated with those of landscape A. It is then straightforward to generate a vector $\bar{B}$, a linear combination of $\bar{A}$ and $\bar{A}_\perp$, such that the fitness values of landscapes A and B are correlated to a tunable degree $-1 \leq \rho \leq 1$, where ρ is the Pearson correlation coefficient between the two vectors $\bar{A}$ and $\bar{B}$. At the end of this procedure, we rescale $\bar{A}$ and $\bar{B}$ so that both have mean and variance equal to that of

the original A landscape.

4.4.2 Evolution on the landscapes

The SSWM assumption allows the evolutionary trajectories to be modeled as a Markov chain [56, 55]. We follow the "random move SSWM model", which says that the probability of transitioning between adjacent genotypes $i \to j$ is given by $T_{ij} = 1/m$, with m the total number of i-adjacent genotypes with fitnes greater than that of i in the given environment. Each environment (A or B) has its own transition matrix, which we designate as T_A and T_B. Evolution in environment A is then given by

$$\bar{p}(t) = (T_A)^t \bar{p}(0) \tag{4.1}$$

with $\bar{p}(t)$ the vector whose i^{th} component is the probability to be in genotype i at time step t. We refer to the steady state ($t \to \infty$) limit of this process as $\bar{p}_A$. Similarly, we can describe rapidly alternating landscapes (A-B-A-B...) with

$$\bar{p}(t') = (T_B T_A)^{t'/2} \bar{p}(0) \tag{4.2}$$

with $t' \equiv 2t$ an even time step. We refer to the steady state ($t \to \infty$) limit of this process as $\bar{p}_{AB}$. In practice, we define steady state using the condition $\|(\bar{p}(2t+1) - \bar{p}(2t-1))\| < \epsilon = 0.001$. In words, we require the change in $\bar{p}$ between consecutive steps in environment A to be sufficiently small. To facilitate comparison with static evolution in landscape A, we always end the process after a step in landscape A, meaning there are always an odd number of steps. Ending instead in landscape B results in qualitatively similar behavior, though the fitness is often shifted, indicating that a single step in A or B–even in steady state–can lead to significant changes in fitness 4.9.

4.5 Appendix

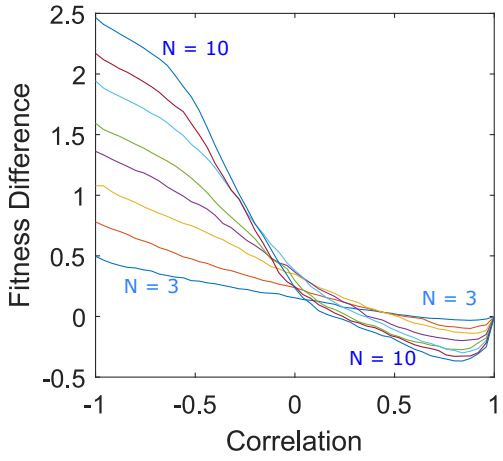

Figure 4.7: **Rugged landscapes of different sizes show qualitatively similar changes in fitness as a function of correlation.** Difference in average fitness (at steady state) between populations adapted to a single static landscape (landscape A) or rapidly alternating landscape pairs (A-B cycles) as a function of correlation between landscapes A and B. Average fitness is defined as the mean fitness of the steady state genotype distribution (which arises following adaptation to either static or switching protocols) measured in landscape A. Different curves range from $N = 3$ to $N = 10$, and $\sigma = N/12$ for each landscape to achieve relatively similar magnitudes of epistasis as N varies.

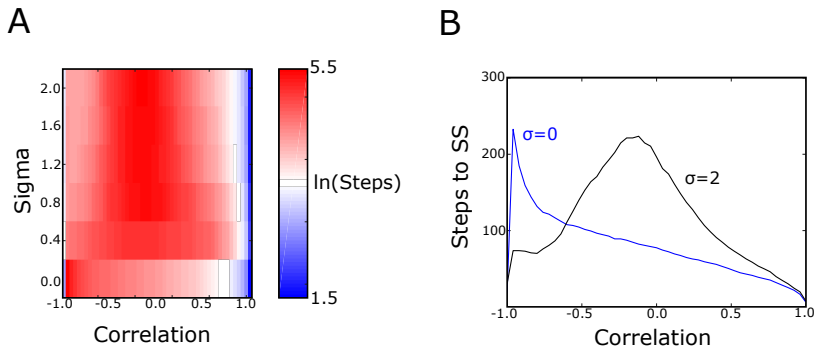

Figure 4.8: **Adaptation to static and alternating environments approach steady state at different timescales.** A. Number of time steps (log scale) until steady state for alternating landscapes of a given ruggedness (σ) and correlation (ρ). Full correlated landscapes ($\rho = 1$) correspond to static evolution in a single landscape. B. Example slices through panel A corresponding to $\sigma = 0$ and $\sigma = 2$.

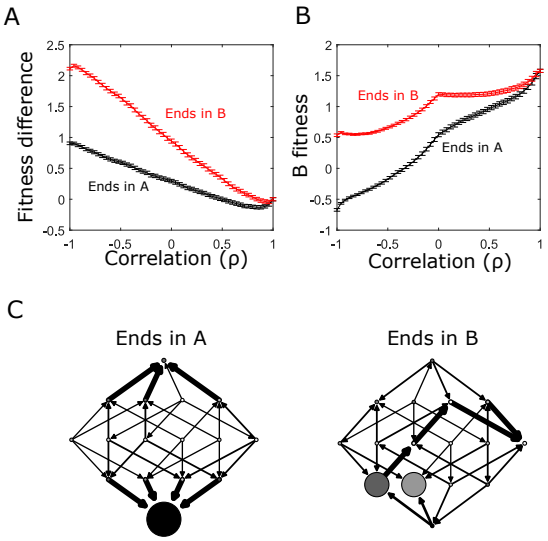

Figure 4.9: **Adapted fitness depends on whether final step is taken in landscape A or B when landscapes are anticorrleated.** A. Difference in average fitness (at steady state) between populations adapted to a single static landscape (landscape A) or rapidly alternating landscape pairs (A-B cycles) as a function of correlation between landscapes A and B. Average fitness is defined as the mean fitness of the steady state genotypte distribution (which arises following adaptation to either static or switching protocols) measured in landscape A. Curves correspond to steady state with a final step in landscape A (black) or a final step in landscape B (red). B. Collateral fitness change for populations adapted to alternating environments A and B as a function of inter-landscape correlation. Collateral fitness change is defined as the increase in average fitness in landscape B (relative to ancestor) associated with the steady state genotype distribution arising from adaptation to alternating A-B landscapes. C. Network representation of example fitness landscapes and transition probabilities following long-term adaptation to uncorrelated ($\rho = 0$) landscapes; adaptation ends either in landscape A (left) or B (right). $N = 4$ in all panels.

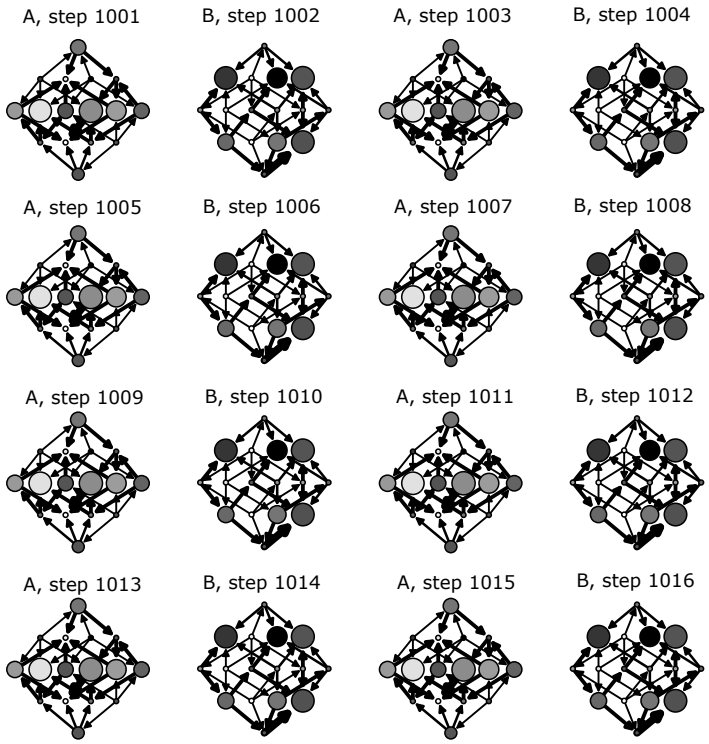

Figure 4.10: **Adaptation to anti-correlated landscapes can produce cycles that sample large fractions of genotype space.** Network representations of 16 consecutive steps in the steady state for paired landscape evolution with $\rho = -0.88$. Each circle represents a genotype (ancestral genotype at the top), with shading indicating the relative fitness of that genotype and size representing the occupation probability at that time step. Arrows represent transitions between genotypes that occur with nonzero probability and are accessible starting from the ancestor genotype. The width of the arrow represents the magnitude of the transition probability.

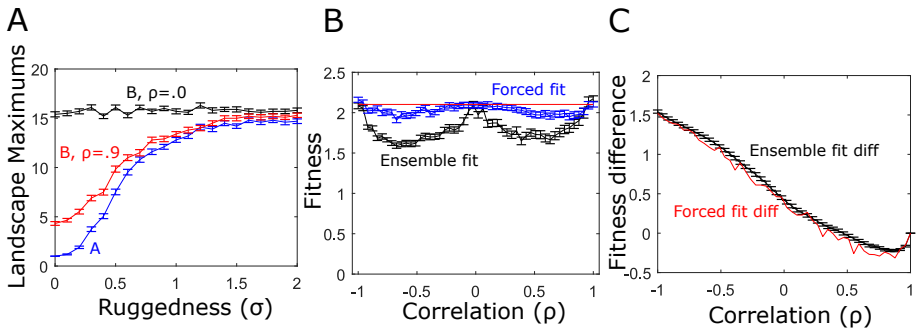

Figure 4.11: **Statistical properties of landscape B differ from those of A but do not appreciably impact fitness differences between static and alternating landscapes.** A. Average number of local maxima in landscape A (blue) and two different B landscapes correlated with A to different degrees ($\rho = 0$, black; $\rho = 0.9$, red). B. Evolved fitness following static adaptation to landscape A (red) or B (black). Blue curve is fitness in a reduced "forced fit" ensemble of B landscapes, which includes only those B landscapes that lead to similar levels of fitness as in landscape A. C. Fitness difference between static and switching environments for the full paired landscape ensemble (black) and for the reduced "forced fit" ensemble (black).

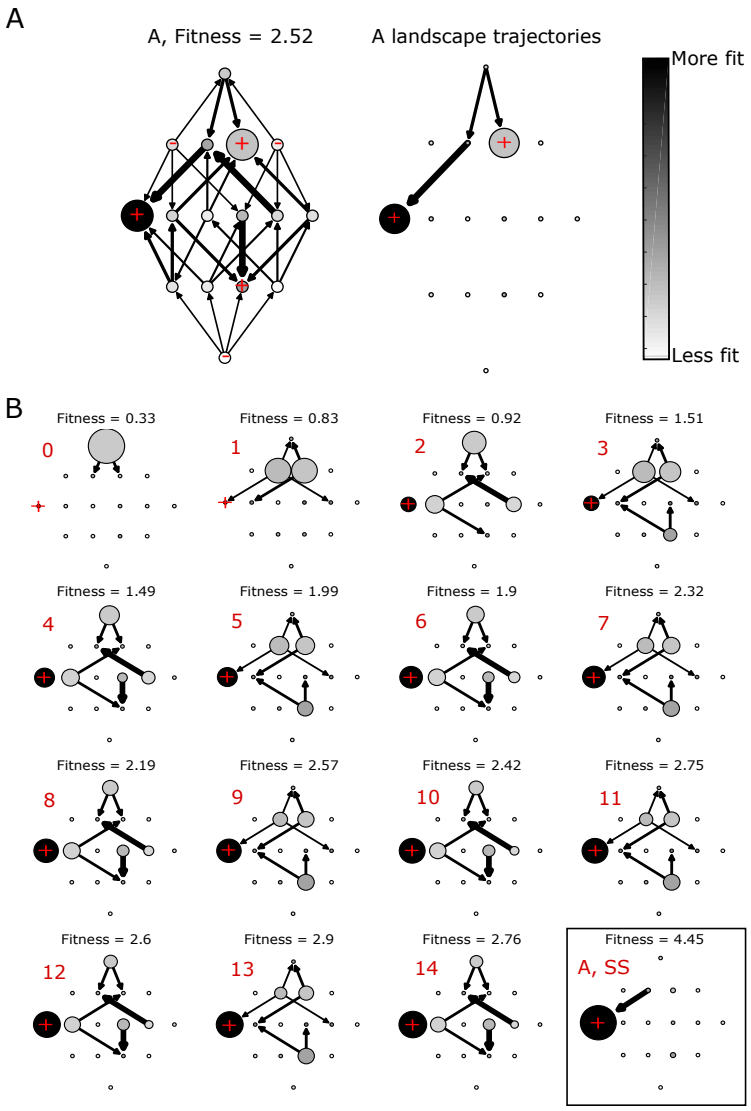

Figure 4.12: **Evolutionary dynamics in alternating landscapes with positively correlated fitness peaks.** A. Left panel: network representation of adaptation on a static landscape (environment A) of size $N = 4$. Each circle represents a genotype (ancestral genotype at the top), with shading indicating the relative fitness of that genotype and size representing the occupation probability in the steady state. Red + symbols mark genotypes corresponding to local fitness maxima. Arrows represent transitions between genotypes that occur with nonzero probability–that is, the entries of the transition matrix. The width of the arrow represents the magnitude of the transition probability. Right panel: same as left panel, but showing only transitions that occur during adaptation starting from the ancestral genotype (top circle).

Figure 4.12: B. Network representations of adaptation (at different time points) in alternating landscapes with positively correlated fitness peaks. Red number above each landscape represents the current evolutionary time point (ranging from 0 to SS, indicating steady state of approximately 200 steps). Directed arrows represent possible transitions between genotypes based on the current genotype distribution (indicated by the circle sizes) and the current landscape (A or B). Average fitness at each time point (calculated over the current genotype distribution) are listed above each plot. Even numbered steps correspond to landscape A, odd to landscape B.

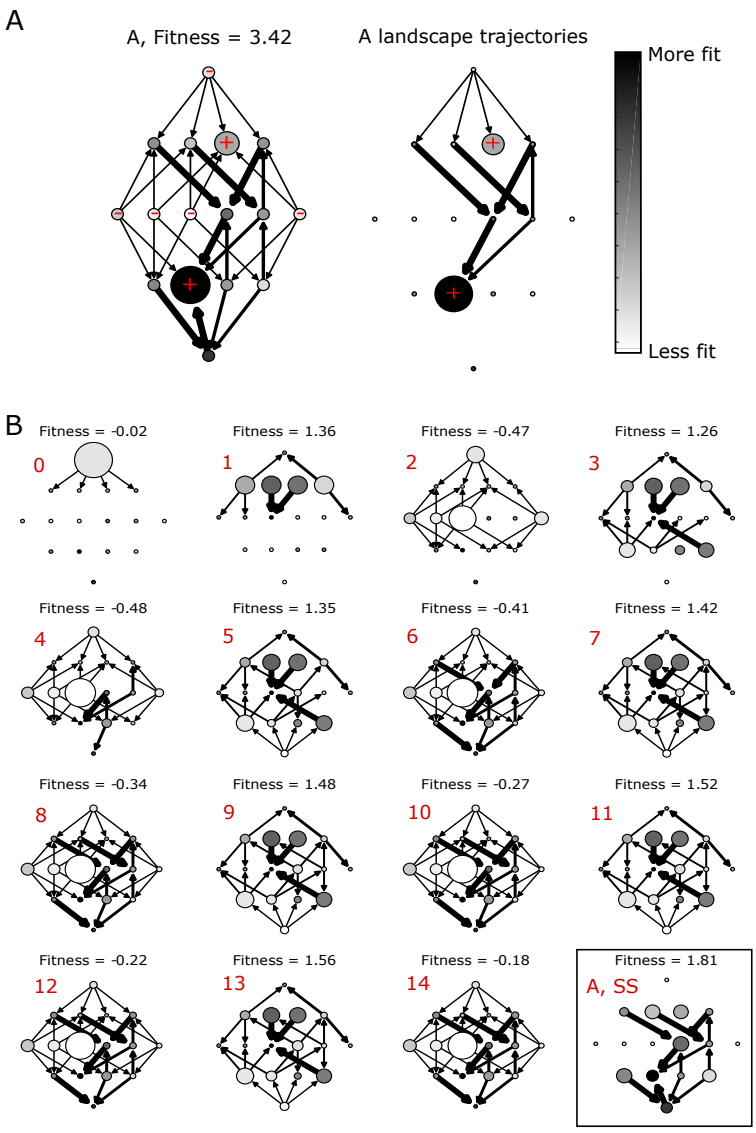

Figure 4.13: **Evolutionary dynamics in alternating landscapes with negatively correlated fitness peaks.** A. Left panel: network representation of adaptation on a static landscape (environment A) of size $N = 4$. Each circle represents a genotype (ancestral genotype at the top), with shading indicating the relative fitness of that genotype and size representing the occupation probability in the steady state. Red + symbols mark genotypes corresponding to local fitness maxima. Arrows represent transitions between genotypes that occur with nonzero probability.

Figure 4.13: he width of the arrow represents the magnitude of the transition probability. Right panel: same as left panel, but showing only transitions that occur during adaptation starting from the ancestral genotype (top circle). B. Network representations of adaptation (at different time points) in alternating landscapes with negatively correlated fitness peaks. Red number above each landscape represents the current evolutionary time point (ranging from 0 to SS, indicating steady state of approximately 200 steps). Directed arrows represent possible transitions between genotypes based on the current genotype distribution (indicated by the circle sizes) and the current landscape (A or B). Average fitness at each time point (calculated over the current genotype distribution) are listed above each plot. Even numbered steps correspond to landscape A, odd to landscape B.

4.6 References

1 S. Farhang-Sardroodi, A. Darooneh, M. Nikbakht, *et al.*, "The effect of spatial randomness on the average fixation time of mutants.," *PLoS computational biology* **13**(11), e1005864 (2017).

2 R. Hermsen and T. Hwa, "Sources and sinks: a stochastic model of evolution in heterogeneous environments," *Physical review letters* **105**(24), 248104 (2010).

3 Y. T. Lin, H. Kim, and C. R. Doering, "Demographic stochasticity and evolution of dispersion ii: Spatially inhomogeneous environments," *Journal of Mathematical Biology* **70**, 679–707 (2015).

4 J. N. Waddell, L. M. Sander, and C. R. Doering, "Demographic stochasticity versus spatial variation in the competition between fast and slow dispersers," *Theoretical population biology* **77**(4), 279–286 (2010).

5 M. C. Whitlock and R. Gomulkiewicz, "Probability of fixation in a heterogeneous environment," *Genetics* **171**(3), 1407–1417 (2005).

6 G. W. Constable and A. J. McKane, "Population genetics on islands connected by an arbitrary network: An analytic approach," *Journal of theoretical biology* **358**, 149–165 (2014).

7 G. W. Constable and A. J. McKane, "Fast-mode elimination in stochastic metapopulation models," *Physical Review E* **89**(3), 032141 (2014).

8 M. G. Habets, D. E. Rozen, R. F. Hoekstra, *et al.*, "The effect of population structure on the adaptive radiation of microbial populations evolving in spatially structured environments," *Ecology letters* **9**(9), 1041–1048 (2006).

9 R. Korona, C. H. Nakatsu, L. J. Forney, *et al.*, "Evidence for multiple adaptive peaks from populations of bacteria evolving in a structured habitat," *Proceedings of the National Academy of Sciences* **91**(19), 9037–9041 (1994).

10 A. Agarwala and D. S. Fisher, "Adaptive walks on high-dimensional fitness landscapes and seascapes with distance-dependent statistics," *bioRxiv* , 435669 (2018).

11 R. C. Lewontin and D. Cohen, "On population growth in a randomly varying environment," *Proceedings of the National Academy of Sciences* **62**(4), 1056–1060 (1969).

12 R. D. Cook and D. L. Hartl, "Uncorrelated random environments and their effects on gene frequency," *Evolution* **28**(2), 265–274 (1974).

13 D. L. Hartl and R. D. Cook, "Autocorrelated random environments and their effects on gene frequency," *Evolution* **28**(2), 275–280 (1974).

14 J. H. Gillespie and H. A. Guess, "The effects of environmental autocorrelations on the progress of selection in a random environment," *The American Naturalist* **112**(987), 897–909 (1978).

15 P. B. Gupta, C. M. Fillmore, G. Kiang, *et al.*, "Stochastic state transitions give rise to phenotypic equilibrium in populations of cancer cells," *Cell* **146**, 633–644 (2011).

16 E. Kussell and S. Leibler, "Phenotypic diversity, population growth, and information in fluctuating environments," *Science* **309**(5743), 2075–2078 (2005).

17 N. Kashtan, E. Noor, and U. Alon, "Varying environments can speed up evolution," *Proceedings of the National Academy of Sciences* **104**(34), 13711–13716 (2007).

18 V. Mustonen and M. Lässig, "Molecular evolution under fitness fluctuations," *Phys. Rev. Lett.* **100**, 108101 (2008).

19 M. Acar, J. T. Mettetal, and A. van Oudenaarden, "Stochastic switching as a survival strategy in fluctuating environments," *Nature Genetics* **40**, 471 EP – (2008).

20 V. Shahrezaei, J. F. Ollivier, and P. S. Swain, "Colored extrinsic fluctuations and stochastic gene expression," *Molecular Systems Biology* **4**(1), 196 (2008).

21 V. Mustonen and M. Lässig, "From fitness landscapes to seascapes: non-equilibrium dynamics of selection and adaptation," *Trends in genetics* **25**(3), 111–119 (2009).

22 B. Gaál, J. W. Pitchford, and A. J. Wood, "Exact results for the evolution of stochastic switching in variable asymmetric environments," *Genetics* **184**(4), 1113–1119 (2010).

23 T. F. Cooper and R. E. Lenski, "Experimental evolution with e. coli in diverse resource environments. i. fluctuating environments promote divergence of replicate populations," *BMC evolutionary biology* **10**(1), 11 (2010).

24 L. Tan, S. Serene, H. X. Chao, *et al.*, "Hidden randomness between fitness landscapes limits reverse evolution," *Phys. Rev. Lett.* **106**, 198102 (2011).

25 L. Tan and J. Gore, "Slowly switching between environments facilitates reverse evolution in small populations," *Evolution* **66**(10), 3144–3154 (2012).

26 I. Cvijović, B. H. Good, E. R. Jerison, *et al.*, "Fate of a mutation in a fluctuating environment," *Proceedings of the National Academy of Sciences* **112**(36), E5021–E5028 (2015).

27 P. Patra and S. Klumpp, "Emergence of phenotype switching through continuous and discontinuous evolutionary transitions," *Physical biology* **12**(4), 046004 (2015).

28 A. Skanata and E. Kussell, "Evolutionary phase transitions in random environments," *Physical review letters* **117**(3), 038104 (2016).

29 B. Steinberg and M. Ostermeier, "Environmental changes bridge evolutionary valleys," *Science advances* **2**(1), e1500921 (2016).

30 R. Canino-Koning, M. J. Wiser, and C. Ofria, "Fluctuating environments select for short-term phenotypic variation leading to long-term exploration," *PLOS Computational Biology* **15**, 1–32 (2019).

31 M. G. J. de Vos, A. Dawid, V. Sunderlikova, *et al.*, "Breaking evolutionary constraint with a tradeoff ratchet," *Proceedings of the National Academy of Sciences* **112**(48), 14906–14911 (2015).

32 M. O'Neill, L. Vanneschi, S. Gustafson, *et al.*, "Open issues in genetic programming," *Genetic Programming and Evolvable Machines* **11**(3-4), 339–363 (2010).

33 J. Gerhart and M. Kirschner, "The theory of facilitated variation," *Proceedings of the National Academy of Sciences* **104**(suppl 1), 8582–8589 (2007).

34 M. Parter, N. Kashtan, and U. Alon, "Facilitated variation: how evolution learns from past environments to generalize to new environments," *PLoS computational biology* **4**(11), e1000206 (2008).

35 Q. Zhang, G. Lambert, D. Liao, *et al.*, "Acceleration of emergence of bacterial antibiotic resistance in connected microenvironments," *Science* **333**(6050), 1764–1767 (2011).

36 R. Hermsen, J. B. Deris, and T. Hwa, "On the rapidity of antibiotic resistance evolution facilitated by a concentration gradient," *Proceedings of the National Academy of Sciences* **109**(27), 10775–10780 (2012).

37 P. Greulich, B. Waclaw, and R. J. Allen, "Mutational pathway determines whether drug gradients accelerate evolution of drug-resistant cells," *Physical Review Letters* **109**(8), 088101 (2012).

38 F. Fu, M. A. Nowak, and S. Bonhoeffer, "Spatial heterogeneity in drug concentrations can facilitate the emergence of resistance to cancer therapy," *PLoS Comput Biol* **11**(3), e1004142 (2015).

39 S. Moreno-Gamez, A. L. Hill, D. I. Rosenbloom, *et al.*, "Imperfect drug penetration leads to spatial monotherapy and rapid evolution of multidrug resistance," *Proceedings of the National Academy of Sciences* **112**(22), E2874–E2883 (2015).

40 M. Baym, T. D. Lieberman, E. D. Kelsic, *et al.*, "Spatiotemporal microbial evolution on antibiotic landscapes," *Science* **353**(6304), 1147–1151 (2016).

41 M. G. De Jong and K. B. Wood, "Tuning spatial profiles of selection pressure to modulate the evolution of drug resistance," *Physical review letters* **120**(23), 238102 (2018).

42 C. T. Bergstrom, M. Lo, and M. Lipsitch, "Ecological theory suggests that antimicrobial cycling will not reduce antimicrobial resistance in hospitals.," *Proc. Natl. Acad. Sci. USA* **101**, 13285–13290 (2004).

43 E. M. Brown and D. Nathwani, "Antibiotic cycling or rotation: a systemic review of the evidence of efficacy.," *Journal of Antimicrobial Chemotherapy* **55**, 6–9 (2005).

44 O. Shoval, H. Sheftel, G. Shinar, *et al.*, "Evolutionary trade-offs, pareto optimality, and the geometry of phenotype space," *Science* **336**(6085), 1157–1160 (2012).

45 Y. Hart, H. Sheftel, J. Hausser, *et al.*, "Inferring biological tasks using pareto analysis of high-dimensional data," *Nature methods* **12**(3), 233–235 (2015).

46 J. H. Gillespie, "Some properties of finite populations experiencing strong selection and weak mutation," *The American Naturalist* **121**(5), 691–708 (1983).

47 J. H. Gillespie, "A simple stochastic gene substitution model," *Theoretical Population Biology* **23**(2), 202 – 215 (1983).

48 J. H. Gillespie, "Molecular evolution over the mutational landscape," *Evolution* **38**(5), 1116–1129 (1984).

49 P. J. Gerrish and R. E. Lenski, "The fate of competing beneficial mutations in an asexual population," *Genetica* **102**, 127 (1998).

50 M. M. Desai and D. S. Fisher, "Beneficial mutation–selection balance and the effect of linkage on positive selection," *Genetics* **176**(3), 1759–1798 (2007).

51 M. M. Desai, D. S. Fisher, and A. W. Murray, "The speed of evolution and maintenance of variation in asexual populations," *Current Biology* **17**, 385–394 (2007).

52 S. Wang and L. Dai, "Evolving generalists in switching rugged landscapes," *PLOS Computational Biology* **15**(10), e1007320 (2019).

53 D. R. Burton, P. Poignard, R. L. Stanfield, *et al.*, "Broadly neutralizing antibodies present new prospects to counter highly antigenically diverse viruses," *Science* **337**(6091), 183–186 (2012).

54 S.-Y. Rhee, J. Taylor, W. J. Fessel, *et al.*, "Hiv-1 protease mutations and protease inhibitor cross-resistance," *Antimicrobial agents and chemotherapy* **54**(10), 4253–4261 (2010).

55 R. Durrett and R. Durrett, *Essentials of stochastic processes*, vol. 1, Springer (1999).

56 D. Nichol, P. Jeavons, A. G. Fletcher, *et al.*, "Steering evolution with sequential therapy to prevent the emergence of bacterial antibiotic resistance," *PLOS Computational Biology* **11**, 1–19 (2015).

57 T. Aita and Y. Husimi, "Adaptive walks by the fittest among finite random mutants on a mt. fuji-type fitness landscape," *Journal of Theoretical Biology* **193**(3), 383 – 405 (1998).

58 J. Neidhart, I. G. Szendro, and J. Krug, "Adaptation in tunably rugged fitness landscapes: the rough mount fuji model," *Genetics* **198**, 699–721 (2014). 25123507[pmid].

59 P. C. Phillips, "Epistasis—the essential role of gene interactions in the structure and evolution of genetic systems," *Nature Reviews Genetics* **9**(11), 855 (2008).

60 M. D. Ritchie, L. W. Hahn, N. Roodi, *et al.*, "Multifactor-dimensionality reduction reveals high-order interactions among estrogen-metabolism genes in sporadic breast cancer," *The American Journal of Human Genetics* **69**, 138–147 (2001).

61 J. Xu, J. Lowey, F. Wiklund, *et al.*, "The interaction of four genes in the inflammation pathway significantly predicts prostate cancer risk," *Cancer Epidemiology and Prevention Biomarkers* **14**(11), 2563–2568 (2005).

62 C.-T. Tsai, J.-J. Hwang, M. D. Ritchie, *et al.*, "Renin–angiotensin system gene polymorphisms and coronary artery disease in a large angiographic cohort: Detection of high order gene–gene interaction," *Atherosclerosis* **195**, 172–180 (2007).

63 J. da Silva, M. Coetzer, R. Nedellec, *et al.*, "Fitness epistasis and constraints on adaptation in a human immunodeficiency virus type 1 protein region," *Genetics* **185**(1), 293–303 (2010).

64 D. M. Weinreich, N. F. Delaney, M. A. DePristo, *et al.*, "Darwinian evolution can follow only very few mutational paths to fitter proteins," *Science* **312**(5770), 111–114 (2006).

65 D. W. Anderson, A. N. McKeown, and J. W. Thornton, "Intermolecular epistasis shaped the function and evolution of an ancient transcription factor and its dna binding sites," *eLife* **4**, e07864 (2015).

66 R. E. Lenski, "Experimental studies of pleiotropy and epistasis in escherichia coli. ii. compensation for maldaptive effects associated with resistance to virus t4," *Evolution* **42**(3), 433–440 (1988).

67 C. L. Burch and L. Chao, "Evolution by small steps and rugged landscapes in the rna virus phi-6," *Genetics* **151**(3), 921–927 (1999).

68 W. D. Crill, H. A. Wichman, and J. J. Bull, "Evolutionary reversals during viral adaptation to alternating hosts," *Genetics* **154**(1), 27–37 (2000).

69 S. Kim, T. D. Lieberman, and R. Kishony, "Alternating antibiotic treatments constrain evolutionary paths to multidrug resistance," *Proceedings of the National Academy of Sciences* **111**(40), 14494–14499 (2014).

CHAPTER V

Conclusion

This research sought to better understand the possibilities and limitations of collateral sensitivity. We began with an extensive quantitative study of the phenotypic and genetic collateral effects in *E. faecalis* . We demonstrate that not only are collateral resistance and sensitivity common, but these profiles can be highly heterogeneous with collateral profiles often times varying between mutants evolved to the same selection pressure. While these results may be discouraging, we also demonstrate that the variability in collateral profile is sensitive to the selecting drug, suggesting that some drugs may be better suited for optimal control strategies than others due to the stability of the evolutionary response. Interestingly, we show that despite the heterogeneity in collateral profiles of individual mutants, these profiles mutants from the same drug class tend to cluster into statistically similar groups.

As a proof of principle, using a simple mathematical model inspired by a Markov Decision Process, we demonstrate how these profiles may inform optimal drug protocols that can account for both the stochasticity of evolution and varying time horizons. Optimizing over these different time horizons may be useful when considering a single patient (short-term time horizon) or a hospital (long-term time horizon). We then confirmed these predictions with extensive lab-evolution experiments and demonstrate the predicted optimal outperforms all single-drug and two-drug cycles as well as a representative four-drug cycle.

We expand on this work to include nonantibiotic selecting conditions such as acidic and basic pH, high salt environments, preservatives and disinfectants. These results provide the first systems-level picture of the collateral effects between antibiotic and nonantibiotic conditions. Indeed, we see collateral effects between these conditions are quite common. These collateral effects suggest more work is needed to understand the role of food additives, preservatives, biocides or common natural environments in the spread of multidrug resistance. As a proof-of-principle, we showed experimentally that consecutive adaption to different environments may be used to increase the total

number of sensitivities than either environment can induce alone.

When taken together we have learned much about the potential of collateral sensitivity as an evolutionary-based therapy, however many questions remain. It is unclear how our results might differ when performed in a different ancestral strain. V583 is highly resistant to multiple antibiotics, and as such might differ substantially from a strain without high native resistance. In addition, our sequencing results are conservative and only report mutations with a frequency above 30 percent. It is likely we are missing mutations that occur at a low frequency, but nonetheless play a large role in the resistance of the population. In addition, our technique is not sensitive to mobile elements, and as such we are unable to identify any that may be responsible for the observed phenotypic changes. Our MDP is not meant to be a detailed, clinically accurate model. Instead, we first focused on proving this approach can work for in vitro laboratory experiments. Extensions to this work to incorporate host and immune effects or drug-free periods may help bridge the gap between laboratory evolution and in-patient evolution. In addition, we only measured the collateral profiles at one time point. It is plausible that the collateral profiles are changing dramatically over time and more precise time-sensitive measurements are required to fully utilize this approach therapeutically.

Finally, we sought to understand how collateral effects manifest in the evolutionary dynamics between a pair of statistically related fitness landscapes. Collateral effects manifest themselves in the correlation between a pair of landscapes, where highly correlated landscapes are analogous to collateral resistance, and anti-correlated landscapes are analogous to collateral sensitivity. Our results suggest that both intra-landscape disorder (ruggedness or epistasis) and inter-landscape correlation (collateral effects) impact the fitness in rapidly alternating fitness landscapes. When compared to evolution in either landscape alone, we see that highly correlated landscape pairs reach a higher mean fitness while anti-correlated landscape pairs reach a significantly

lower mean fitness. Interestingly, we see that higher fitness achieved due to paired landscapes with positive correlations only occurs in the presence of epistasis. We show these results are largely driven by the location and prevalence of shared maxima between landscapes. Rugged, correlated landscapes are much more likely to exhibit shared fitness maxima than anti-correlated landscapes. In the case of positive correlations, these shared maxima lead to stepping stones to higher fitness as the population rapidly samples each landscape. In the case of anti-correlations, the absence of shared maxima results in ergodic-like behavior where the population endlessly wanders the genotype space.

While our results are inspired and informed by drug cycling, our model is highly idealized and should not be used to predict clinical outcomes. Our model relies on the Strong Selection Weak Mutation (SSWM) limit and thus ignores many of the complicating factors associated with horizontal gene transfer, large clonal interference effects, and the fixation of deleterious mutants. In addition, practical genotype spaces can be billions of base pairs long, while our landscape range from 2 to 10. This approach is impractical for large genotype spaces as the landscape size grows as 2^N, where N is the length of the genome. Future work may aim to investigate the impact of large clonal interference, deleterious mutations, or temporally-varying landscapes.